All-optical signal processing and regeneration

Wolfson, David

Publication date:
2001

Document Version
Publisher's PDF, also known as Version of record

David Wolfson

All-optical signal processing and regeneration

Ph.D. Thesis
February 2001

Research Center COM
Technical University of Denmark

Acknowledgements

I would like to start out by expressing my sincere gratitude to my supervisor Professor Kristian E. Stubkjaer for encouragement, support and fruitful discussions during my Ph.D. project but also for giving me the opportunity to work within a unique research group. In addition, I am grateful to Benny Mikkelsen, who inspired me to pursue the Ph.D. degree.

I would also like to thank Søren Lykke Danielsen, Allan Kloch, Peter Bukhave Hansen and Tina Fjelde for the joint efforts and long hours we had together during experiments in the laboratories. Experimental work usually requires a lot of patience and hard work, why having good colleagues is invaluable. I am furthermore indebted to Tina Fjelde and Allan Kloch for proof-reading and commenting the thesis. Special thanks are extended to Peter Bukhave Hansen and Allan Kloch for our joint efforts in 'Wombat Wagon'.

My other colleagues at Research Center COM, Henrik N. Poulsen, Anders Clausen, Alvaro Buxens, Emmanuel Limal, Xueyan Zheng, Fenghai Lui and Leif Oxenløwe are acknowledged for good team work and inspiring discussions. Moreover, the mechanical workshop is acknowledged for their kind help and creative solutions to different practical problems. I am also indebted to IT Support at Research Center COM for being there when my computer wasn't.

Finally, thanks are extended to all partners in the European ACTS project REPEAT and especially Alcatel Opto+ and Alcatel Alsthom Recherche for good collaboration and supply of state-of-the-art components for the experiments.

Kgs. Lyngby, Denmark David Wolfson

February 23rd, 2001

List of abbreviations

1R	Re-amplification
2R	Re-amplification + Re-shaping
3R	Re-amplification + Re-shaping + Re-timing
ACTS	Advanced Communications Technologies and Services
ASE	Amplified Spontaneous Emission
BER	Bit Error Rate
CW	Continuos Wave
DBR	Distributed Bragg Reflector
DCF	Dispersion Compensating Fiber
DFB	Distributed FeedBack (laser)
DOMO	Dual-Order Mode
EA	Electro-Absorption (converter/modulator)
EDFA	Erbium Doped Fiber Amplifier
EXC	Electrical Cross-Connect
FWHM	Full Width Half Maximum
FWM	Four-Wave Mixing
GC-SOA	Gain-Clamped Semiconductor Optical Amplifier
IP	Internet Protocol
IPDR	Input Power Dynamic Range
ISSR	Input Signal Suppression Ratio
IWC	Interferometric Wavelength Converter
KEOPS	KEys to Optical Packet Switching
MEMS	Micro-ElectroMechanical Switches
MI	Michelson Interferometer
MMI	Multi-Mode Interference (coupler)
MZI	Mach-Zehnder Interferometer
MQW	Multi-Quantum Well
NOLM	Non-linear Optical Loop Mirror
NRZ	Non Return-to-Zero
OADM	Optical Add Drop Multiplexer
OPEN	Optical Pan-European Network
OSNR	Optical Signal-to-Noise Ratio

OTDM	Optical Time Division Multiplexing
OXC	Optical Cross-Connect
PRBS	Pseudo Random Bit Sequence
REPEAT	REgeneration of PulsE shape, Amplitude and Timing
RZ	Return-to-Zero
SDH	Synchronous Digital Hierarchy
SOA	Semiconductor Optical Amplifier
TOAD	Terahertz Optical Asymmetric Demultiplexer
UNI	Unidirectional Non-linear Interferometer
WDM	Wavelength Division Multiplexing
XGM	Cross-Gain Modulation
XPM	Cross-Phase Modulation

Abstract

The trend in the industry today is that more and more complex functionalities are moving from the electrical domain and into the optical domain, demonstrating that all-optical networks are coming closer to realisation. In order for this progress to continue, there is a need for advanced optical components. The objective of this thesis is therefore to present an investigation and evaluation of key components that will be important enablers for future optical networks, namely optical space switches, wavelength converters and regenerators. The focus in the present work is on semiconductor optical amplifier (SOA)-based devices.

The thesis starts out by giving a description of the motivations and driving forces for the current evolution of optical networks from point-to-point systems to all-optical network topologies.

The use of SOA-based devices for all-optical gating is investigated with the use of a detailed large-signal model. An important parameter for SOA-based gates is the input power dynamic range (IPDR) as it determines the cascadability of the devices. Guidelines on how to maximise the IPDR are therefore established. Important trends are that short SOAs with low confinement factors and a low applied bias current should be used. These guidelines are verified by an investigation of the cascadability of the SOAs. Another type of SOA-based gate, namely the gain-clamped SOA (GC-SOA), is investigated. GC-SOAs have a higher saturation input power than conventional SOAs, making them attractive for multi-channel operation. It is shown that the cascadability of GC-SOAs is superior at 2.5 Gbit/s compared to conventional SOAs for up to at least 16 wavelength channels, whereas the benefit is reduced at higher bit rates due to influence from relaxation oscillations in the GC-SOA.

Furthermore, all-optical wavelength converters are treated. Initially, cross-gain modulation (XGM) in SOAs is described and guidelines as how to achieve a high modulation bandwidth are outlined. It is demonstrated that using long SOAs with high confinement factors and high bias currents together with high optical powers is beneficial to improve the performance. Moreover, issues concerning counter-directional coupling are discussed and advantages and disadvantages of the scheme are highlighted. A scheme, that can be used as a part of all-optical re-timing, is also investigated. The scheme has some advantages compared to conventional wavelength conversion since conversion of an optical clock signal is used instead of CW light. An investigation of these advantages is carried out and the feasibility of the scheme is demonstrated at 20 Gbit/s.

A description of interferometric wavelength converters (IWCs) is also given. The high-speed capabilities are investigated and conversion at 20 Gbit/s is demonstrated

in a single Mach-Zehnder interferometer (MZI) and a cascade of two Michelson interferometers (MIs). Furthermore, wavelength conversion at 40 Gbit/s is achieved with a penalty of ~0.6 dB. The challenge of conversion to the same wavelength is discussed and two approaches are described and demonstrated experimentally. The first solution is based on a dual-stage converter employing an XGM-converter in the first stage and an IWC in the second stage. An assessment of the dual-stage converter at 20 Gbit/s shows a insertion penalty of ~1.5 dB. The second approach is based on a dual-order mode (DOMO) MZI and a detailed investigation at 10 Gbit/s is presented. In addition, a conversion scheme that exhibits excellent transmission and speed performance will be described and evaluated at 10 Gbit/s.

Besides wavelength conversion, IWCs are also attractive for all-optical regeneration. Experiments carried out at 40 Gbit/s demonstrate excellent performance for 2R regeneration, which is emphasised by a clear improvement of the optical signal-to-noise ratio and a noise suppression capability. 3R regeneration is also illustrated at 40 Gbit/s, where insertion of the regenerator results in a penalty of ~0.5 dB. The scheme for 3R regeneration is extended to also include demultiplexing and demonstrated experimentally for demultiplexing from 40 to 10 Gbit/s. Finally, a scheme for 2R regeneration in IWCs, without the normally accompanying wavelength conversion, is presented. The performance of the scheme is investigated at 2.5 and 10 Gbit/s in an MI showing excellent results. The high-speed capabilities are also demonstrated in an experiment carried out at 40 Gbit/s, where clear noise suppression is achieved in an MZI.

Resumé (in Danish)

Tendensen i industrien i dag er, at stadig mere komplekse funktionaliteter bevæger sig fra det elektriske domæne til det optiske domæne, hvilket viser at rent optiske netværk kommer tættere på realisering. For at denne udvikling kan fortsætte, er der brug for avancerede optiske komponenter. Formålet med denne afhandling er derfor at præsentere en undersøgelse og evaluering af nøglekomponenter, som er vigtige for fremtidens optiske netværk. Disse er optisk-baserede rumlige koblere, bølgelængde-konvertere og regeneratorer. I dette arbejde er der fokuseret på komponenter baseret på optiske halvlederforstærkere (SOAer).

I starten af afhandlingen gives en beskrivelse af motivationerne bag den eksisterende udvikling af optiske netværk fra punkt-til-punkt systemer til rent optiske netværks-topologier.

Brugen af SOAer som optiske kontakter undersøges ved brug af en detaljeret storsignalmodel. En vigtig parameter for SOAer er det dynamiske indgangs-effektområde (IPDR), idet det bestemmer hvor mange SOAer, der kan kaskade-kobles. Retningslinjer for hvordan IPDR maksimeres opstilles derfor. Vigtige tendenser er, at en kort SOA med lav effektbegrænsningsfaktor og en lille fødestrøm bør bruges. Disse retningslinjer verificeres efterfølgende ved hjælp af en undersøgelse af hvor mange SOAer, der kan kaskadekobles. En anden type SOA-baseret kontakt, en forstærkningsfastholdt SOA (GC-SOA), undersøges ligeledes. GC-SOAer har højere mætningsindgangseffekter end konventionelle SOAer, hvilket gør dem attraktive til brug i et flerbølgelængdesystem. Det vises, at der kan kaskadekobles mange flere GC-SOAer end SOAer ved 2.5 Gbit/s i et system med op til 16 bølgelængder. Ved højere bithastigheder er fordelen dog mindre, grundet ind-flydelsen af relaksationsfrekvensen i GC-SOAerne.

Endvidere behandles optiske bølgelængdekonvertere. Indledningsvist beskrives krydsforstærkningsmodulation, og retningslinjer for hvordan en høj modulations-båndbredde opnås skitseres. Det demonstreres, at lange SOAer med høje effektbegrænsningsfaktorer, høj fødestrøm samt høje optiske effekter er optimale. Desuden diskuteres problemer vedrørende modsatkoblede indgangssignaler, og fordele samt ulemper ved teknikken fremhæves. En teknik der kan benyttes til optisk tidsrammegendannelse undersøges også. Teknikken har nogle fordele sammenlignet med den almindelige konverteringsteknik, idet et optisk kloksignal benyttes istedet for kontinuert lys. Disse fordele undersøges, og teknikken demonstreres ved 20 Gbit/s.

En beskrivelse af interferometriske bølgelængdekonvertere (IWCer) bliver ligeledes foretaget. Muligheden for operation ved høje bithastigheder undersøges, og konvertering demonstreres ved 20 Gbit/s i et enkelt Mach-Zehnder interferometer

(MZI) og to Michelson interferometre (MI). Desuden er bølgelængdekonvertering ved 40 Gbit/s opnået med en følsomhedsforringelse på 0.6 dB. Problemet vedrørende konvertering til samme bølgelængde diskuteres og to løsninger beskrives og demonstreres eksperimentelt. Den første løsning er baseret på en konverter bestående af krydsforstærkningsmodulation og en IWC. Ved eksperimentel undersøgelse af teknikken demonstreres en følsomhedsforringelse ved indsættelse af den samlede konverter på ~1.5 dB ved 20 Gbit/s. Den anden løsning er baseret på en MZI, hvor indgangssignalerne udbredes i to forskellige modes (DOMO), og her foretages en detaljeret undersøgelse af komponenten ved 10 Gbit/s. Derudover præsenteres og undersøges en bølgelængdekonverteringsteknik ved 10 Gbit/s, der er karakteriseret ved gode transmissionsegenskaber og høj modulationsbåndbredde.

Udover bølgelængdekonvertering er IWCer også attraktive til optisk regenerering. Eksperimenter foretaget ved 40 Gbit/s demonstrerer gode egenskaber for 2R regenerering, hvilket understreges af en klar forbering i signalstøjforhold samt støjundertrykkelse. 3R regenerering demonstreres ligeledes ved 40 Gbit/s, hvor indsættelse af regeneratoren resulterer i en følsomhedsforringelse på ~0.5 dB. Teknikken til 3R regenerering udvides til også at inkludere demultipleksning og demonstreres eksperimentelt for demultipleksning fra 40 til 10 Gbit/s. Slutteligt præsenteres en teknik til 2R regenerering i IWCer uden den normalt medfølgende bølgelængdekonvertering. Teknikken undersøges ved 2.5 and 10 Gbit/s i en MI, hvor der vises gode resultater. Højhastighedsegenskaberne demonstreres ligeledes i et eksperiment udført ved 40 Gbit/s, hvor en klar støjundertrykkelse opnås i en MZI.

Contents

Chapter 1

Introduction

People are slowly beginning to comprehend the true meaning of the 'information era'. The real enabler for this awakening has been the Internet and the possibilities that it has provided. Just within the last decade, there have been significant changes in people's daily habits and since the majority has embraced these changes, the Internet is boosted even further. The rapid evolution of the Internet and its importance for the future should therefore not be underestimated. The possibilities are immense, and will be in an even higher degree in the future. Today the Internet is a natural part of many people's daily life and is used for retrieval of information of almost any kind, sending e-mails and an area like e-commerce is gaining more and more foothold. There are no indications that this evolution will come to a stop and already new multimedia services such as video conferencing, video-on-demand, etc. are beginning to dawn. As a consequence of this evolution, bandwidth requirements are immense. Furthermore, there is a steady increase in the number of new users. An estimation given by RHK[1] predicts that by July 2002 there will be around 800 million Internet users world-wide, more than twice the current level [1]. This, together with the continuing adoption of high-speed access in companies and homes, which will enable new high-speed applications, will trigger an even higher demand for bandwidth. Conservative estimations concerning Internet traffic growth is that the capacity doubles every 6th month [2].

The traffic growth is therefore a tremendous challenge for the telecommunications companies that have to provide network solutions that are able to handle the capacity requirements. Wavelength division multiplexing (WDM) has proven to be the most cost-effective technology that is capable of fulfilling the demand. Consequently, WDM transmission systems are deployed on a global scale by all major vendors and the success of WDM is clearly illustrated by the fact that commercial systems are reaching fiber capacities of 1.6 Tbit/s [3]. In comparison, state-of-the-art commercial systems in 1997 had a fiber capacity of 40 Gbit/s [4].

WDM systems today are mainly point-to-point systems as is also the case for most systems currently being implemented. Due to the increase in demand for transmission bandwidth, however, the current trend is that more and more functionalities, which traditionally are carried out in the electrical domain, are moving into the optical domain. This has been made possible by the development and commercialisation of components that constitute some of the important

[1] RHK: Ryan Hankin Kent, Inc. - Telecommunications Industry Analysis.

building blocks necessary in an optical network node, e.g., amplifiers [5], tuneable filters [6], tuneable add-drop multiplexers [7] and space switches [8]. As a result of this progress, true optical networking, i.e., a network with an all-optical core where optical signals only are terminated at the edges of the network, is a realistic vision in the near future. Initial steps in this direction have already begun in that ring networks employing all-optical add-drop multiplexers have become commercially available [9]. However, for more complex network architectures like meshed networks, optical cross-connects (OXCs) that are able to switch information between different input and output ports, with the use of optical space switches, become necessary. Consequently, there is a significant activity in research and development of practical gates. As a result of the efforts, different promising technologies exist today both for circuit-switched [8] and packet-switched networks [10]. Although OXCs are technically more demanding than the individual building blocks mentioned above, different field trials [11,12], and especially product-offerings [13], demonstrate that the vision of all-optical networks is coming closer to realisation.

Once OXCs are deployed to a higher degree than today, optical signals will traverse many network nodes before the connections are terminated. In such a network, the use of all-optical wavelength converters [14-16,p6,p29] in OXCs will offer a significant advantage since they will allow full exploitation of the wavelength domain. Thereby flexibility will be provided in the optical network since converters enable wavelength assignment on a link-by-link basis rather than on a global basis [17] as well as reduction of wavelength contention in OXCs due to the possible wavelength re-use [18-20]. Both these features are attractive as they ease the network management and increase the bandwidth utilisation.

An important issue to consider in the process of building all-optical networks is that the detrimental effects that the signals undergo during transmission are accumulated through the network. This imposes a serious limitation on the size of optical networks, which can only be avoided through the implementation of the all-optical regenerator [21,22]. The all-optical regenerator will therefore be as important for large-scale optical networks as the optical amplifier was for the commercial success of WDM systems [21], why the research in this area is very intense world-wide.

This thesis contains both theoretical and experimental work concerning all-optical gates, wavelength converters and regenerators. The results presented throughout this thesis are all carried out with devices based on semiconductor optical amplifiers (SOAs). The objective of the work is to investigate and evaluate these devices, with special focus on the system performance. Regarding SOA-based gates guidelines on how to maximise the cascadability will be presented since this number to a large degree determines whether they are practical for implementation. Furthermore, guidelines concerning the conversion speed of SOA-based wavelength converters will

be established and a detailed experimental investigation of interferometric wavelength converters (IWCs) will be carried out. Since the transfer function of IWCs is non-linear, noisy input signals are re-shaped during wavelength conversion. This also makes IWCs attractive for all-optical regeneration and consequently, the regenerative properties these devices will be investigated.

More specifically, the thesis is organised as follows:

To set the scene for the rest of this thesis, chapter 2 gives a description of the various driving forces for the current evolution of optical networks from point-to-point systems to all-optical network topologies. Moreover, an overview of some of the different techniques for all-optical wavelength conversion and regeneration, that exist today, will be given.

Chapter 3 presents an evaluation of SOA-based gates. Using a detailed theoretical model, basic characteristics such as gain and optical bandwidth are considered. Furthermore, guidelines for optimisation of the input power dynamic range are given. Following this, an investigation of the cascadability of SOAs in single channel systems is carried out. A description and evaluation of gain-clamped SOAs (GC-SOAs) is also carried out followed by a comparison of the performance in a multi-channel system between conventional SOAs and GC-SOAs.

In chapter 4, cross-gain modulation (XGM) in SOAs will be described. First the operating principle of XGM will be explained and then guidelines for high-speed operation are established followed by a 40 Gbit/s system experiment. Moreover, an investigation of the difference between co- and counter-directional propagation in XGM-based converters is presented. A scheme that can be used for all-optical re-timing in XGM-based converters is also investigated and the feasibility of the scheme is evaluated experimentally at 20 Gbit/s.

Cross-phase modulation (XPM) in IWCs is treated in chapter 5, which starts out with a description of the operating principle of these devices. After an investigation of the basic performance at 10 Gbit/s, the high-speed capabilities will be evaluated by a 20 Gbit/s system experiment. Furthermore, a technique that allows for an increase in the conversion speed will be described and demonstrated at 40 Gbit/s together with a scheme for increasing the input power dynamic range of IWCs. Two solutions to the problem of converting to the same wavelength as the input signal are also presented. The first solution is based on a dual-stage converter consisting of an XGM converter in the first stage and an XPM converter in the second stage. The second scheme is based on a new type of IWC called a dual-order mode (DOMO) Mach-Zehnder interferometer. Finally, a new scheme for wavelength conversion in IWCs, that exhibits good speed and transmission properties, will be presented.
The results presented in section 5.1.2 and 5.3.2 are obtained in collaboration with my colleagues Allan Kloch and Tina Fjelde from Research Center COM. The

straight-line experiment in section 5.2.1 with two Michelson interferometers and the experiments in section 5.3.1 were carried out with Allan Kloch and Peter Bukhave Hansen (former COM, now with Ericsson Denmark). The 20 Gbit/s experiment in section 5.2.1 with a Mach-Zehnder interferometer and the results presented in section 5.2.2 and 5.2.3 are obtained together with Peter Bukhave Hansen, Allan Kloch and Tina Fjelde.

In chapter 6, the regenerative properties of IWCs are investigated experimentally. After a short introduction to all-optical regeneration, 2R and 3R regeneration is demonstrated at 40 Gbit/s together with a scheme that enables simultaneous 3R regeneration, wavelength conversion and demultiplexing. The 2R regenerative capabilities of a novel conversion scheme are also assessed. Following this, a novel scheme for 2R regeneration, without the normally accompanying wavelength conversion, will be described and evaluated experimentally at 2.5, 10 and 40 Gbit/s. Finally, an investigation of the transmission properties of the scheme is presented.
The results demonstrated in section 6.1 are obtained together with Peter Bukhave Hansen and Allan Kloch, while the results in section 6.2.1-3 and 6.3.3 are obtained in collaboration with Peter Bukhave Hansen, Allan Kloch and Tina Fjelde.

Chapter 7 presents the conclusion of the thesis.

Chapter 2

Keys to optical networking

Over the last decade, tele and data communication has experienced a tremendous increase in the need for transmission bandwidth. So, in order to accommodate the capacity requirements, point-to-point WDM systems have been installed on a global scale. These systems have proven to be an efficient and cost-effective way to realise high-capacity links and consequently, much research and development is focussed on increasing the capacity on the optical fibres by increasing both the number of wavelength channels [23] and the channel bit rate [24]. As a means to further boost the growth in network capacity, steps are currently being taken in order to avoid electrical termination of all connections in each network node as is done today. Much effort is therefore put into development of optical techniques to interconnect fibers in optical cross-connects performing some of the functionalities that are handled by electronics today.

The purpose of this chapter is to give a general description of the evolution of optical backbone networks with special focus on some of the important functionalities that will be required to build true all-optical networks and not just point-to-point connections. This description will create a basis for the remaining chapters in this thesis, which will focus on the design and realisation of optical components that are able to fulfil these requirements.

Section 2.1 deals with the technological evolution of optical networks from WDM point-to-point systems to all-optical network topologies that can be envisaged in the near future. Following this, a discussion of the important building blocks to realise these all-optical networks will be carried out in section 2.2.

2.1 Evolution of optical networks

The envisaged structure of the optical backbone network is constantly changing as a result of higher bandwidth requirements and new technological progress. One possible evolution, however, is shown in Fig. 2.1 [25]. In the following the motivations for such a network evolution will be described with focus on the functionalities needed to realise true all-optical networks.

The first step that is currently being taken by vendors world-wide is installation of WDM point-to-point connections consisting of WDM transmitters, optical links including optical fiber amplifiers and WDM receivers. The reason for deployment of these systems is that this is the only technology today that can handle the enormous amount of capacity that is generated world-wide in a cost-effective and efficient way.

The successful progress in using wavelengths as a means to upgrade the capacity is also clearly illustrated by the fact that commercial systems are reaching fiber capacities of 1.6 Tbit/s [3]. Recent experiments carried out in laboratories even show transmission capacities of 6.4 Tbit/s [26]. Since most commercial systems employed today are point-to-point systems, all connections are terminated in every network node after which signal processing is carried out in the electronic domain. However, as WDM deployment continues and network traffic grows, electronic solutions become increasingly cumbersome, making optical solutions more attractive. There are several reasons why this is the case and arguments will consequently be given throughout this section. One reason, however, is that since a large part of the IP traffic today is international, it passes several network nodes before its final destination. This means that termination of the information is performed at many nodes and since electronics operate on bit level, costly high-speed equipment is necessary each time. On the other hand, simple optical signal processing, such as wavelength add/drop or space switching, operates on the wavelength or multiplex level and is therefore bit rate transparent. Consequently, cost savings are envisaged by keeping the information in the optical domain.

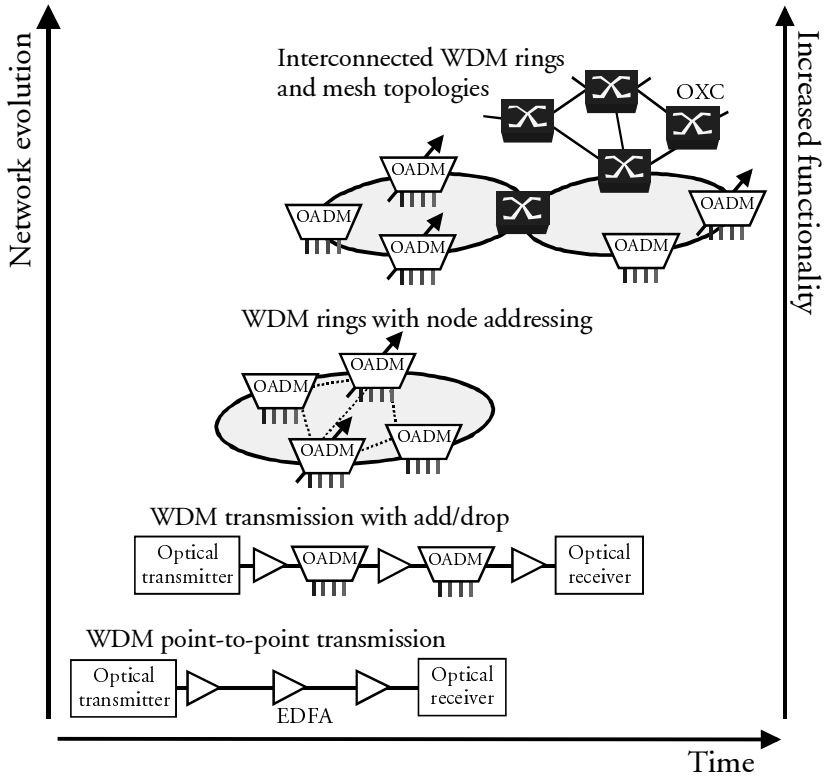

Fig. 2.1: Evolution of the optical transport network from WDM point-to-point links through WDM rings with tuneable add-drop multiplexers (OADM) to finally full interconnection of rings and meshed networks using optical cross-connects (OXC). From [25].

An initial step towards an increased functionality in the optical domain is the introduction of an optical add-drop multiplexer (OADM) as shown in Fig. 2.1. OADMs allow for adding and dropping of one or more specific wavelengths at intermediate sites in the network, while the rest of the wavelength channels are passed transparently[2] through. An even higher degree of functionality will be obtained with the introduction of tuneable or reconfigurable OADMs capable of adding and dropping any of the incoming wavelengths. As indicated in Fig. 2.1, a ring network with reconfigurable OADMs will correspond to a logically meshed network, whereby full connectivity can be provided since every node can address all nodes in the network. These devices are already commercial both as stand-alone components and as part of network solutions [7].

The next step in the network evolution will be introduction of building blocks that are able to switch information transparently between input and output ports. So, in much the same way as electrical cross-connects (EXCs) emerged to manage capacity at the electrical layer, optical cross-connects (OXCs) will be attractive in the optical domain [27]. As indicated in Fig. 2.1, the OXC will enable interconnection of WDM rings and physical meshed topologies. The basic building block in OXCs will therefore be space switches, which provide the connectivity between the channels on the input ports and the channels on the output ports. Some vendors have already announced various OXCs, incorporating all-optical space switches, with throughput capacities above 1 Tbit/s [13].

Apart from the fact that termination will be avoided in OXCs, there is another crucial reason why optical solutions are attractive compared to EXCs. EXCs today can handle channel bit rates up to ~10 Gbit/s per input port, however, problems arise when a large throughput capacity has to be obtained. The reason is that as the number of fibers and wavelengths on each fiber increase, the number of electrical interconnections in the EXC increases rapidly making it increasingly difficult to maintain short electrical path lengths. This imposes a considerable concern at high bit rates since loss at high frequencies becomes a significant factor, thereby limiting the possible number of interconnections and ultimately the possible throughput capacity. One solution to this is to fragment the EXC into smaller units so that the number of interconnections in each unit is limited. However, this approach scales with the number of ports squared making it a very bulky and costly solution. Optical solutions, on the other hand, do not struggle with these problems to the same degree. First of all, optical fibers, used as interconnects, can be long without influencing the signal quality. Secondly, the wavelength domain can be utilised to build OXCs that scale better than EXCs. The 'feeling' today, is therefore that for

[2] Unless explicitly stated, the term transparency is in this thesis used when no electro-optic conversion takes place, i.e., it does not relate to format or service transparency.

throughput capacities above 1-2 Tbit/s, optical solutions should be applied. This boundary may naturally move with time but the point is that above a certain throughput capacity, optical solutions appear superior. The drawback of present optical solutions, however, is that some functionalities that are handle by electronics today, e.g., bit error rate monitoring, are still difficult to implement optically. This raises the problem of fault detection, i.e., where in the network an error has occurred, which obviously is an important functionality. Much effort is therefore put into development of different techniques that are able to fulfil these requirements. It should also be pointed out that for deployment of OXCs to become reality there has to be ways or rules to manage the optical channels. Consequently, there is much work going on in different standardisation bodies to achieve this [28,29].

To fully exploit the wavelength domain and thereby increase the flexibility, another important building block in OXCs is the all-optical wavelength converter. One of the obvious advantages offered by the converter is reduction of wavelength blocking in OXCs [18,19], which will have a significant impact on the management of the network as it enables wavelength re-use [20]. Although optical converters already are commercial for 10 Gbit/s [30], there are still several challenges that have to be overcome before deployment in real systems. Still, the research in this area is very intense, as it is an important part of the OXC for full flexibility. One impressive realisation of a strictly non-blocking OXC incorporating both semiconductor optical amplifier (SOA)-based space switches and wavelength converters was achieved in the European ACTS project OPEN[3], for which the aim was to demonstrate the feasibility of an optical backbone meshed network covering major cities in Europe [31]. In the project, two successful field trials were conducted where the OXC played an essential part [32].
In section 2.2.1 different techniques for all-optical wavelength conversion will be reviewed, while chapter 4 and 5 deals with two specific methods, namely cross-gain and cross-phase modulation in SOA-based components.

The result of performing signal processing on the optical channel level is that the granularity in the network is coarse, i.e., corresponding to a wavelength channel. The drawback of this is that transmission bandwidth is wasted when not enough information is transmitted. In order to obtain a higher bandwidth utilisation, optical packet switching is therefore attracting attention as a means to achieve a finer granularity. In the European ACTS project KEOPS[4], optical packet switching was studied thoroughly [33,34] with special focus on a possible architecture for a packet-based switch. The main conclusions drawn in the project was that, although possible to realise, there are two main obstacles in connection with such a packet switch.

[3] OPEN: Optical Pan-European Network.
[4] KEOPS: KEys to Optical Packet Switching.

Firstly, the ability to realise stable and compact units that can synchronise the optical packets and secondly, optical buffers, which are necessary to minimise the packet loss in the packet switch. Due to these problems, optical networks will be circuit-switched in the near future, whereas a packet-switched layer can be added on in time when the above-mentioned problems are solved.

A very important issue to consider in the attempt to build transparent large-scale all-optical networks is the analogue transmission nature of optical signals, which means that the detrimental effects that the optical signals undergo during transmission are accumulated through the network. This sets a severe limitation on the realisation of true optical networks. The analogue nature naturally also plays an important role for systems today but nevertheless commercial long-haul point-to-point systems are already successfully installed, e.g., sub-marine systems crossing the Pacific or Atlantic Ocean. The important point is, however, that these systems have been very carefully designed so that parameters such as transmission distance, power levels, optical signal-to-noise ratio (OSNR) of individual wavelength channels, fiber dispersion, timing jitter, etc. are well known in the system. Also, since the nodes in point-to-point systems are electrical, regeneration of the signals is straightforward. This has the very important benefit that expansion of the network is relatively easy. In the case of all-optical networks, signals will be transmitted over different distances, amplified by a different number of optical amplifiers, etc. depending on the path through the network and the number of nodes traversed. In practice, this means that the network would have to be designed from a worst-case scenario, thereby imposing a considerable limitation on the size of the network. This, however, is neither very cost-effective nor future-proof since any expansion of the network would in principle require an upgrade of the entire network. Because of this limitation, the vision of transparent all-optical networks has subsided during the recent years and the concept of transparent optical domains has emerged instead [29]. Fig. 2.2 illustrates this idea with a representation of two optical transparent WDM domains. Here, each domain can be carefully designed so that a certain signal quality is maintained. In addition, different domains are interconnected with an electronic transponder performing full 3R regeneration[5], thereby avoiding further degradation of the optical signals. Besides ensuring high quality of signals entering a new domain, this also has the advantage that much of the high-speed electronics will be moved from the core of the network to the edges, where different networks are interconnected.

[5] 3R regeneration: Re-amplification + Re-shaping + Re-timing.

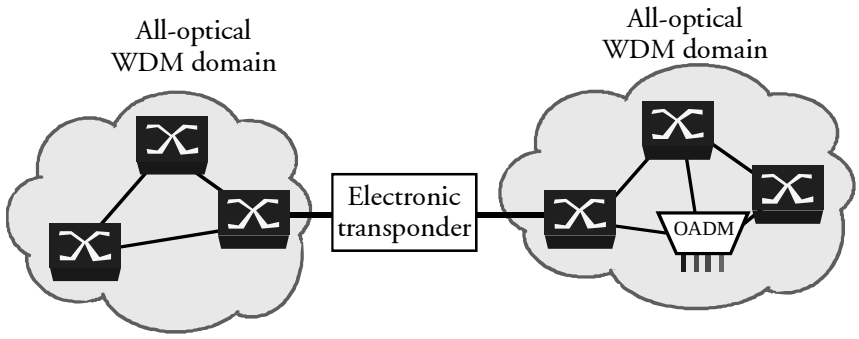

Fig. 2.2: Illustration of two transparent all-optical WDM domains interconnected with an electronic transponder performing full 3R electronic regeneration. The electronic transponder ensures that optical signals are delivered to the next WDM island with satisfactory quality.

The vision of large-scale transparent networks still exists, however, since it is believed that once optical channels can be managed in the optical domain, it will be easier and less expensive than to perform electrical processing. The key component to realise this dream is the all-optical regenerator. The research in this area is very intense world-wide and although the field is far from having a practical solution yet, different techniques are showing very promising results [p34,35-38]. It should be mentioned that the effort is not only put into 3R regenerators but also on 2R regenerators (re-amplification + re-shaping). The reason is that a cost-effective network solution might be to have several smaller networks or domains, where only 2R regeneration is necessary to maintain satisfactory signal quality. In much the same way as illustrated in Fig. 2.2, these small networks can then be interconnected with 3R regenerators for full regeneration.
To give an overview of the area, section 2.2.2 deals with different techniques for all-optical regeneration.

2.2 Key functionalities for all-optical networking

Some of the important functionalities or building blocks needed to achieve true all-optical networks will be discussed here. As outlined in section 2.1, both OADMs and optical space switches are important components in order to bring flexibility to optical networks. Seen from a commercial point of view, however, this process has already started and these devices will therefore not be described in this section. Note that an overview of the various approaches for space switching will be given in chapter 3 followed by a detailed description of SOA-based gates. There are two specific areas that are still under heavy research and which could prove to be very important for future all-optical networks. Namely all-optical wavelength conversion, which is desirable due to the added flexibility in WDM networks and all-optical regeneration, which will be crucial in the attempt to realise large-scale optical networks that are not limited by accumulation of degrading effects.

To set the scene for chapter 4, 5 and 6, where all-optical wavelength conversion and regeneration is covered, an overview of some of the different techniques that exist today is given here. It is emphasised that the focus will be on recent experimental results rather than giving an in-depth description of the different techniques. Section 2.2.1 deals with all-optical wavelength conversion, while regeneration is covered in section 2.2.2.

2.2.1 All-optical wavelength conversion

Even though the requirements to all-optical wavelength converters will be system dependent, there are several general features that should be fulfilled. Below, a list of the most relevant is given:

- Polarisation independence.
- High input power dynamic range.
- Moderate optical input power requirements.
- High-speed operation, preferably 40 Gbit/s and above.
- Large optical bandwidth (both for input and output wavelength).
- Low chirp to facilitate transmission over non-dispersion shifted fiber.
- High conversion efficiency[6], OSNR and extinction ratio of converted signals.
- Good cascadability performance for large-scale optical network applications.
- Compactness, simple implementation and low power consumption.

In the following, different techniques for all-optical wavelength conversion will be reviewed and the advantages and disadvantages of the techniques will be discussed.

Four-wave mixing

Converters that rely on four-wave mixing (FWM) have been investigated using optical fibers [39], laser converters [40] and SOAs [41] as non-linear elements. FWM converters have several desirable features such as format transparency, high-speed operation (100 Gbit/s conversion is shown in [42]) and the ability to convert several WDM channels simultaneously (32x10 Gbit/s conversion is shown in [43]). A problem associated with FWM, however, is that the conversion efficiency is low (typically below -10 dB), why high optical powers have to be used for both the pump and signal (10-20 dBm). Furthermore, the efficiency decreases as the detuning between the pump and signal wavelength increases, thereby limiting the conversion range [44]. Using two orthogonal polarised pumps solves the problem of wavelength dependent efficiency [45,46] (conversion over 80 nm is shown in [46]) and can result in polarisation insensitive operation [47], however, at the expense of added

[6] The conversion efficiency is defined as the ratio between the power of the converted output signal and the input data signal.

complexity. Still, as a result of low efficiencies, the converted signals usually exhibit a low OSNR. As shown in [48], where two converters are cascaded at 10 Gbit/s, an initial OSNR of ~40 dB is reduced to ~20 dB after two conversions, clearly limiting the cascadability to two converters. Although the OSNR can be improved by using a pre-filtering technique [49], the cascadability performance of FWM-based converters still has to be demonstrated. Moreover, since the output wavelength is dependent on both the pump and signal wavelengths, the pump must be tuneable even for fixed output wavelengths.

Electro-absorption converters
Wavelength converters based on electro-absorption (EA) are very simple devices and recently BER measurements for conversion at 10 Gbit/s over 20 nm was reported with negligible polarisation sensitivity [50]. Furthermore, conversion at 40 Gbit/s has also been achieved with high Q-values [37]. The main drawbacks of EA converters are low conversion efficiencies, high insertion losses and the need for high optical powers to achieve good absorption modulation (typically 10-15 dBm) [50].

TOAD/NOLM/UNI
The terahertz optical asymmetric demultiplexer (TOAD) [51], non-linear optical loop mirror (NOLM) [52] and ultrafast non-linear interferometer (UNI) [53] are all fiber-based devices (even though the TOAD and UNI use an SOA as the non-linear element). They have all shown good results, e.g., 40 Gbit/s conversion is demonstrated in the NOLM [54] and 80 Gbit/s in the UNI [55], however, since these devices are fiber-based they are bulky and difficult to stabilise.

Cross-gain modulation in SOAs
The cross-gain modulation (XGM) scheme can be polarisation independent, has a large conversion range [56], a high input power dynamic range (typically >7 dB), is very power efficient and high-speed operation is possible (100 Gbit/s conversion is shown in [57]). There are, however, also some shortcomings related to XGM. The scheme suffers from a chirped output signal limiting transmission on standard fibers and the extinction ratio of the converted signal may degrade for conversion to longer wavelengths [15]. Chapter 4 deals with XGM in SOAs in more detail.

Cross-phase modulation in SOAs
A technique that, compared to the previous schemes, eliminates most of the drawbacks is based on cross-phase modulation (XPM) in SOA-based interferometers, i.e., monolithically integrated Mach-Zehnder [58] or Michelson interferometers [59]. The following features characterise the converters: High-speed operation (40 Gbit/s conversion is shown in [p19,60-62]), low and controllable chirp [15] and a large conversion range [61] are obtainable. Also, a high OSNR of the converted signal is achievable (typically ~40 dB in 0.1 nm [p23]). It should be pointed out that since the performance of the interferometers is sensitive to the phase conditions between the

interferometer arms, active control of the converters is an issue that needs special attention. A detailed evaluation of the performance of Mach-Zehnder and Michelson interferometers will be given in Chapter 5.

Delayed-interference signal wavelength converter

This type of converter has recently been proposed [63,64] and a record-breaking operation at 168 Gbit/s has been demonstrated [65,66]. Very importantly, this device has also been realised as a monolithically integrated structure, where 100 Gbit/s conversion has been achieved [67]. Besides the high conversion speed, this type of converter has not been investigated fully yet, so the general performance is difficult to comment on. It should be mentioned, though, that the converter resembles other interferometric structures, why similar performance can be expected.

2.2.2 All-optical regeneration

As mentioned in section 2.1, realisation of the all-optical regenerator will probably be the most important enabler for large-scale transparent all-optical networks. An illustration of a 2R and 3R regenerator is given in Fig. 2.3. Both regenerators have a re-amplification stage and a non-linear decision element to re-shape the input signal. In addition, the 3R regenerator has a clock recovery, which can be either optical or electrical, generating clock pulses that perform re-timing by sampling the input signal. If necessary, e.g., if the decision element has a small input power dynamic range, the amplification stage can also function as a power equaliser.

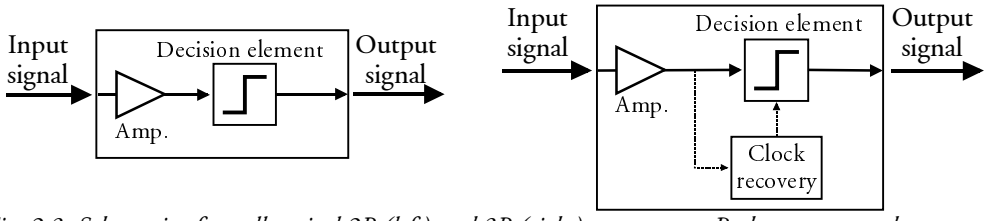

Fig. 2.3: Schematic of an all-optical 2R (left) and 3R (right) regenerator. Both regenerators have a re-amplification stage and a non-linear decision element to re-shape the input signal. In addition, the 3R regenerator has a clock recovery circuitry performing re-timing by sampling the input signal.

It is crucial that the transfer function of the decision gate, i.e., the output power as a function of the input power, is non-linear. The larger degree of non-linearity, the better the re-shaping capability [68,p3]. The best transfer function is that of an ideal decision gate since all noise on both logical zeros and ones is effectively re-shaped. In the following list, different requirements that should be associated with an all-optical regenerator are given:

- Polarisation independence.
- High input power dynamic range.
- Moderate optical input power requirements.
- High-speed operation, preferably 40 Gbit/s and above.
- Large optical bandwidth.
- 2R regeneration: Should accept a low OSNR and extinction ratio of the input signal but result in a high OSNR and extinction ratio of the output signal.
- 3R regeneration: In addition to 2R a large amount of jitter on the input signal should be accepted but result in a small jitter on the output signal.
- Low power consumption, compactness and simple implementation.

Due to the requirements for a non-linear transfer function and the ability to accept a low OSNR and still result in a high OSNR, there are not as many different promising techniques for all-optical regeneration as for wavelength conversion. So, even though there are other techniques than those discussed in the following, these are the most promising.

Electro-absorption modulator
Due to the highly non-linear transfer function of EAs, a 2R capability is inherent when performing wavelength conversion and has been demonstrated at 20 Gbit/s [69]. Furthermore, transmission over 30.000 km has been achieved at 10 Gbit/s [70], emphasising the 2R regenerative properties. 3R regeneration is also possible, simply by replacing the CW light, necessary for wavelength conversion, with a re-timed optical clock signal [71]. This has been used to demonstrate 3R regeneration both at 10 and 40 Gbit/s [72,37]. As already mentioned, the main drawbacks of EAs are low conversion efficiencies, high insertion losses and the need for high optical input powers.

Soliton techniques
Soliton systems employing 3R techniques have shown very impressive results such as transmission over 1 million km at 10 Gbit/s [73], transmission over 10.000 km at 8x20 Gbit/s [74], transmission over 70.000 km at 40 Gbit/s [75] and transmission over 10.000 km at 80 Gbit/s [76]. The biggest disadvantage of these techniques, however, is that the fiber link has to be very carefully designed in order to maintain the soliton effect. This is of course only possible in a point-to-point link, where each path can be designed regardless of other optical paths. This has been partly overcome in [77], where a 'black box' solution has been proposed that in principle can be adapted to a wide variety of RZ transmission systems regardless of the transmission line characteristics. In the 'black box', RZ-to-soliton transformation is performed and regeneration is achieved using soliton methods. After the 'black box', i.e., on the transmission link, there is a back-conversion to RZ pulses, which then propagate on

the fiber. The advantage is that the transmission line does not have to be designed for soliton transmission but that the 'black box' can be adapted to the transmission line [77]. Still, the 'black box' is rather complex since it requires different specially designed parts [38,78]. A disadvantage of soliton techniques in general is that high optical power levels are required.

SOA-based interferometers

As for EAs, 2R regeneration is also inherent in Mach-Zehnder or Michelson interferometers due to the non-linear transfer function [p3,p5,p11,79]. Here, regeneration at 40 Gbit/s has been demonstrated [p16,p23] as well as transmission over 3.600 km at 2.5 Gbit/s [80]. If an optical clock signal is used instead of the CW light, re-timing can also be obtained [81] (3R regeneration at 40 Gbit/s is shown in [p23,82]). Owing to these features, an impressive cascadability performance has been demonstrated in loop experiments. 1000 3R regenerators at 10 Gbit/s including transmission over 170.000 km [35] and 200 regenerators at 20 Gbit/s including transmission over 20.000 km [36]. It can also be mentioned that by using a 'pass-through' scheme in interferometric converters, all-optical 2R regeneration without wavelength conversion can be achieved [p13]. Also with this scheme, extinction ratio improvement and noise suppression has been demonstrated [p13,p16]. As already pointed out, active control of the converters is an issue that needs special attention. A detailed evaluation of the regenerative capabilities of Mach-Zehnder and Michelson interferometers will be given in Chapter 6.

2.3 Summary

A possible evolution of optical networks has been described where it has been argued that the increasing network capacity raises the need for all-optical techniques to handle some of the functionalities that are performed by electronics today. This progress has already started with the emergence of commercial optical add-drop multiplexers and optical space switches but will most likely continue so that even more complex operations will be taken care of in the optical domain, e.g., wavelength conversion and regeneration. Finally, different techniques that exist today to perform all-optical wavelength conversion and regeneration have been discussed with special focus on recent results as well as advantages and disadvantages seen from a system perspective. These areas still require maturing before commercial deployment is realistic but the research is very intense, as they will play an important role to realise large-scale flexible all-optical networks.

Chapter 3

SOA-based gates for all-optical space switching

All-optical space switches will be important in future optical networks to realise OXCs so that transparent connections can be established in the optical domain. The requirements to space switches naturally depend on the network and the specific application, but in general the optical gates should possess the following features:

- Wavelength and polarisation independence.
- High on-off ratio of 40-50 dB to suppress impact from cross-talk.
- Low insertion loss to maintain a good OSNR and relax the power budget.
- Switching time as required by the application, i.e., ~ms for circuit switching and ~ns for packet switching.
- Low power consumption, compactness and scalability.

There are many candidates for space switching, where each solution has different advantages and disadvantages. Among free-space switches, macromechanical techniques are the most attractive from the perspective of optical impairments [83]. High on-off ratio, polarisation insensitivity and low insertion losses even for large switch fabrics are some of the attractive features. However, since the switching is based on mechanically moving parts, they are bulky and the switching speed is slow (up to several hundred ms) making them unpractical for optical networks.

Micro-electromechanical switches (MEMS) may offer the compactness needed for practical use. This technology combines free-space interconnect with the advantages of monolithic integration on silica platforms. Some of the attractive features are low power consumption, on-off ratios in excess of 50 dB [8], negligible polarisation dependent loss [8] and potentially low insertion loss even for large switch fabrics. The switching time for MEMS is in the ms region [8] making them appropriate only for circuit-switched networks. The biggest concern of MEMS, however, is the long-term stability of the components, which is a critical but still unanswered question.

Switches based on electro-absorption modulators can have switching times of ~1 ns, be polarisation independent and have a high optical bandwidth [84,85]. They also feature a fairly high on-off ratio of 30-40 dB [84]. A shortcoming, however, is an insertion loss of up to ~10 dB [86] making them unpractical for large switch fabrics.

Optical Mach-Zehnder switches and digital switches based on, e.g., $LiNbO_3$ or InP have desirable properties such as high switching speed and they can also be wavelength and polarisation independent [10,87-89]. The main limitations, however, are fairly high insertion loss [10] and problems in achieving sufficiently

high on-off ratios [10,83], although the latter can be improved by using dilated structures [88] at the expense of an increased complexity.

Thermo-optic switches such as silica-on-silicon or polymers are relatively easy to fabricate and are therefore low-cost devices. Both can be made with very low polarisation dependent loss and large optical bandwidths. The insertion loss for individual elements, e.g., 1x2 or 2x2 switches, is fairly low (<1 dB) but the loss scales with increasing switch size making large switch fabrics unpractical. Furthermore, special attention must be given to the cross-talk levels of individual elements but also here dilated schemes improve the performance noticeably. The switching time is in the ms range, which means that the application is for circuit-switched networks.

SOA-based gates overcome the problem of insertion loss since they can supply a gain of ~30 dB [10]. Furthermore, they have switching times of less than 1 ns [90,91] and very high on-off ratios of 40-50 dB [90] needed to overcome the impact from cross-talk. Moreover, they can be made polarisation insensitive and offer an optical bandwidth of more than 50 nm [92,93]. The drawback, however, is that SOAs have a limited input power dynamic range (IPDR) due to amplified spontaneous emission (ASE) at low input powers and gain saturation at high input powers.

The objective of this chapter is to give a detailed investigation of the linear properties of SOA-based gates. The investigation will especially focus on optimisation of the cascadability of the gates since this number to a large degree determines whether the SOA-based gates are practical for implementation.

Basic characteristics such as gain and optical bandwidth are considered in section 3.1 and furthermore, guidelines for optimisation of the IPDR are given. In section 3.2, an investigation of the cascadability of SOAs in single channel systems is presented, while section 3.3 describes gain-clamped SOAs (GC-SOAs) [94,95]. GC-SOAs are essentially like conventional SOAs but have the advantage of being able to operate at higher input powers, making them attractive for WDM operation. This will be evident by a comparison of the performance of GC-SOAs and conventional SOAs in a WDM environment. Finally, the influences of the modulation format, i.e., RZ and NRZ, on the performance of GC-SOAs will also be investigated in section 3.3.

3.1 Conventional SOAs

In order to get an understanding of basic SOA characteristics, this section considers the influence of bias current, optical confinement factor and SOA length on important parameters such as optical bandwidth, gain and noise figure. Furthermore, guidelines on how to optimise the IPDR of SOA gates are given, as this will determine the cascadability of the gates.

3.1.1 Static characteristics of conventional SOAs

An illustration of the SOA gate considered here is given in Fig. 3.1. The device consists of an active region designed to ensure single mode propagation in the waveguide. Since the refractive index in semiconductor material is ~3.5 and ~1.5 in optical fibers, tapered sections are introduced at each end of the waveguide. This makes the mode profile in the SOA compatible with that in optical fibers, thereby reducing the coupling losses to ~2 dB pr. facet [93]. Furthermore, to reduce reflections from the end-facets, anti-reflex (AR) coating and tilted facets are used so that reflections in the range of 10^{-5} are achieved [93].

In the following, the static performance of an SOA realised by Alcatel Alsthom Recherche will be described. The device is a 450 μm long bulk SOA with a width of 0.7 μm, thickness of 0.3 μm and an optical confinement factor (Γ) of 0.45. For a detailed description of the device, the reader is referred to [96]. Fig. 3.2 shows the chip gain as a function of the applied bias current to the SOA. At low bias currents the semiconductor material is not inverted, why loss is experienced. Increasing the bias current increases the inversion and consequently gain is achieved and as seen, a gain of ~30 dB is possible for a bias current of 100 mA. It should be noted that the gain saturates at high bias currents due to an increased ASE. An obtainable on-off ratio of ~50 dB is observed in Fig. 3.2 and although this is for the static case, the fast carrier dynamics inside the semiconductor makes it possible to achieve on-off ratios in this range within ~1 ns [90,91]. Consequently, this type of gate is very attractive for packet-switched applications, where the switching must take place between subsequent packets. The calculations shown in Fig. 3.2, as well as in the rest of this thesis, are carried out using a model that combines the theory for the material gain [97] with equations for propagation of the signal [98] and spontaneous emission [92,99]. A detailed description of the complete model can be found in [92,98,99].

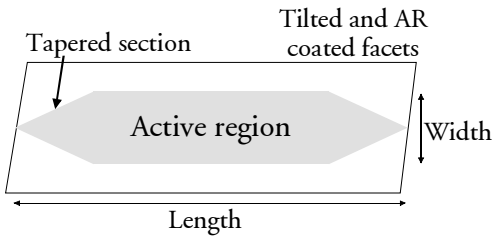

Fig. 3.1: Schematic of an SOA gate in top-view. At each end the facets are AR coated and tilted to minimise reflections, whereas the tapered sections perform spot size conversion to optimise coupling to optical fibers.

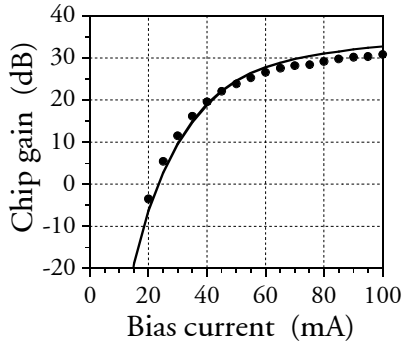

Fig. 3.2: Measured (dots) and calculated (line) unsaturated chip gain as a function of the bias current to a 450 μm long bulk SOA. The signal wavelength is 1544 nm. The measurements are from [92,99].

Besides a high gain, a large optical bandwidth with a flat gain spectrum is also desirable for WDM applications. Fig. 3.3 shows the measured and calculated gain as a function of the wavelength with the bias current as a parameter. Due to the band filling effect [100], the gain peak shifts towards shorter wavelength as the bias current increases. Furthermore, the bandwidth of the material gain increases [97] leading to an increased optical bandwidth. As seen in Fig. 3.3, at 80 mA the 3 dB optical bandwidth is ~50 nm, which covers the EDFA bandwidth of ~30 nm well.

The optical bandwidth is not only dependent on the bias current but also very much on the length of the SOA and Γ. This is illustrated in Fig. 3.4, giving the calculated optical 3 dB bandwidth and chip gain as a function of the SOA length with Γ as a parameter. The applied bias current corresponds to a current density of 30 kA/cm^2, which here will be used as the maximum allowed current density[7]. It is evident from the figure that as the SOA length increases, the optical bandwidth decreases. The reason is that it corresponds to a concatenation of several SOAs with a shorter length. So, just as the bandwidth decreases if several filters are concatenated this is also the case for long SOAs. Furthermore, it can be shown [101] that the optical bandwidth is inversely proportional to the square root of the length times Γ. The decrease in bandwidth as Γ increases is also apparent in the figure.

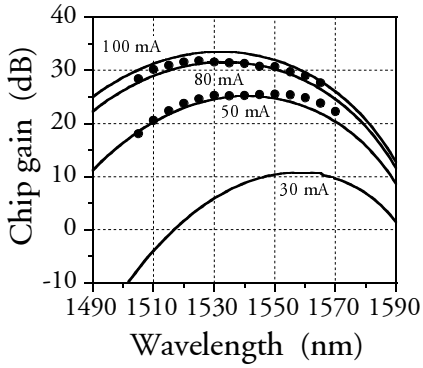

Fig. 3.3: Measured (dots) and calculated (lines) unsaturated chip gain vs. the wavelength. The bias current is a parameter. The measurements are from [92,99] and are for 50 and 80 mA.

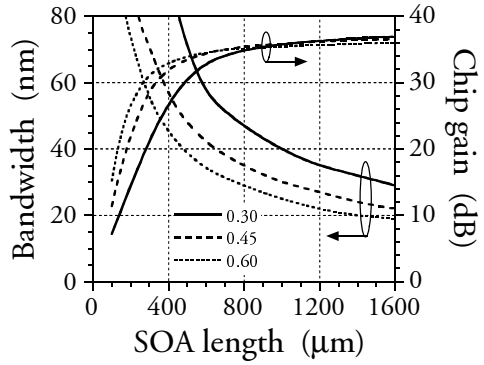

Fig. 3.4: Optical 3 dB bandwidth and chip gain at the gain peak vs. the SOA length. The confinement factor is a parameter and the applied bias current corresponds to 30 kA/cm^2.

This means that in order to have an SOA with a large optical bandwidth, short SOAs with a low Γ are preferable. On the other hand, since the gain is proportional to $\exp(\Gamma g_m L)$ [97], where g_m is the material gain and L is the SOA length, the gain increases as the SOA length or Γ increases. Consequently, there is a clear trade-off between a large optical bandwidth and a high gain. It is noted that for long SOAs,

[7] The current density is defined as the applied bias current divided by the waveguide area (length times width, see Fig. 3.1). 30 kA/cm^2 is used to ensure long term operation.

the gain saturates due to ASE and since the power of the ASE is proportional to Γ, the saturation sets in earlier for a high Γ.

The gain of the SOA is also dependent on the optical input power. This is illustrated in Fig. 3.5, giving the measured and calculated chip gain versus the input power to the 450 μm long SOA. As the input power increases the carrier concentration drops and consequently the gain saturates. Furthermore, as the bias current increases, the gain increases resulting in saturation at lower input powers. The saturation input power, i.e., the power where the gain has dropped 3 dB compared to the unsaturated gain, is a very important parameter for SOAs. The reason is that for input powers higher than the saturation input power, a logical one will experience a lower gain than a zero and since the SOA responds on bit level, this will lead to extinction ratio degradation. Consequently, the saturation input power should be as high as possible. However, this is in contrast to the desire of having a high gain as shown in Fig. 3.5.

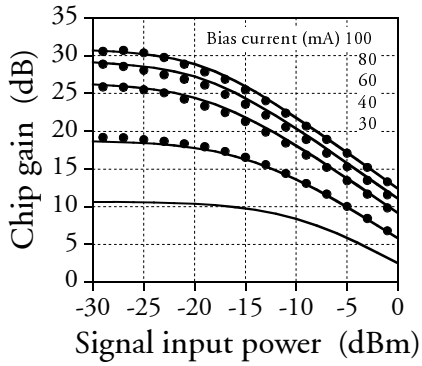

Fig. 3.5: Measured (dots) and calculated (lines) chip gain vs. input power to the 450 μm long SOA with the bias current as a parameter. The measurements are from [101,102].

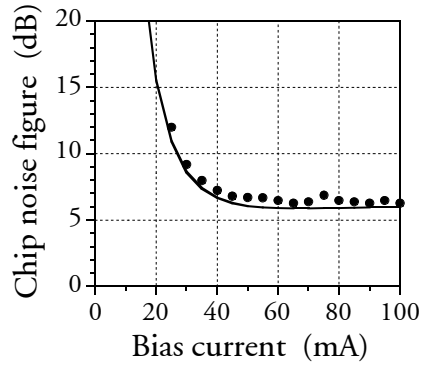

Fig. 3.6: Measured (dots) and calculated (line) chip noise figure at 1544 nm as a function of the bias current to the 450 μm long SOA. The measurements are from [92,99].

There is also a lower limit of acceptable input power, which is given by the noise figure of the SOA. Fig. 3.6 shows the measured and calculated noise figure as a function of the bias current to the 450 μm long SOA. At a low bias current the inversion is low resulting in a high noise figure. Increasing the bias current, however, increases the inversion and therefore the noise figure decreases. Naturally, the noise figure should be as low as possible to minimise degradations of the OSNR.

The lower and upper limit of the input power defines the IPDR[8] for the SOA and should be as high as possible as this figure determines the cascadability of the gates. The cascadability of SOA-based gates is the topic of section 3.2 and 3.3.3.

[8] Defined as the input power range where the power penalty stays below 1 and 2 dB for non pre-amplified and pre-amplified receivers, respectively. Note that the penalty is measured at BER = 10^{-9} throughout this thesis.

Fig. 3.7 shows explicitly the important trends seen in Fig. 3.5 and 3.6, respectively. The noise figure and saturation input power is shown in the left part of Fig. 3.7 as a function of the bias current with Γ as a parameter. Clearly, the noise figure decreases as the bias current increases and slightly higher noise figures are experienced for higher Γ. On the other hand, the saturation input power decreases with increasing current and is lowest for a high Γ since the gain increases (see Fig. 3.4). As a static measure of the IPDR, a figure of merit is defined as the saturation input power divided by the noise figure, and should consequently be as high as possible. This figure of merit is shown in the right part of Fig. 3.7 as a function of the bias current with Γ as a parameter. Here, it can be seen that a low Γ and a low current, i.e., a low gain, is preferable to obtain a large figure of merit. It is noted that the lower limit in bias current is set so that there is still gain in the SOA.

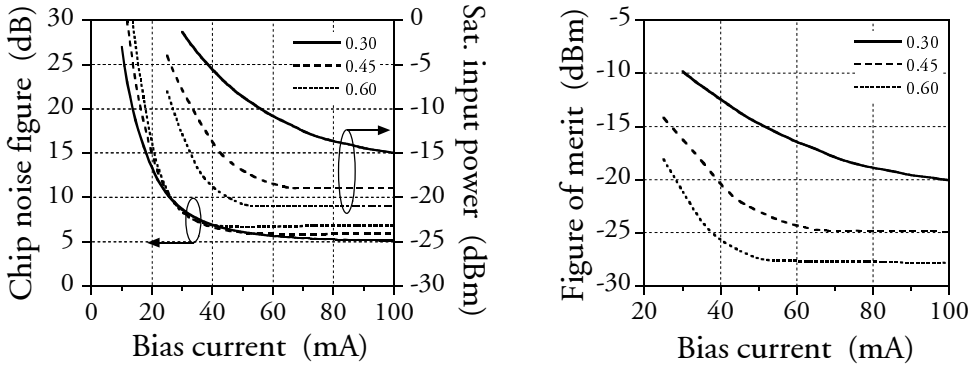

Fig. 3.7: Chip noise figure and saturation input power (left) and figure of merit (right) vs. the bias current to the 450 μm long SOA. The figure of merit is defined as the saturation input power divided by the noise figure. The confinement factor is a parameter and the wavelength is 1550 nm.

The influence of the SOA length on the noise figure and saturation input power at 30 kA/cm^2 can be seen in left part of Fig. 3.8. As illustrated, the noise figure increases with the SOA length or Γ. The reason is that as the length or Γ increases, the gain increases resulting in a high ASE power that saturates the front part of the amplifier. Noting that the noise figure of the entire amplifier is determined mainly by the inversion in the front part of the amplifier, the saturation will lead to a higher noise figure. Furthermore, the saturation input power decreases as the length or Γ increases, which also is due to a higher gain. The resulting figure of merit is given in the right part of Fig. 3.8 and here it clearly can be seen that short SOAs with a low Γ are preferable to obtain a high figure of merit.

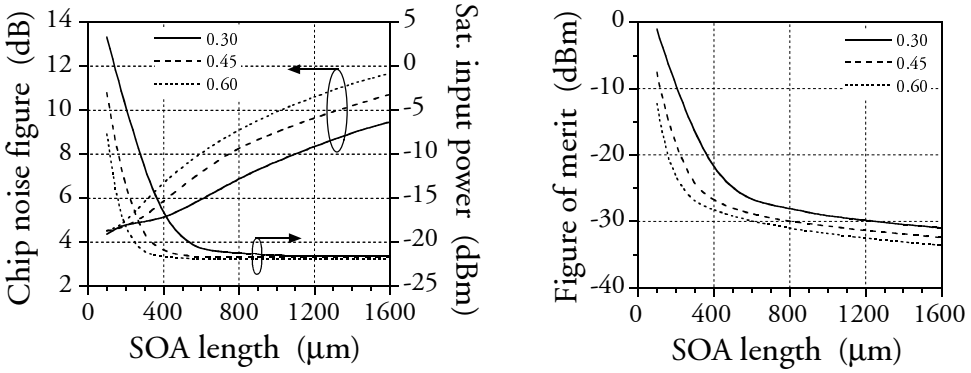

Fig. 3.8: Chip noise figure and saturation input power (left) and figure of merit (right) at the gain peak vs. the SOA length. The confinement factor is a parameter and the applied bias current corresponds to a current density of 30 kA/cm^2.

3.1.2 Dynamic performance of conventional SOAs

Based on static characteristics, guidelines on how to increase the IPDR of SOAs were established in the previous section. Here, the influence of the bit rate will be described. Fig. 3.9 shows the extinction ratio as a function of the input power to a 400 (left) and 800 μm (right) long SOA with the bit rate as a parameter. The input signal is an NRZ PRBS signal with an extinction ratio of 13 dB. The extinction ratio as predicted by the static case, i.e., the static gain characteristics, is for comparison also included in the figures.

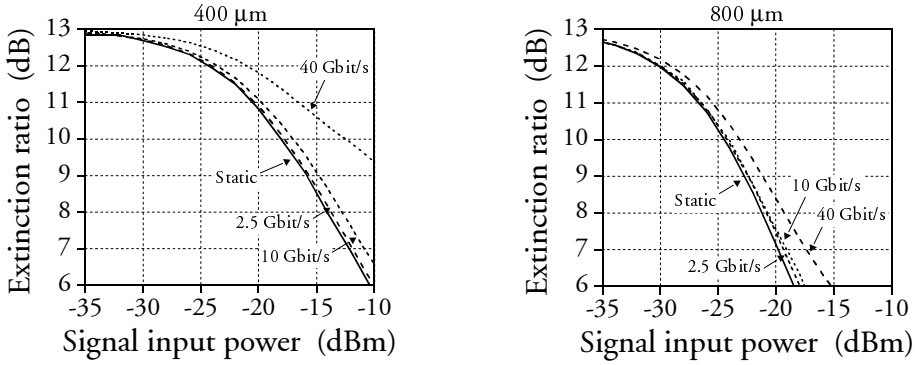

Fig. 3.9: Extinction ratio vs. input power to a 400 (left) and 800 μm long SOA (right) with the bit rate as a parameter. The confinement factor is 0.45, while the bias current is 42 and 82 mA (15 kA/cm^2), respectively. The input signal is an NRZ signal with an extinction ratio of 13 dB and the wavelength is at the gain peak.

As illustrated, the extinction ratio decreases as the input power to the SOAs increases, which is caused by the gain saturation effect described in the previous section. Furthermore, since the saturation input power is lower for the 800 μm long SOA (due to a gain of ~30 dB compared to ~25.5 dB for the short SOA) degradations appear at lower input powers. It can also be noticed that as the bit rate increases, the

extinction ratio increases, which is due to the fact that the bit period gets comparable to the response time or carrier lifetime of the SOA. This is identical to EDFAs operated in the Gbit/s range, where the ms response of the EDFAs does not cause extinction ratio degradations at high input powers. For the 800 μm long SOA, however, the improvement is smaller compared to the 400 μm long SOA. This is because the carrier lifetime decreases as the length of the SOA increases, thereby enabling the device to respond to a higher bit rate. This will be covered in more detail in chapter 4.

3.2 Cascadability of SOA gates for single channel operation

Here, a detailed theoretical investigation of the cascadability of SOAs at 10 Gbit/s will be presented. As illustrated in Fig. 3.2, controlling the bias current to the SOA changes the gain. This be exploited for two different switching schemes. The first scheme considered here is for compensation of losses in switch blocks, where by applying the correct current to the amplifier in the on-state, the total losses can be compensated for. This is attractive for realisation of large switch fabrics, where other switch technologies can result in large losses as described in the beginning of this chapter. The second scheme is for power equalisation, where the bias current in the on-state is changed in accordance with the optical input power so that a constant average output power is achieved. This will be a required functionality in optical networks, where signals entering a network node can have different power levels due to transmission over different paths as described in chapter 2. Furthermore, it also has the very attractive feature that fast equalisation is possible with SOAs, which is desirable for optical packet switching.

These two schemes will be investigated in detail in the following and the presented results are partly based on [p36]. All calculations in this section are carried out for a 10 Gbit/s NRZ PRBS signal with an extinction ratio of 13 dB. In addition, the wavelength of the signal is at the gain peak of the SOA considered, which for all cases has a confinement factor of 0.45. In order to focus on the performance of the SOA alone, no transmission effects are taken into account in the calculations concerning the cascadability of the SOAs. ASE accumulation from cascading SOAs, on the other hand, is taken into account, where an optical bandpass filter with a bandwidth of 1 nm centred around the signal wavelength is used after each SOA. In the detection process, low-pass filtering of the signal with a 4^{th} order electrical Bessel filter is performed. The filter has a 3 dB bandwidth of 7 GHz, corresponding to 70% of the bit rate, i.e., the optimal bandwidth for NRZ signals.

3.2.1 SOAs as loss compensators in switch blocks

In this case the SOA is biased to give a desired gain and the performance of a single 200 μm long SOA is illustrated in Fig. 3.10. The left part of Fig. 3.10 shows the

extinction ratio and OSNR of the output signal from the SOA as a function of the input power, while the right part shows the resulting penalty. The SOA is biased to give an unsaturated gain of 5, 10 and 20 dB, respectively.

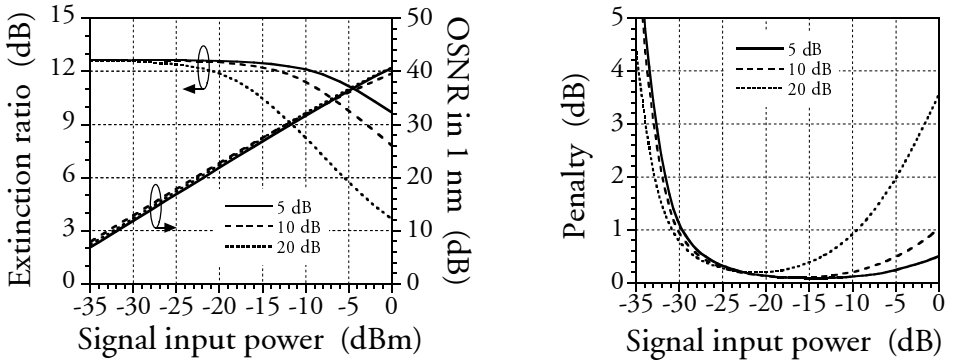

Fig. 3.10: Extinction ratio and OSNR (left) and penalty (right) vs. input power to a 200 μm long SOA at 10 Gbit/s. The SOA is biased to give an unsaturated gain of 5, 10 and 20 dB, respectively.

As seen, the extinction ratio is high at low input powers but since the OSNR is low a penalty is experienced. At high input powers the OSNR is high but the extinction ratio has dropped due to gain saturation also resulting in a penalty. It can be noted that for the case of 5 dB gain the penalty is highest at low input powers. The reason is that for a 5 dB gain the bias current is lower compared to 10 or 20 dB gain. This gives a higher noise figure as shown in Fig. 3.6 and the left part of 3.7, which in turn results in a lower OSNR (see left part of Fig. 3.10). On the other hand, the penalty is lowest for high input powers since low bias currents result in higher saturation input power as illustrated in Fig. 3.5 and the left part of 3.7, thereby resulting in less extinction ratio degradation (see left part of Fig. 3.10).

These characteristics naturally have a severe impact on the cascadability of the SOA. This is illustrated in Fig. 3.11, showing the number of SOAs that can be cascaded at 1 dB penalty as a function of the input power to each SOA. At low input powers, ASE accumulation limits the cascadability, while increasing the input power increases the OSNR and consequently the cascadability. At high input powers, however, extinction ratio degradation becomes a limiting factor also decreasing the cascadability. This effect is more severe for a high gain since the saturation input power decreases as the gain increases. Therefore, superior performance is achieved in the case of an amplifier gain of 5 dB, where a maximum of 19 SOAs can be cascaded compared to a maximum of only 5 SOAs for 20 dB gain. This clearly shows a trade-off between the cascadability, which is an important issue for large-scale networks, and the desired gain of the gate. It should be pointed out that the input powers that result in the highest cascadability correspond in each case to input powers giving minimum penalty after one SOA, as evident by comparing the right part of Fig. 3.10 and 3.11.

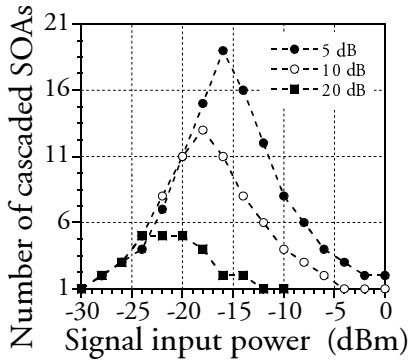

Fig. 3.11: Number of cascaded SOAs (@ 1 dB penalty) at 10 Gbit/s vs. the input power to a 200 μm long SOA. The SOA is biased to give an unsaturated gain of 5, 10 and 20 dB, respectively.

The cascadability is also illustrated in Fig. 3.12, showing the maximum number of SOAs that can be cascaded at 1 dB penalty as a function of the SOA length. As seen, an improvement is achieved by using short SOAs since they have lower noise figures and higher saturation input powers compared to long SOAs even for equal gain conditions. Therefore, a guideline in construction of optical switches, using SOA-gates for loss compensation, is as follows: The losses should be minimised by proper switch design so that the lowest possible gain is required. Then, the shortest possible SOAs should be used in order to obtain a high cascadability, which also has the benefit of increasing the optical bandwidth (see Fig. 3.4).

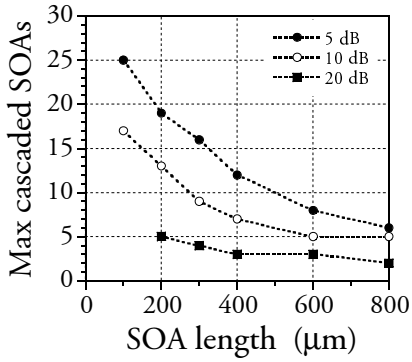

Fig. 3.12: Maximum number of cascaded SOAs (@ 1 dB penalty) at 10 Gbit/s as a function of the SOA length. An input power to each SOA that results in the highest cascadability is used in each case. The SOAs are biased to give an unsaturated gain of 5, 10 and 20 dB, respectively.

Finally, it should be stressed that these calculations were performed for SOAs with a confinement factor of 0.45. Reducing the confinement factor would improve the overall cascadability performance as indicated in the right part of Fig. 3.7 and 3.8. As an example it can be mentioned that the maximum cascadability of a 100 μm long SOA with a confinement factor of 0.3 is 37 compared to 25 in Fig. 3.12.

3.2.2 SOAs as power equalisers

In contrast to the previous section, where the SOA was operated with a constant bias current, the SOA is in this case biased to give a desired output power, why the bias current must be adjusted when the input power changes. In the case of an average output power of -5 dBm, Fig. 3.13.a illustrates the needed bias current as a function of the input power for different SOA lengths. Please note that a gain of less than 5 dB has not been accepted in the calculations, e.g., for an output power of -5 dBm, the input power is not above -10 dBm. This has been required so that transparency effects in the SOA are avoided. Additionally, there is also a lower limit on the input power. This is because as the input power decreases a higher gain is required to obtain a constant output power. However, at some point this requirement cannot be fulfilled since the amplifier gain saturates and as seen in Fig. 3.13.a, this restriction is more severe for short SOAs due to a lower maximum gain compared to long SOAs. Fig. 3.13.b shows the number of SOAs, biased to give an output power of -5 dBm, that can be cascaded at 1 dB penalty as a function of the input power to each SOA. Also in this case, short SOAs have the best performance. It should be pointed out, though, that because short SOAs have a lower gain compared to long SOAs, they are less tolerant to input power variations as seen in Fig. 3.13.b.

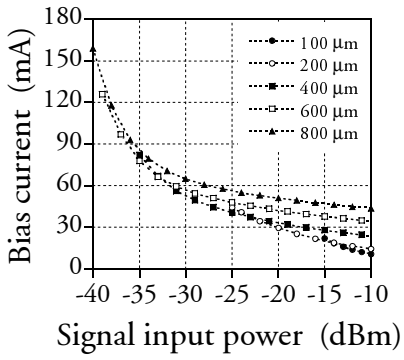

Fig. 3.13.a: Needed bias current to achieve a constant output power of -5 dBm at 10 Gbit/s vs. input power. The SOA length is a parameter.

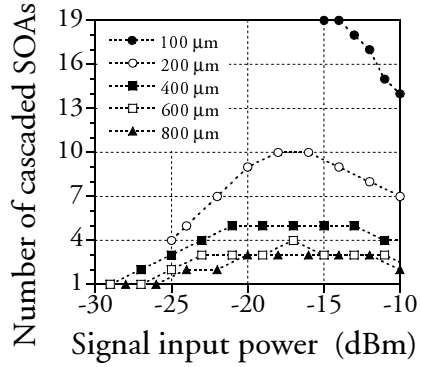

Fig. 3.13.b: Number of cascaded SOAs (@ 1 dB penalty) vs. input power at 10 Gbit/s for different SOA lengths. The SOAs are biased to give an output power of -5 dBm.

The desired level of output power also has an impact on the performance. This is illustrated in Fig. 3.14.a, showing the penalty and extinction ratio versus the input power to a 200 µm long SOA with the output power as a parameter. As seen, there is a penalty at low input powers, which is due to a low OSNR (seen for output powers of -10 and -5 dBm). At high input powers there is a penalty due to extinction ratio degradation (seen for output powers of -5 and 0 dBm), which is more severe for a high output power since a higher gain is necessary. It can also be noticed that for an output power of -10 and -5 dBm, equal penalty is experienced at low input powers, which will result in similar cascadability performance. At high input powers,

however, the lower extinction ratio degradation for an output power of -10 dBm will result in an increased cascadability. This is verified in Fig. 3.14.b, showing the number of gates that can be cascaded at 1 dB penalty versus the input power to the 200 μm long SOA with the output power as a parameter. As illustrated, a maximum of 15 SOAs can be cascaded for a desired output power of -10 dBm, whereas this number has decreased to 10 and 6 SOAs for an output power of -5 and 0 dBm, respectively. Therefore, a trade-off also exists in the case of SOA-based gates used for power equalisation, where superior cascadability is achieved when a low output power is required. It should be noted, however, that decreasing the output power below -10 dBm, will at some point result in a degradation of the cascadability performance due to ASE accumulation.

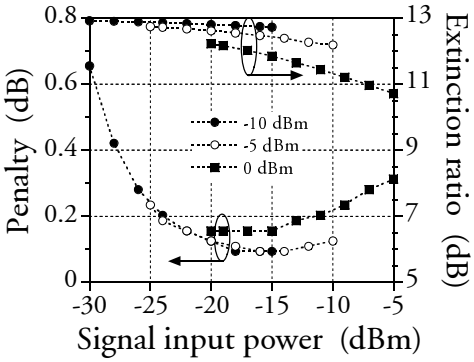

Fig. 3.14.a: Penalty and extinction ratio vs. input power at 10 Gbit/s to a 200 μm long SOA. The average output power is a parameter.

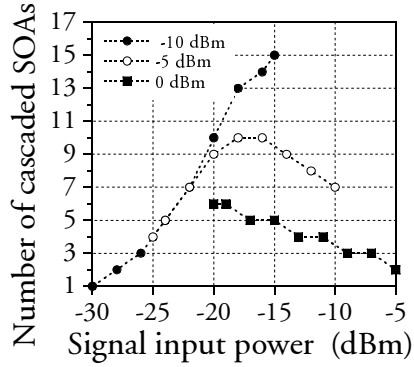

Fig. 3.14.b: Number cascaded SOAs (@ 1 dB penalty) vs. the input power at 10 Gbit/s for different output powers. SOA length: 200 μm.

Fig. 3.15, that gives the maximum number of SOAs that can be cascaded at 1 dB penalty as a function of the SOA length, clearly shows that short SOAs with low output powers are preferable.

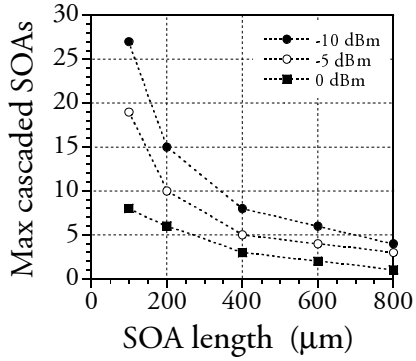

Fig. 3.15: Maximum number of cascaded SOAs (@ 1 dB penalty) vs. SOA length at 10 Gbit/s. In each case an input power that results in the highest cascadability is used. The SOAs are biased to give an average output power of -10, -5 and 0 dBm, respectively.

3.3 Gain-clamped SOAs

As described and illustrated in the previous sections, gain saturation in conventional SOAs leads to extinction ratio degradation and thereby a substantial limitation in the cascadability. Furthermore, since the gain is much dependent on the input power, this effect will be even more pronounced for WDM operation due to a higher total input power and cross-gain modulation between the different wavelength channels. So in order to minimise this, gain-clamped SOAs (GC-SOAs) have been proposed [94,95]. Here, an internal laser clamps the carrier concentration, and consequently the gain, allowing for higher input powers before saturation. Furthermore, since the carrier concentration is clamped, the gain will be constant until the laser is forced below threshold by the amplified input signal making WDM operation more feasible. The objective of the present section is to give a description of the static and dynamic behaviour of GC-SOAs as well as an investigation of the cascadability performance in a WDM system.

3.3.1 Static characteristics of GC-SOAs

The GC-SOA is basically a distributed Bragg reflector (DBR) laser incorporating passive Bragg regions at each end facet to facilitate lasing. A schematic of the device, used for the experiments and modelling results presented in this section, is shown in Fig. 3.16. The bulk-based GC-SOA, which is fabricated by Alcatel Alsthom Recherche, has an active region length of 600 μm, while each Bragg region is 200 μm long. In order for the laser light not to have an influence on the EDFA gain spectrum, the passive Bragg regions are designed to achieve a lasing wavelength well outside the EDFA window. This is illustrated in Fig. 3.17, giving the measured laser output power at 200 mA as a function of the wavelength, where it can be seen that the lasing wavelength is at ~1508 nm. If the lasing light is unwanted after the GC-SOA, filtering has to be applied.

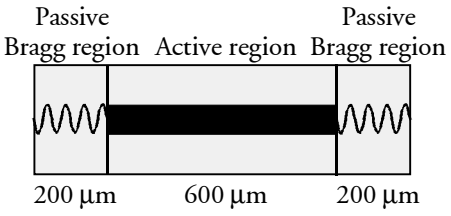

Fig. 3.16: Schematic of an 1000 μm long GC-SOA incorporating 200 μm long passive Bragg regions at the facets.

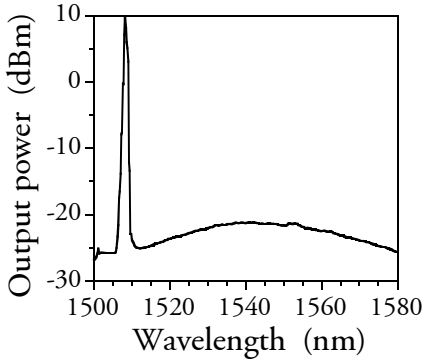

Fig. 3.17: Measured optical spectrum at the output of the 1000 μm long GC-SOA biased at 200 mA.

Since the GC-SOA basically is a laser, the carrier concentration, and consequently the gain of an optical input signal, will be clamped for bias currents above the lasing threshold. This is verified in Fig. 3.18, showing the measured and calculated chip gain for an input signal at 1550 nm and lasing output power versus the bias current. The model for the GC-SOA is based on the SOA model but also includes theory for wave propagation in Bragg gratings [97]. The parameters used for the calculations can be found in [101]. As observed in Fig. 3.18, lasing starts for a bias current above 60 mA after which the gain of the input signal is effectively clamped at ~21 dB. Therefore, a further increase in the bias current only serves to increase the lasing output power.

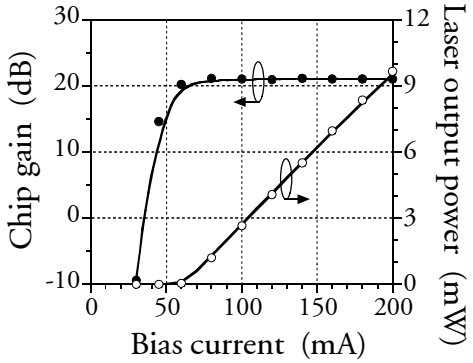

Fig. 3.18: Measured (dots) and calculated (lines) chip gain at 1550 nm and laser output power vs. the bias current to the 1000 μm long GC-SOA.

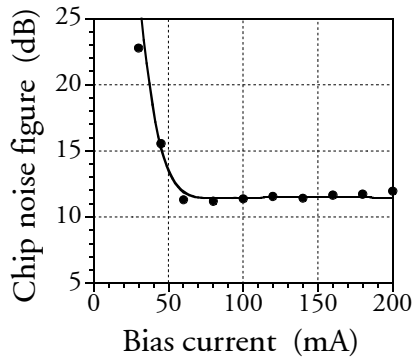

Fig. 3.19: Measured (dots) and calculated (line) chip noise figure at 1550 nm vs. the bias current to the 1000 μm long GC-SOA.

It should be pointed out that GC-SOAs inherently have higher noise figures than conventional SOAs with similar physical dimensions in the active region. The reason is that the lasing light saturates the input part of the amplifier leading to a low inversion and thus a high noise figure. In addition to this, the passive Bragg section at the input represents a loss that adds directly to the noise figure. Fig. 3.19 illustrates the measured and calculated chip noise figure as a function of the bias current for an input signal at 1550 nm and as demonstrated, a minimum noise figure of ~11.5 dB is experienced.

The advantage of the carrier clamping is illustrated in Fig. 3.20, showing the measured and calculated chip gain at 150 and 200 mA as a function of the input power at 1550 nm. Clearly, the gain of the GC-SOA is clamped, independent of the bias current and input power, until saturation sets in, which occurs when the amplified signal power is comparable with the power of the lasing light. Therefore, it can also be observed that increasing the bias current increases the saturation input power. This is in contrast to conventional SOAs, where the unsaturated gain is dependent on the bias current as depicted in Fig. 3.2 and an increase in current results in a decrease in the saturation input power (see left part of Fig. 3.7).

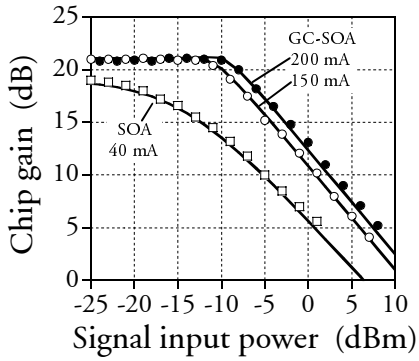

Fig. 3.20: Measured (symbols) and calculated (lines) chip gain vs. the input power to the 1000 μm long GC-SOA and 450 μm long conventional SOA. The signal wavelength is 1550 nm and the bias current is a parameter.

For comparison, the gain curve of the 450 μm long conventional SOA operated at 40 mA is also given in Fig. 3.20. It can clearly be seen that the linear behaviour of the GC-SOA results in a much higher saturation input power. This indicates that the extinction ratio degradation due to gain saturation will be reduced compared to conventional SOAs and thereby result in superior cascadability performance. Especially in the case of WDM operation, the linear behaviour of the GC-SOA will have a significant influence on the performance as will be discussed in section 3.3.3.

3.3.2 Dynamic performance of GC-SOAs

Although the static characteristics of the GC-SOA show far superior performance at high input powers compared to the conventional SOA, the performance is strongly dependent on the bit rate [p2,p10]. This dependency is caused by the relaxation oscillations, which are inherent in laser-based devices. The impact becomes significant for input powers near the saturation input power, i.e., where the laser is forced below threshold, and are more severe for bit rates approaching or exceeding the relaxation frequency. This is demonstrated in Fig. 3.21 that gives the calculated extinction ratio at the output of the GC-SOA as a function of the signal input power for an input extinction ratio of 13 dB. The results are for the static case, 2.5, 10 and 20 Gbit/s, where the extinction ratio has been found for the electrically low pass filtered signals (4^{th} order Bessel filter with a 3 dB bandwidth equal to 70 % of the bit rate). As illustrated, there is not much difference in the extinction ratio in the case of 2.5 Gbit/s and the static case. However, going to 10 or even 20 Gbit/s results in a large degradation at high input powers, which is in contrast to conventional SOAs, where a small improvement can be experienced (see Fig. 3.9). The reason for this is that the input signal induces an amplitude modulation of the lasing light with transient times given by the relaxation frequency, which for the 1000 μm long GC-SOA has been measured to ~14 GHz [103]. Increasing the bit rate decreases the bit period compared to the relaxation time, why a more significant impact is observed.

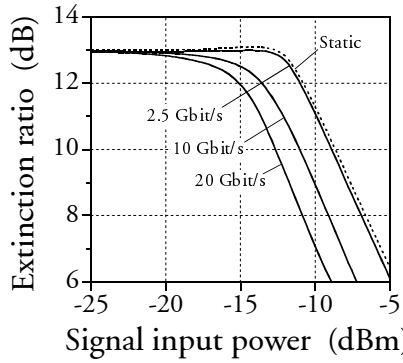

Fig. 3.21: Extinction ratio at 2.5, 10 and 20 Gbit/s vs. input power to the 1000 μm long GC-SOA biased at 200 mA. The extinction ratio as predicted by the static gain curve is also included in the figure. The signal wavelength is 1550 nm.

The effect of increasing the bit rate on the pulse deterioration is also very clearly illustrated in Fig. 3.22, showing the calculated unfiltered pulse traces after the GC-SOA at 2.5, 10 and 20 Gbit/s for an input power of -10 dBm. Here, the impact from the relaxation oscillations is quite evident, when going from 2.5 to 20 Gbit/s.

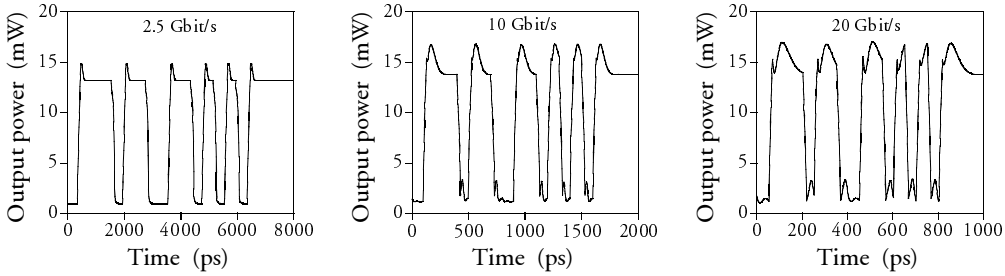

Fig. 3.22: Unfiltered pulse traces after the 1000 μm long GC-SOA at 2.5 (left), 10 (middle) and 20 Gbit/s (right). The input power to the GC-SOA is -10 dBm in each case, the bias current is 200 mA and the signal wavelength is 1550 nm.

3.3.3 Cascadability of SOAs and GC-SOAs in a multi-wavelength system

The linear behaviour of GC-SOAs makes them very attractive for WDM applications [104,105] since cross-gain modulation between different channels due to gain saturation will be minimised compared to the case when using conventional SOAs. However, as illustrated in the previous section, a problem with GC-SOAs is that the relaxation frequency causes pulse pattern effects that deteriorates the signal if the bit rate is close to the relaxation frequency. Moreover, the noise figure of GC-SOAs is inherently larger than for comparable SOAs. Both will have an influence on the cascadability and a comparison with conventional SOAs is therefore of interest.

Consequently, the objective of this section is to carry out a detailed theoretical comparison of the cascadability of conventional SOAs and GC-SOAs in a multi-wavelength system. The presented results are based on [p15,p22] and all calculations

in this section are carried out for 2.5 or 10 Gbit/s NRZ PRBS signals (up to 16 channels) that are synchronised but modulated independently of each other. The signals have an extinction ratio of 13 dB and are equally spaced around a central wavelength of 1550 nm with a channel spacing of 2 nm. It is noted that the bandwidth allocated by the channels is smaller than the optical bandwidth of the SOA and GC-SOA, being 69 and 55 nm, respectively. In the detection process, low-pass filtering of the signals with a 4^{th} order electrical Bessel filter is performed (3 dB electrical bandwidth equal to 70% of the bit rate).

In order to make a fair comparison between the GC-SOA and the conventional SOA, equal unsaturated gains of 21 dB are used. This is accomplished by shortening the device length of the SOA from 450 μm to 250 μm and using the appropriate bias current. It is emphasised that this is in favour of the SOA as shown in section 3.2. The resulting gain characteristic for the two amplifiers, in the case of a single channel, is shown in Fig. 3.23. As seen the GC-SOA has a much higher saturation input power compared to the SOA. Therefore, a better dynamic performance of the GC-SOA in a multi-wavelength system can be expected at high input powers.

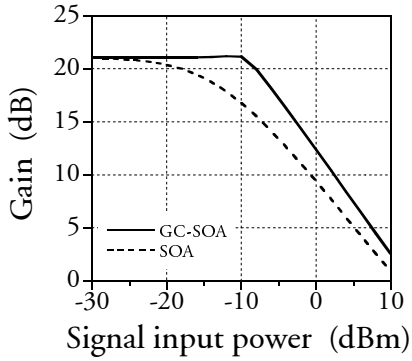

Fig. 3.23: Calculated gain vs. input power to the 1000 μm long GC-SOA biased at 200 mA and a 250 μm long conventional SOA biased at 43 mA. The unsaturated gain of both amplifiers is 21 dB and the signal wavelength is 1550 nm. These amplifiers are the basis of the comparison in this section.

This is verified in Fig. 3.24, showing the extinction ratio of the channel at 1550 nm at the output of the amplifiers as a function of the signal input power per channel to the conventional SOA (left) and the GC-SOA (right). The calculations are performed with 4 and 8 channels and at a channel bit rate of 2.5 and 10 Gbit/s, respectively. A fundamental difference between the SOA and the GC-SOA can be seen. For the SOA, the extinction ratio decreases as the input power or the number of channels increase. However, increasing the channel bit rate to 10 Gbit/s improves the extinction ratio considerably since the influence of gain modulation from other channels becomes less pronounced. This is illustrated in Fig. 3.25, giving calculated pulse traces at the output of the SOA at a channel bit rate of 2.5 and 10 Gbit/s in the case of 4 input channels.

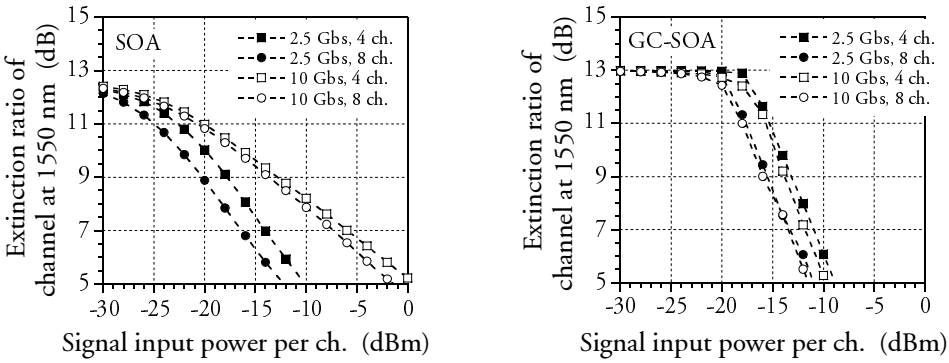

Fig. 3.24: Calculated extinction ratio of the channel at 1550 nm at the output of the SOA (left) and the GC-SOA (right) vs. the signal input power per channel. The number of channels and the channel bit rate is a parameter and the input extinction ratio for all channels is 13 dB.

For the GC-SOA, there is no degradation of the extinction ratio before the amplifier starts to saturate but in contrast to the conventional SOA, there is no improvement by increasing the channel bit rate. This is due to the limited (~14 GHz) relaxation frequency of the GC-SOA, which causes pulse pattern effects that limits the performance (see Fig. 3.22). So the improvement due to a lower gain modulation between the different channels is cancelled by the degradations due to the relaxation oscillations. Once saturation sets in, another effect of these oscillations is a much more rapid decrease in the extinction ratio compared to the conventional SOA as observed in Fig. 3.24. Nevertheless, for input powers below the saturation point of the GC-SOA, clearly the performance of the SOA is the worst.

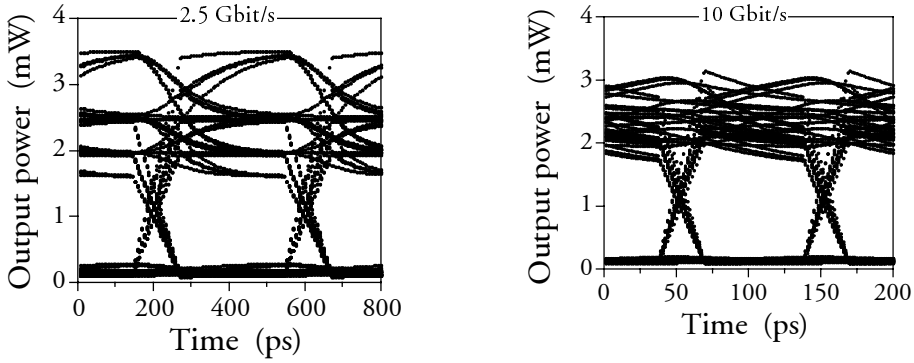

Fig. 3.25: Calculated pulse traces at 1550 nm at the output of the conventional SOA in the case of 4 input channels at a channel bit rate of 2.5 Gbit/s (left) and 10 Gbit/s (right). The input power per channel is -15 dBm.

The superior dynamic characteristics of the GC-SOAs in a multi-wavelength system, as seen in Fig. 3.24, can be used to substantially increase the cascadability of optical gates. This is illustrated in Fig. 3.26, showing the number of GC-SOAs and SOAs that can be concatenated at 1 dB penalty versus the signal input power per channel. The calculations are performed with 4 channels at a channel bit rate of 2.5 Gbit/s. As

seen in Fig. 3.26, a higher number of SOAs can be concatenated at low input powers. This is because the SOA has a noise figure of only ~5 dB, while the GC-SOA has a noise figure of ~10.5 dB. Since ASE accumulation rather than extinction ratio degradation limits the cascadability at low input powers, the lower noise figure for the SOA results in better performance. Increasing the input power increases the OSNR and consequently the cascadability of both types of gates. At high input powers, however, the extinction ratio degradation becomes a limiting factor as shown in Fig. 3.24 and is much more severe in SOAs compared to GC-SOAs. Therefore, better performance is achieved for the GC-SOA as shown in Fig. 3.26 even when compared to a short cavity SOA gate. As seen, a maximum of 15 GC-SOAs can be cascaded, compared to a maximum of only 5 SOAs.

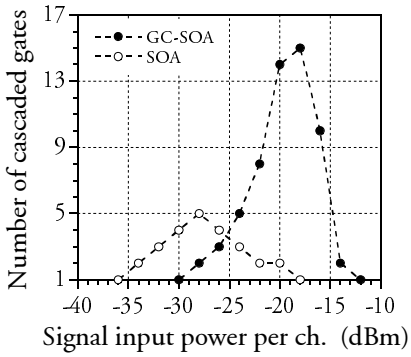

Fig. 3.26: Number of cascaded GC-SOAs and SOAs (@ 1 dB penalty) vs. the input power per channel. There are 4 channels at a channel bit rate of 2.5 Gbit/s.

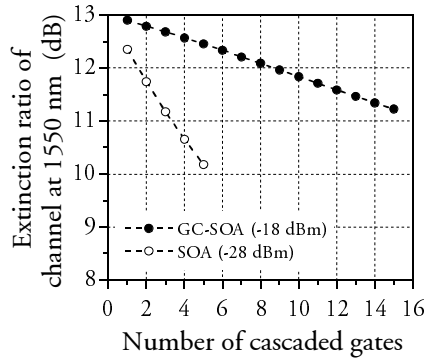

Fig. 3.27: Extinction ratio of the channel at 1550 nm vs. the number of cascaded gates at the optimum input powers. There are 4 channels at a channel bit rate of 2.5 Gbit/s.

In order to highlight what limits the cascadability for the two kind of gates, Fig. 3.27 shows the extinction ratio of the channel at 1550 nm as a function of the number of gates that are cascaded for the optimum input powers to the gates. As seen the extinction ratio is ~10.2 after 5 SOAs, whereas, it is ~11.2 dB after 15 GC-SOAs. This means that for the SOAs it is a combination of extinction ratio degradation and OSNR degradation that limits the cascadability. For the GC-SOA, on the other hand, it is OSNR degradation rather than extinction ratio degradation that limits the cascadability, which is due to the linear behaviour of the GC-SOA before saturation sets in. Therefore, fabrication of GC-SOAs with low noise figures is essential to fully exploit the benefits from the higher saturation input power.

Even at a channel bit rate of 10 Gbit/s, the GC-SOA performs best as illustrated in Fig. 3.28, giving the number of GC-SOAs and SOAs that can be cascaded at 1 dB penalty as a function of the input power per channel in a 4 channel system. However, the improvement in cascadability has decreased considerably compared to a channel bit rate of 2.5 Gbit/s, which is due to the influence from the relaxation oscillations in the GC-SOA. Therefore, an equally important challenge is to fabricate

GC-SOAs with a high relaxation frequency. Devices with a low threshold current can accomplish that [97] and therefore, multi-quantum well (MQW) devices can be of interest to achieve this [106]. The use of MQW devices for GC-SOAs has, however, not been investigated yet.

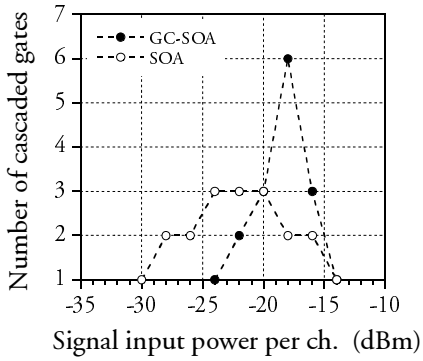

Fig. 3.28: Number of cascaded GC-SOAs and SOAs (@ 1 dB penalty) vs. the input power per channel. There are 4 channels at a channel bit rate of 10 Gbit/s.

It should be noted that the overall decrease in cascadability of the two gates at 10 Gbit/s compared to 2.5 Gbit/s is because ASE accumulation becomes a limiting factor. This is also the reason for the decreased performance of the SOA compared to 2.5 Gbit/s, even though the extinction ratio is higher at 10 Gbit/s (see Fig. 3.24).

In order to illustrate the cascadability of the two gates for a different number of wavelength channels, Fig. 3.29 shows the maximum number of GC-SOAs and SOAs that can be cascaded at 2.5 and 10 Gbit/s as a function of the number of channels.

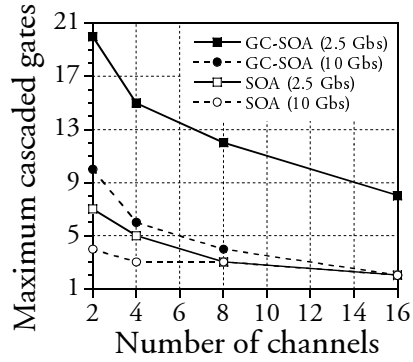

Fig. 3.29: Maximum number of cascaded GC-SOAs and SOAs (@ 1 dB penalty) vs. the number of wavelength channels. The channel bit rate is a parameter.

As seen, the use of GC-SOAs at a channel bit rate of 2.5 Gbit/s allows a much higher number of gates to be cascaded up to at least 16 channels. Even at 10 Gbit/s, where relaxation oscillations limit the performance, the GC-SOA performs equal or even better than a short cavity SOA at 2.5 Gbit/s.

3.3.4 Influence of NRZ and RZ operation in GC-SOAs

Here, a comparison of the influence between NZR and RZ operation in GC-SOAs will be given. This is of interest since it can be expected that the RZ signal format will perform better than NRZ. An explanation of this is given in Fig. 3.30, showing input pulses with different pulse widths coupled into a GC-SOA. The corresponding output pulses are also given in the figure. As illustrated, the influence from the relaxation oscillations on the logical one diminishes as the pulse duration gets below the characteristic relaxation time of the device, which is because the device is not fast enough to respond to the short pulse. The influence on the logical zeros will of course be the same in all cases but since the logical ones are less influenced, this indicates that RZ operation will be beneficial.

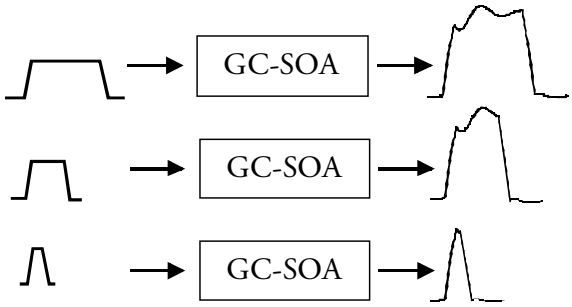

Fig. 3.30: Schematic of the influence from relaxation oscillations on pulses with different pulse widths. (top) Pulse duration higher than the relaxation time. (middle) Pulse duration close to the relaxation time. (bottom) Pulse duration much lower than the relaxation time.

In order to verify this, measurements at 20 Gbit/s with RZ signals have been conducted [p25] and compared to 15 Gbit/s operation with NRZ signals. Fig. 3.31 shows the experimental set-up used for the 20 Gbit/s RZ measurements. In the transmitter a gain-switched laser at 1550 nm produces a 10 GHz pulse train, which is modulated at 10 Gbit/s and then passively multiplexed to a 20 Gbit/s signal with a pulse width of ~25 ps. The signal is then coupled into the 1000 μm long GC-SOA and at the output a filter is used to reject the lasing light. In the receiver an EA modulator is used to demultiplex the signal back to 10 Gbit/s before detection.

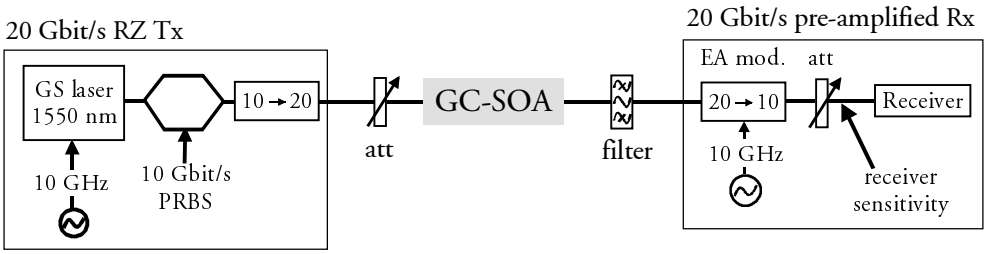

Fig. 3.31: Experimental set-up used for 20 Gbit/s RZ measurements on the 1000 μm long GC-SOA biased at 200 mA.

The set-up for 15 Gbit/s NRZ operation is similar to that shown in Fig. 3.31 except that the CW light is directly modulated at 15 Gbit/s in the modulator and that demultiplexing is done electrically.

The left part of Fig. 3.32 shows the measured penalty versus signal input power to the GC-SOA for both the 20 Gbit/s RZ signal and the 15 Gbit/s NRZ signal. Pulse traces after the GC-SOA are included for the two cases in the middle and right part of the figure. The better performance at low input powers for the NRZ signal is mainly due to a lower electrical bandwidth of the receiver when using the 15 Gbit/s NRZ signal compared to the 20 Gbit/s RZ signal. At high input powers there is a penalty due to extinction ratio degradation and pulse distortion. Nevertheless, it is seen that the performance is best when using the RZ signal, i.e., a 4 dB higher input power can be tolerated at a penalty of 2 dB. This is because the relaxation oscillations have less influence on the logical ones as confirmed by the pulse traces. As seen, the NRZ signal has experienced pattern effects on both logical ones and zeros, whereas the RZ signal only has distortions on the logical zeros even though the input power is ~6 dB higher and the bit rate is 5 Gbit/s higher. It should be noted that gain saturation and not relaxation oscillations cause the difference in pulse amplitude for the RZ signal.

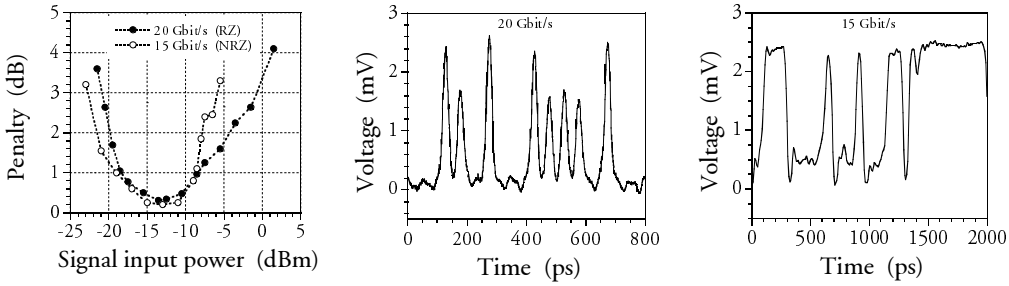

Fig. 3.32: (left) Penalty vs. the input power to the GC-SOA in the case of a 20 Gbit/s RZ signal and 15 Gbit/s NRZ signal. (middle) Pulse trace after the GC-SOA for a 20 Gbit/s RZ signal (signal input power = -1dBm) and (right) 15 Gbit/s NRZ signal (signal input power = -7 dBm). The measurements for the NRZ signal are from [101,102].

In terms of cascadability, the RZ signal format is therefore preferable to NRZ. This is also demonstrated in Fig. 3.33, showing the unfiltered extinction ratio as a function of the number of GC-SOAs that are cascaded. The calculations are performed for NRZ and RZ signals at 20 Gbit/s with an input extinction ratio of 13 dB. Clearly, the RZ signal format performs better and for an extinction ratio of 6 dB, only ~5 GC-SOAs can be cascaded when using NRZ, whereas, this number increases to ~14 for the RZ format.

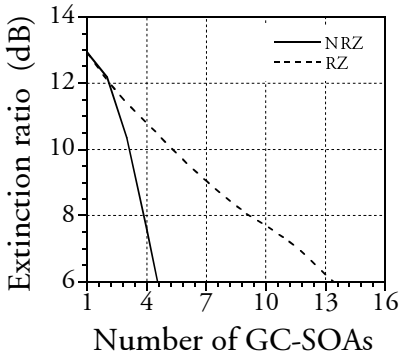

Fig. 3.33: Unfiltered extinction ratio vs. number of traversed GC-SOAs at 20 Gbit/s for NRZ and RZ (FWHM = 20 ps) signal formats. The input extinction ratio is 13 dB and the input power in a logical one and zero is -11 and -24 dBm, respectively. The signal wavelength is 1550 nm.

3.4 Summary

The use of SOA-based devices for all-optical space switching has been investigated and the performance has been analysed both experimentally and theoretically. For the conventional SOA, the influence of the applied bias current, the confinement factor and device length on the gain, optical bandwidth and noise figure has been described. In general, a high bias current together with a high confinement factor and a long device results in a large gain, whereas a high optical bandwidth and low noise figure requires a low confinement factor and a short SOA.

The main drawback of SOA-based space switches, however, is that the IPDR is limited due to ASE at low input powers and gain saturation at high input powers. As a consequence of the limited IPDR, the cascadability will also be limited. Therefore guidelines on how to optimise the IPDR have been established, i.e., low noise figure and large saturation input power. It has been demonstrated theoretically that the largest IPDR is obtained using short SOAs with low confinement factors and a low gain, i.e., low bias current. In this context, the cascadability of the conventional SOA for single channel operation has been investigated theoretically. In the case where the SOA was used as a loss compensator, i.e., biased to give a certain unsaturated gain, the analysis clearly confirmed the above-mentioned guidelines to obtain a large IPDR. As an example, when biased to give a gain of 5 dB, the maximum number of 200 μm long SOAs, that could be cascaded at 1 dB penalty, was 19. When biased to give a gain of 20 dB, this number was decreased to 5. In the case where the SOA was used as a power equaliser, i.e., biased to give a constant average output power, the analysis also clearly confirmed the guidelines only that instead of a low gain a low output power was important. As an example, when biased to give an output power of -10 dBm, the maximum number of 100 μm long SOAs, that could be cascaded at 1 dB penalty, was 27. Biased to give an output power of 0 dBm, the maximum number was 8. Consequently, for a given required gain or output power, superior

performance is achieved when the SOA length and confinement factor is minimised as much as possible.

The problem of gain saturation is partly overcome in GC-SOAs that have a more linear gain characteristic than conventional SOAs and therefore much higher saturation input powers. Due to this, they are also more attractive for WDM applications since cross-gain modulation between different wavelength channels is minimised. Through a theoretical analysis it has been demonstrated that the cascadability of GC-SOAs is superior at 2.5 Gbit/s compared to conventional SOAs for up to at least 16 channels. At a channel bit rate of 10 Gbit/s the performance of the GC-SOAs is still better but the improvement has dropped substantially due to the influence from relaxation oscillations, a phenomena that does not exist in the conventional SOA. Finally, an investigation of the influence of RZ and NRZ operation in GC-SOAs has been carried out. It has been shown that the cascadability can be improved by using RZ signal formats instead of NRZ due to less influence from the relaxation oscillations.

Chapter 4

High-speed cross-gain modulation in SOAs

The trend in the optical network evolution today is deployment of WDM systems using an increasing number of wavelength channels to accommodate the need for transmission capacity. As a consequence of this, there will be a need to manage the capacity on the optical channel level as pointed out in chapter 2. Here, all-optical wavelength converters will play an important role to realise flexible all-optical networks, the reason being that they reduce wavelength blocking in OXCs [18,19], packet loss in packet switches [107,108] and enable easier management and protection switching [16,20,109]. The most important techniques for all-optical wavelength conversion are discussed in chapter 2, and as pointed out in chapter 2 there are several requirements that the converters have to fulfil before deployment will be realistic. These requirements will, however, be system dependent and the advantages and disadvantages of a specific technique should therefore be related to the application.

Here, a technique for wavelength conversion relying on cross-gain modulation (XGM) in SOAs will be treated. To get an initial idea of the performance of XGM, a list of its most important characteristics is given below:

+ Can be made polarisation independent.
+ Relatively high input power dynamic range (>7 dB).
+ Optical bandwidth of more than 50 nm [110].
+ High-speed operation (100 Gbit/s shown in [57]).
+ Good conversion efficiency and high OSNR of the converted signal.
+ Good cascadability performance (cascade of 25 converters shown in [111]).
+ Low power consumption, compact and easy to realise.
÷ Extinction ratio degradation can occur, especially for conversion to longer wavelengths due to a wavelength-dependent differential gain [15].
÷ Chirped converted output signal resulting in degradation for transmission over non-dispersion shifted fiber [112].

Especially, the last point concerning the chirped output signal is a significant disadvantage since it requires the usage of dispersion compensation or dispersion shifted fibers. However, due to the simplicity of the scheme and the positive features listed above it still remains interesting for several applications.

In section 4.1, the basic operating principle of XGM converters will be discussed, whereas optimisation for high-speed operation is performed in section 4.2 followed

by a 40 Gbit/s system experiment. Section 4.3 presents an investigation of the difference between co- and counter-directional operation, while section 4.4 presents a scheme that can be used for all-optical re-timing.

4.1 Principle of operation of XGM in SOAs

In contrast to SOAs used as optical gates, where only the linear properties are of interest, XGM relies on gain saturation in order to achieve wavelength conversion. This is illustrated in Fig. 4.1, showing how the gain saturates in an SOA as the input power increases. Therefore, injecting both a modulated signal and CW light into the SOA will cause the CW light to experience the gain modulation introduced by the modulated input signal. Consequently, when the power of the input signal is high, the gain of the CW light will be low and vice versa, resulting in a converted signal with inverted polarity compared to the input signal.

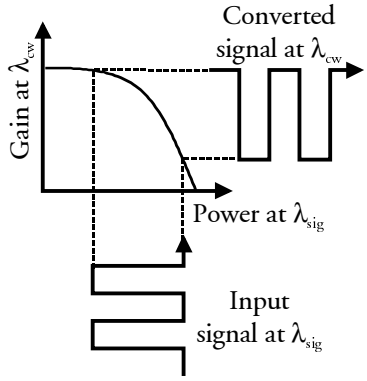

Fig. 4.1: Illustration of the XGM scheme in SOAs, where gain saturation is exploited. The modulated input signal modulates the gain that is experienced by a simultaneously injected CW light resulting in a wavelength converted signal with inverted polarity.

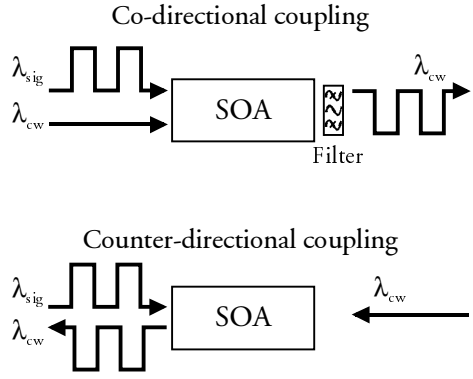

Fig. 4.2: Wavelength conversion by XGM in an SOA for two coupling schemes. (top) Input signal and CW light co-propagate, why a filter is needed at the output. (bottom) Input signal and CW light are injected from opposite directions, why filter-less operation is possible.

As illustrated in Fig. 4.2, XGM conversion can be achieved using two different schemes. In the top of Fig. 4.2, the co-directional coupling scheme is shown where the input signal and CW light co-propagate through the device. Since both signals are coupled out at the same end of the SOA, an optical bandpass filter is required to filter out the original data signal. Using a counter-directional scheme, as depicted in the bottom of Fig. 4.2, enables filter-less operation, which is especially attractive if a tuneable output wavelength is required. Moreover, conversion to the same wavelength is possible. This coupling scheme has, however, some disadvantages [92,113,114] as will be discussed in section 4.3.

So, as indicated by Fig. 4.1 and 4.2, the operation of XGM-based converters is very simple. To illustrate the performance of a specific SOA at 20 Gbit/s, Fig. 4.3 shows

measured eye diagrams of the input signal at 1560 nm (left), the XGM converted signal at 1555 nm (middle) and the BER curves (right). The SOA used for this experiment is a 1200 μm long bulk device with a confinement factor of 0.6 fabricated by Alcatel Alsthom Recherche.

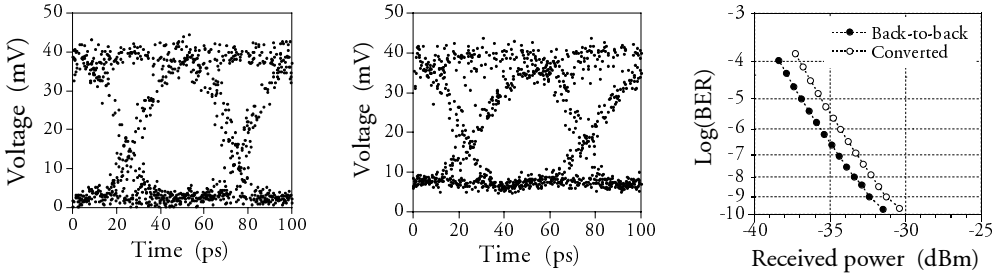

Fig. 4.3: Experimental results for XGM conversion at 20 Gbit/s in a 1200 μm long bulk-type SOA. Eye diagram of the input signal at 1560 nm (left) and the converted signal at 1555 nm (middle). BER measurements for the back-to-back and converted signal (right). Co-directional coupling is used.

As can be seen in Fig. 4.3, wavelength conversion has been achieved with a clear and open eye diagram of the converted signal having fast rise and fall times. The main effect that can be observed is the degraded extinction ratio, which also is the main reason for the measured pre-amplified power penalty of ~1 dB.

4.2 Guidelines for high-speed XGM in SOAs

In order for all-optical wavelength converters to become attractive for future optical networks, one of the concerns is the achievable conversion speed. Therefore, important guidelines to enable high-speed operation of XGM-based SOAs are described here based on large-signal calculations using a detailed SOA model [92,97-99]. The SOA used in the calculations is the one described in section 3.1 except that the device length and confinement factor will be varied in order to illustrate the trends. The objective of this section, however, is not to give a detailed investigation or optimisation of the conversion speed with respect to all device parameters. For this, most of the answers can be found in [15,56]. It is important to stress that the guidelines obtained in this section are also applicable for interferometric wavelength converters. These types of converters are treated in the following chapters of this thesis.

4.2.1 Influence of the bias current and power levels on the speed

In Fig. 4.4 the influence of the applied bias current (left) and signal input power (right) on the unfiltered extinction ratio of the converted signal at 40 Gbit/s can be seen. Clearly, a high bias current and a high signal input power is needed to obtain a high extinction ratio of the converted signal. The reasons are as follows: For fixed input power levels, a high bias current results in a low saturation input power (see

Fig. 3.5) and therefore a higher gain modulation. On the other hand, for a fixed bias current, the gain modulation also increases when the signal input power is above the saturation input power of the XGM-based converter (see Fig. 4.1). Now, the characteristics illustrated in Fig. 3.5 and 4.1 are of course for the static case. However, the carrier lifetime is dependent on both the carrier density and the total photon density in the SOA [115], and will decrease for high bias currents and power levels, leading to a higher conversion speed. The higher conversion speed enables that the gain modulation can be exploited to achieve a high extinction ratio of the converted signal. These characteristics have also been verified experimentally [15,115,116]. It should be mentioned that since the gain modulation does not increase substantially for high bias currents or high signal power levels, it is seen in Fig. 4.4 that the extinction ratio of the converted signal saturates.

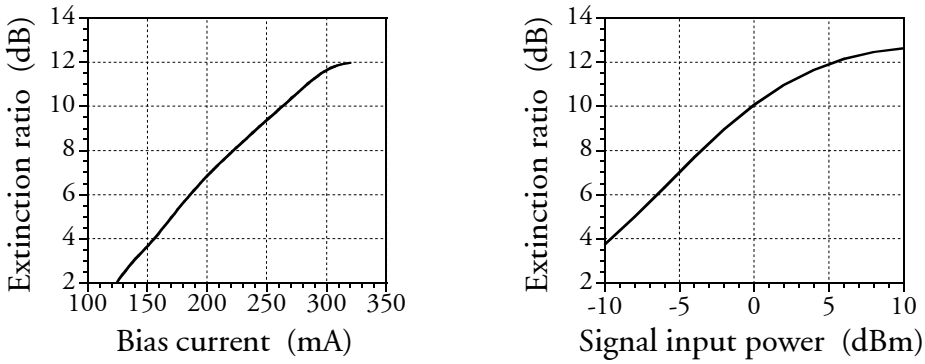

Fig. 4.4: Unfiltered extinction ratio of the converted signal for a 1500 μm long SOA at 40 Gbit/s. (left) vs. the bias current with a signal and CW power of 5 and -5 dBm, respectively. (right) vs. the signal power with a CW power of -5 dBm and a bias current of 315 mA (30 kA/cm^2). An RZ input signal (FWHM=10 ps) with an extinction ratio of 13 dB is used. The confinement factor is 0.45 and conversion is from the gain peak to a wavelength 5 nm shorter. Co-directional coupling is used.

To summarise, the trend in Fig. 4.4, and also in general, is that high bias currents and high optical powers are necessary to obtain a high extinction ratio of the converted signal.

4.2.2 Influence of the device length and confinement factor on the speed

As shown in the previous section, using high bias currents together with high optical power levels increase the conversion speed. Another way to enhance the performance of the converter is to change the physical dimensions of the SOA structure. Here, important parameters are the confinement factor and the device length. The left part of Fig. 4.5 shows the unfiltered extinction ratio of the converted signal at 40 Gbit/s as a function of the SOA length with the confinement factor as a parameter. As seen, the extinction ratio increases as the device length increases, which is due to a longer interaction length between the modulated input signal and the CW light. This has been verified experimentally in [117-119], where it is shown that a cascade of two

SOAs results in a total modulation bandwidth that is higher than the modulation bandwidth of each SOA. Furthermore, it can be seen in Fig. 4.5 that a high confinement factor also results in high extinction ratios. The reason is simply that the optical signals are better confined in the active region yielding a higher photon density inside the active region and therefore a lower carrier lifetime. The trade-off, however, is that the optical conversion bandwidth decreases as the length or confinement factor increase [56,92]. It should be pointed out that changing the confinement factor requires a change in the material composition or the geometry of the active region, i.e., thickness and width of the active region. Taking this into consideration, the trend is that the optical area[9] of the active region has to be minimised [101].

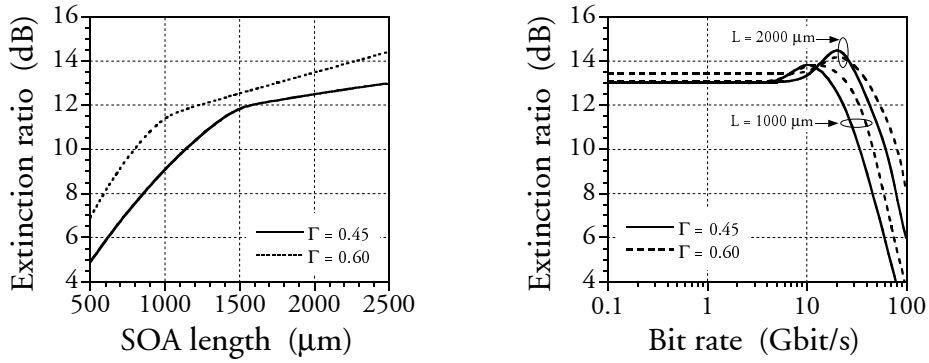

Fig. 4.5: Unfiltered extinction ratio vs. the SOA length at 40 Gbit/s (left) and vs. the bit rate using 1000 and 2000 μm long SOAs (right). In both cases the confinement factor is a parameter. The applied bias current corresponds to a current density of 30 kA/cm² and the signal and CW power is 5 and -5 dBm, respectively. An RZ input signal with a FWHM corresponding to 40% of the time slot and an extinction ratio of 13 dB is used. Conversion is from the gain peak to a wavelength 5 nm shorter and co-directional coupling is used.

The right part of Fig. 4.5 shows the unfiltered extinction ratio of the converted signal as a function of the bit rate for a 1000 and 2000 μm long SOA with the confinement factor as a parameter. Here, it can also be noticed that increasing the length or confinement factor increases the modulation bandwidth. The overshoot that can be observed in the figure is due to a phenomenon usually referred to as 'gain saturation filtering' [15] and is caused by a high-pass filtering of the input data signal, which in turn tends to equalise the low-pass filtering of the CW light. The amount of overshoot, or the strength of the oscillation, depends heavily on the device length and the internal waveguide losses and as observed in the figure, the overshoot is most significant for the 2000 μm long SOA. For a detailed theoretical investigation of this, the reader is referred to [15,120] and the references therein. It is important to stress, however, that the overshoot in the modulation response has been

[9] Optical area = (width×thickness)/confinement factor.

verified experimentally by small-signal measurements [15,91,99]. It should also be emphasised that the 'gain saturation filtering' effect actually is responsible for the high conversion speed that is possible with XGM-based converters, i.e., the response determined by the carrier lifetime predict bandwidths that are well below what has been reported.

In general, a large amount of overshoot can be a problem since the phase transfer function of the converter will be highly non-linear in the frequency region of the overshoot resulting in a deterioration of the converted signal. If designed properly, however, the overshoot can be exploited to increase the total modulation bandwidth of the converter. This together with the fact that the waveguide losses influence the overshoot has been utilised in a so-called gain-attenuation-gain (GAG) device, where a loss section is placed between two SOA sections [121]. Using this scheme it was shown that the small-signal modulation bandwidth could be increased by a factor of ~3 compared to the bandwidth of the single SOAs.

4.2.3 All-optical XGM conversion at 40 Gbit/s

Here, a system experiment performed at 40 Gbit/s with two different bulk SOAs fabricated by Alcatel Alsthom Recherche will be described. Fig. 4.6 shows the set-up used for the measurements. In the transmitter, a gain-switched laser generates 10 GHz pulses at 1546 nm that are compressed by a dispersion compensating fiber (DCF) to ~6 ps. The pulse train is then modulated at 10 Gbit/s and multiplexed to 40 Gbit/s after which the signal is coupled to the wavelength converter together with CW light at 1543 nm. The wavelength converter is either a 1200 or 2200 μm long SOA with a confinement factor of 0.60 or 0.45, respectively. After the SOA, the converted signal is filtered out and detected in a 32 GHz photodiode and displayed on a 50 GHz sampling oscilloscope.

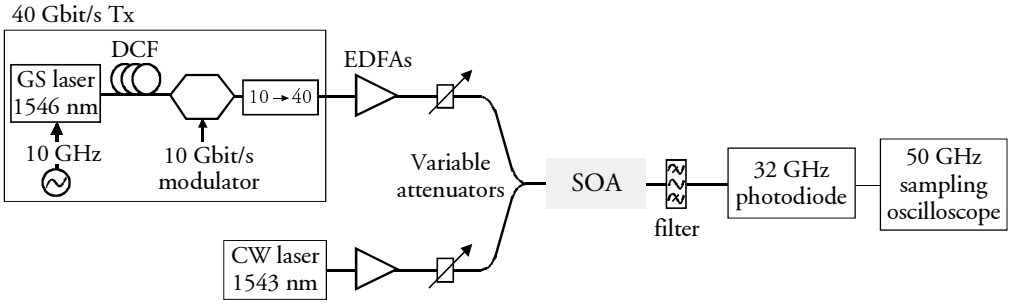

Fig. 4.6: Experimental set-up for XGM conversion at 40 Gbit/s using 1200 and 2200 μm long bulk SOAs with confinement factors of 0.6 and 0.45, respectively. EDFAs and variable attenuators are used to ensure optimum power levels. Co-directional coupling is used.

The measured eye diagrams are shown in Fig. 4.7, giving the back-to-back signal (left), the converted signal using the 1200 μm long SOA (middle) and the 2200 μm long SOA (right). As seen, the eye diagrams of the converted signals are both clear

and open illustrating the good performance. Furthermore, the RZ signal format has been preserved, which indicates a high conversion speed, i.e., a format conversion to NRZ would be observed if the converter was too slow [122].

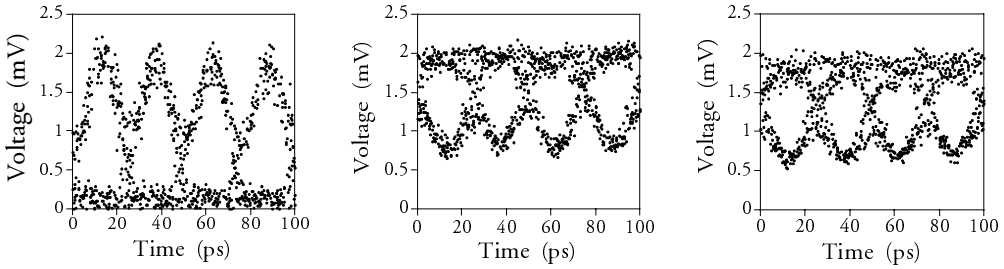

Fig. 4.7: Measured eye diagrams at 40 Gbit/s of the back-to-back signal at 1546 nm (left), the XGM converted signal at 1543 using 1200 μm (middle) and 2200 μm long SOAs (right). Co-directional coupling is used.

It should be mentioned, though, that the extinction ratio clearly is degraded in both cases, although a slightly higher extinction ratio can be observed for the case of the 2200 μm long SOA. Still, the extinction ratios obtained in the measurements are not as high as those shown in Fig. 4.5. The figures should not be compared directly, however, since several parameters, e.g., the optical area, are not known for the devices used in the measurements. As listed in the beginning of this chapter, the extinction ratio degradation is not unusual for XGM-based converters. However, as shown in [119], 40 Gbit/s wavelength conversion in a 2400 μm long SOA resulted in a penalty of only 1.5 dB indicating that only a small degradation in extinction ratio occurred. In the 100 Gbit/s experiment reported in [57] a 2000 μm long MQW-based SOA [123] followed by a grating was used. This resulted in penalties ranging from ~4 to ~10 dB on the individual 10 Gbit/s demultiplexed channels. The purpose of the grating was twofold; firstly to remove the input signal and secondly, if used correct, the grating can result in frequency to intensity modulation, which increases the extinction ratio of the converted signal.

4.3 Co- versus counter-propagation in XGM converters

So far, all results that have been presented are for the co-directional propagation scheme. As illustrated in Fig. 4.2, a counter-directional coupling scheme also exists, to which there are some apparent advantages in that no filter is needed at the output of the converter and that conversion to the same wavelength is possible. Therefore, counter-directional coupling is attractive due to the added flexibility and lower complexity. There are, however, also some shortcomings compared to co-directional coupling, which the purpose of this section is to highlight.

The reason for the difference between co- and counter-directional coupling can be understood from the carrier distribution in the SOA. This is illustrated in Fig. 4.8,

giving the carrier density as a function of the position in a 1000 μm long SOA for co- (left) and counter- (right) directional coupling. The carrier density is shown in the case of a low and high signal input power corresponding to the power in a logical zero and one. In the co-directional case, the carrier density is high in the front of the amplifier, i.e., where the CW light enters, and drops along the amplifier due to the amplified input signal and CW light. As the signal input power increases the carrier density decreases and reaches minimum after a shorter distance. It can be seen, however, that the changes in the carrier density only appear in the front of the amplifier. On the other hand, the situation is quite different in the counter-directional case. For signal input powers higher than the CW light, the maximum carrier concentration will be at the end of the amplifier, whereas for smaller signal input powers, the maximum will move towards the front of the amplifier.

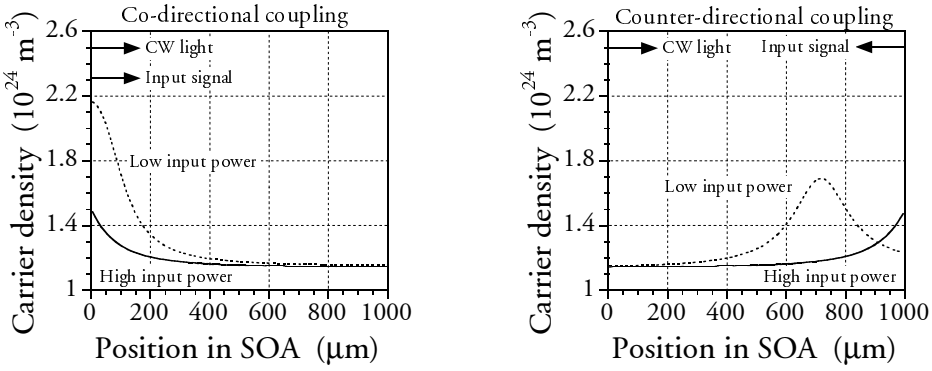

Fig. 4.8: Carrier distribution in a 1000 μm long SOA for co- (left) and counter-directional coupling (right). The high and low input power is 7.8 and -5.2 dBm, corresponding to an average power of 5 dBm and an extinction ratio of 13 dB. The CW power is -5 dBm, while the bias current is 210 mA (30 kA/cm^2). Conversion is from the gain peak and to a wavelength 5 nm shorter.

The movement of the carrier distribution for counter-directional propagation has several disadvantages: First of all, since the carrier density in the front of the amplifier determines the noise figure, it will be higher for the counter-directional case. Secondly, the dynamic movement of the carrier distribution, which happens on a time scale corresponding to the carrier life time, results in jitter on the wavelength converted signal [113,114] that accumulates as the converters are cascaded. Thirdly, transit time effects become important and can decrease the modulation bandwidth compared to the co-directional case [56]. These transit time effects are a result of the limit where the bit duration of the modulated input signal is comparable to or shorter than the time it takes to propagate through the amplifier (transit time). Fig. 4.9 illustrates the two situations, where the time slot is longer (left) and shorter (right) than the transit time. In the case of a long time slot, the CW light inside the amplifier will experience a non-modulated data signal most of the time, as is the case for co-directional propagation. If the time slot is shorter than the transit time, however, the CW light will experience the modulation of the data signal along the

amplifier resulting in a poor conversion since an already converted bit in the front of the amplifier will continue to experience counter propagating data bits.

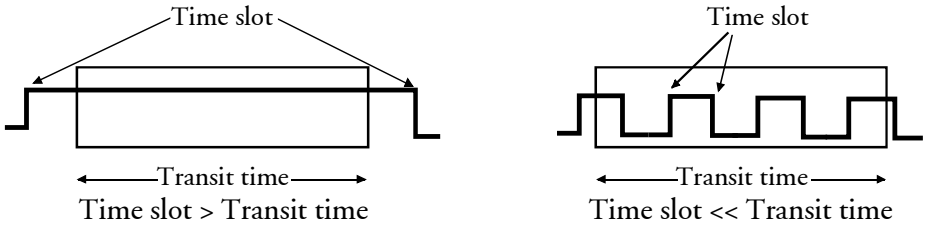

Fig. 4.9: Illustration of the two situations, where the time slot of the modulated input signal is longer than the transit time of the SOA (left) and shorter than the transit time (right). Note that the amplification of the signal is not illustrated in the figures.

As a consequence of the transit time effects, both the amplifier length and the bit rate will play an important role for the performance of the converter. This is verified in Fig. 4.10, showing the extinction ratio of a converted signal at 40 Gbit/s as a function of the signal input power for different device lengths. It can be seen that going from a 500 to a 1000 μm long device results in an improved performance as is the case for co-directional coupling (see Fig. 4.5). However, increasing the length to 1500 or even 2500 μm results in degradations compared to the case of a 1000 μm long device. Keeping in mind that the time slot is 25 ps and that the transit time is ~6 ps per 500 μm of the device, this corresponds well to the comments given above.

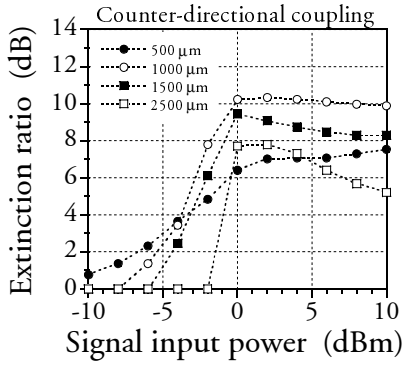

Fig. 4.10: Extinction ratio vs. the input power at 40 Gbit/s with the device length as a parameter. The confinement factor is 0.60, the applied bias current corresponds to a current density of 30 kA/cm^2 and the CW power is -5 dBm. An RZ input signal (FWHM = 10 ps) with an extinction ratio of 13 dB is used. Conversion is from the gain peak to a wavelength 5 nm shorter and counter-directional coupling is used.

In contrast to the co-directional case, it can be noticed that for the long SOAs the extinction ratio has an optimum. The reason is that the converted signal, which continues to be modulated by counter propagating data bits, experiences a higher gain modulation by the data signal at high signal input powers. This leads to extinction ratio degradation of the converted signal as illustrated in Fig. 4.10.

Since these phenomena are characteristic for the counter-directional scheme, this means that for a given bit rate careful optimisation of the SOA with regard to device length, input powers, etc. is necessary. In addition to this, due to the dynamic movement of the carrier distribution, jitter accumulation is unavoidable even at low bit rates. Although, these detrimental effects can be minimised by proper design of the amplifier, the co-directional scheme does not impose any of these limitations. Therefore, if conversion to the same wavelength is unimportant and the added complexity of a filter is of no concern, the co-directional scheme should be applied.

4.4 XGM with optical clock signals

In the previous sections, XGM conversion was described and demonstrated using CW light (see Fig. 4.2). Another possibility is to replace the CW light with an optical clock signal with the same base rate as the data signal. Apart from the increase in complexity, the scheme has some advantages that will be described in this section. An apparent benefit, however, is that all-optical re-timing is obtained. This approach has already been used as part of a 3R regenerator [124]. The synchronisation between the data and clock signal has to be ensured by clock recovery so that any temporal changes in the data signal is followed by the clock signal.

4.4.1 Principle of operation and basic performance

The XGM conversion scheme employing an optical clock signal is illustrated in Fig. 4.11 for the co-directional case and with the use of an RZ data signal. The operation is in principle the same as in the case where CW light is used and the guidelines to achieve high-speed operation are the same as discussed in section 4.2. However, due to a modulated clock signal, there are some additional requirements that need special attention.

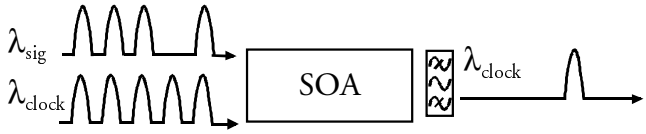

Fig. 4.11: Schematic of XGM conversion in an SOA using an optical clock signal together with the data signal. Co-directional coupling is shown.

Before discussing the additional requirements, it can be noted that the shape of the signal at the output of the converter is different from what can be seen in Fig. 4.7. The converted signal is still logically inverted compared to the input data signal but since a clock signal is used, pulses will only appear at the output when there is a logical zero in the data signal. Therefore, the converted pulses will have the shape of a 'conventional' RZ signal but with the information logically inverted. It should be noted that although an RZ signal is shown in the figure, the scheme is also applicable for NRZ data signals [124]. This will, however, still result in an RZ output signal.

Turning back to the issues that need special attention, one requirement is obviously that pulses in the clock signal are suppressed each time there is a logical one in the data pulse. This implies that sufficiently high signal powers are necessary. In the case where CW light is used, a low signal power will simply result in a low extinction ratio but otherwise an open eye diagram. By using a clock signal, the extinction ratio will also be low for a low signal power but in this case it is caused by non-suppressed pulses. The latter is illustrated in Fig. 4.12, giving calculated converted output pulses at 20 Gbit/s for different signal power levels.

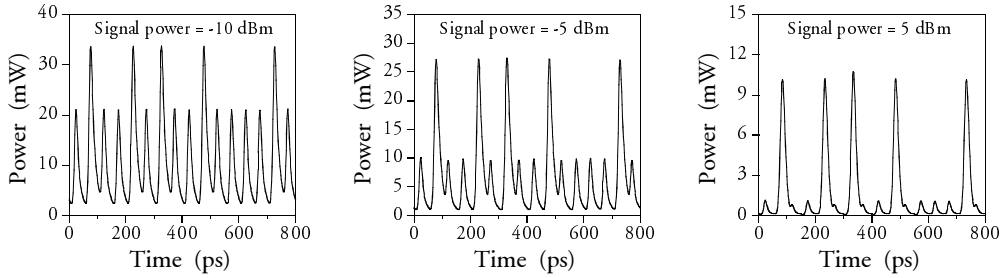

Fig. 4.12: Pulse traces of an XGM converted signal at 20 Gbit/s for a signal input power of -10 dBm (left), -5 dBm (middle) and 5 dBm (right). The power of the clock signal is -5 dBm, while the SOA is 1000 μm long with a confinement factor of 0.6. The applied bias current corresponds to 30 kA/cm². RZ signals are used (FWHM=20ps) with an extinction ratio of 13 dB on both signals. The time delay between the data and clock signal is 0 ps. Conversion is from the gain peak to a wavelength 5 nm shorter and co-directional coupling is used.

Clearly, a low input power results in a poor suppression of the original clock pulses. It can also be seen that even for high input powers, there are still residuals of the pulses. The reason for this is that the data and clock signal are not synchronised perfectly. Fig. 4.13 defines a parameter that will be used in the following, namely the time delay ($\Delta\tau$) between the data and clock signal. In the definition used here, a negative time delay corresponds to the case where the clock signal enters the SOA first and vice versa.

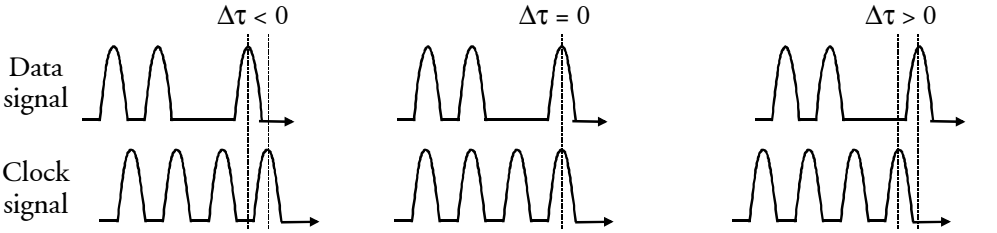

Fig. 4.13: Definition of the time delay ($\Delta\tau$) between the data and clock signal. A negative $\Delta\tau$ corresponds to the situation where the clock signal enters the SOA before the data signal and vice versa.

The importance of synchronisation is demonstrated in Fig. 4.14, showing pulse traces of the converted signal for a time delay between the data and clock signal of -5 ps (left), 0 ps (middle) and 5 ps (right). As observed in the figure, an almost complete suppression can be achieved by choosing the correct time delay. The reason

why a zero time delay is not optimal is due to the finite time response of the gain in the SOA. This means that when the power in the data signal starts to increase, i.e., a pulse enters, a certain amount of time will elapse before saturation of the clock pulse sets in. Due to this, it is also obvious that a positive time delay has to be required, i.e., the data signal has to enter first. The amount of necessary time delay will naturally depend on the speed of the device and therefore on the power levels, applied bias current and dimensions of the SOA. It should be emphasised, however, that for a specific device it is a constant time delay and therefore relatively easy to implement.

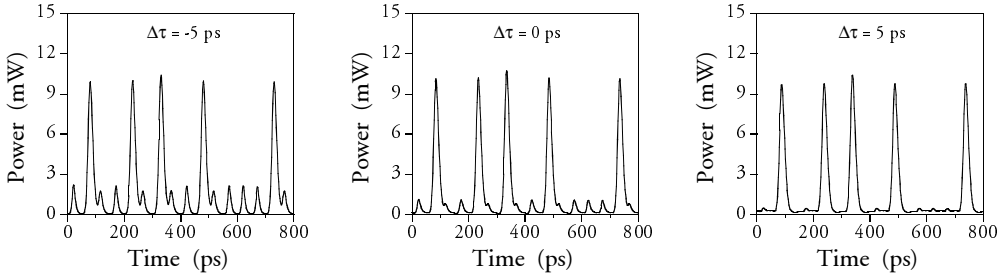

Fig. 4.14: Pulse traces of the converted signal at 20 Gbit/s in the cases of a relative time delay ($\Delta\tau$) between the data and clock pulses of -5 ps (left), 0 ps (middle) and 5 ps (right). The power in the data and clock signal is 5 and -5dBm, respectively. For additional information on the calculations refer to the text in Fig. 4.12.

Since the scheme offers all-optical re-timing, there is also the benefit that the shape of the converted signal to some degree can be determined by the shape of the clock signal. This is of course in contrast to the case where CW light is used since the converted signal in that case solely is determined by the data signal. Although using a clock signal makes optimisation more difficult, it is an attractive feature since the clock signal is generated locally and therefore well controlled. One of the benefits is that it is easier to obtain a high extinction ratio of the converted signal since the clock signal already has a finite extinction ratio. So even though pulses also have to be suppressed on the clock signal, the initial modulation helps to obtain a high extinction ratio of the converted signal. Although this is not evident from a static point of view, it is the experience from dynamic measurements.

Another benefit is that the pulse width of the converted signal depends heavily on the clock signal. This is illustrated in Fig. 4.15, giving pulse traces of the converted signal for a FWHM of the clock signal of 30 ps (left), 20 ps (middle) and 10 ps (right), while keeping the FWHM of the data signal fixed to 20 ps. For a clock pulse width of 30 ps it can be seen that there are still non-suppressed pulses in the converted signal, which is caused by the fact that the signal pulse width is only 20 ps and therefore not sufficiently broad. Decreasing the clock pulse width results in complete suppression and a narrowing of the converted pulses and very importantly, the quality of the converted signal remains unchanged. This is a very attractive

feature, seen from the point of view of re-timing, since the use of short clock pulses increases the jitter tolerance and therefore ensures a better re-timing capability.

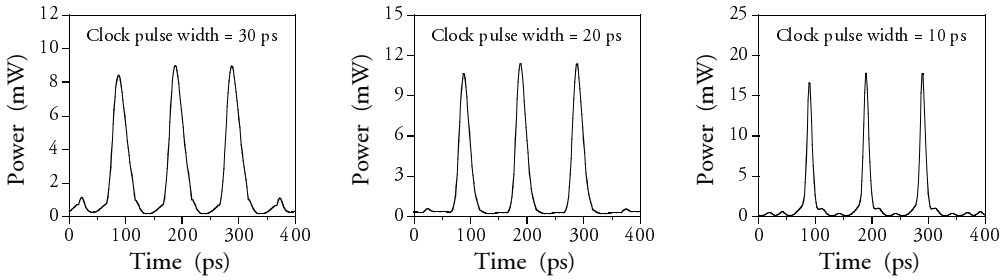

Fig. 4.15: Pulse traces of the converted signal at 20 Gbit/s for a FWHM of the clock signal of 30 ps (left), 20 ps (middle) and 10 ps (right). FWHM of the data pulses is 20 ps. The power in the data and clock signal is 5 and -5 dBm, respectively and the time delay is 5 ps. For additional information on the calculations refer to the text in Fig. 4.12.

4.4.2 20 Gbit/s wavelength conversion using an optical clock signal

In order to demonstrate the feasibility of high-speed operation of the XGM conversion scheme using an optical clock signal, a system experiment carried out at 20 Gbit/s will be described here (the results are based on [p12]). It should be mentioned that all experiments above 10 Gbit/s reported on XGM so far are for co-directional coupling, e.g., [57,119]. Here, conversion for both co- and counter-directional coupling will be demonstrated. The main reason for the good performance that is achieved for counter-directional coupling with the specific SOA is due to the benefits of using a clock signal instead of CW light, as explained in section 4.4.1.

Fig. 4.16 shows the experimental set-ups. The transmitter, optical clock generator and receiver are the same in both coupling schemes. In the transmitter short optical pulses (~25 ps) are generated by a gain-switched DFB laser, modulated at 10 Gbit/s and multiplexed to 20 Gbit/s. The data signal is then coupled into the SOA either co- or counter-directional with respect to the 20 GHz clock signal (also generated by a gain-switched DFB laser, FWHM = ~25 ps).

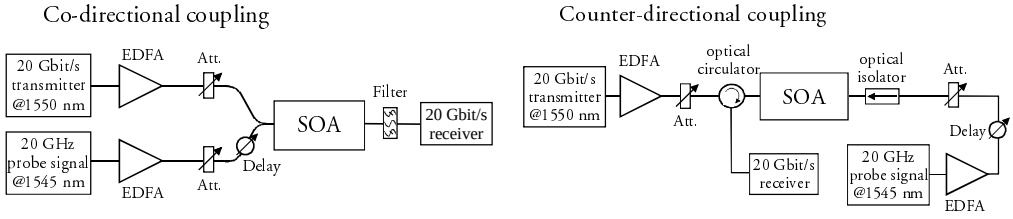

Fig. 4.16: Experimental set-up for co- (left) and counter-directional XGM conversion (right) at 20 Gbit/s using an optical clock signal. The SOA is the one described in section 4.1 biased at 330 mA.

In the co-directional scheme, a filter is applied at the output of the SOA to select the converted signal, while no filter is used in the counter-directional scheme. In the

receiver, the 20 Gbit/s converted signal is optically demultiplexed to 10 Gbit/s by a $LiNbO_3$ Mach-Zehnder modulator before detection. The applied bulk-type SOA is the 1200 μm long device described in section 4.1. It should be pointed out that in these experiments the synchronisation between the data and clock signal is achieved with an optical delay-line, which is adjusted for optimum performance.

The performance of the wavelength converter can be seen in Fig. 4.17, giving the eye diagram of the input signal, pulse trace of the clock signal and eye diagrams of the converted signal for co- and counter-directional coupling. As demonstrated, clear and open eye diagrams are obtained in both cases with a good suppression of the clock signal in the converted logical zeros.

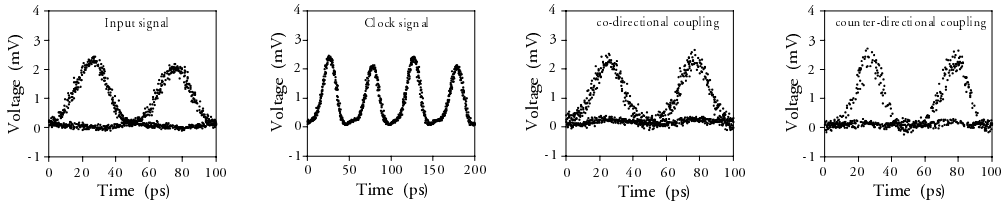

Fig. 4.17: Measured eye diagrams at 20 Gbit/s of the input signal, clock signal and converted signal for co- and counter-propagation. Power levels for co: 1.7 and -1 dBm for the data and clock signals. Power levels for counter: 6.3 and 0.2 dBm for the data and clock signals.

The measured BER curves shown in the left part of Fig. 4.18 verify that the converter indeed has good performance. For co propagation, a pre-amplified penalty of 1.2 dB is achieved, while using counter-directional coupling results in a penalty of 2.5 dB. The slightly higher penalty in the counter-directional scheme is mainly due to a higher noise figure of the SOA compared to co-directional operation as explained in section 4.3. Still, good BER performance is achieved for both operation schemes and in addition to the low penalties, it is emphasised that the wavelength converter is polarisation independent and loss-less with an output power of more than 6 dBm.

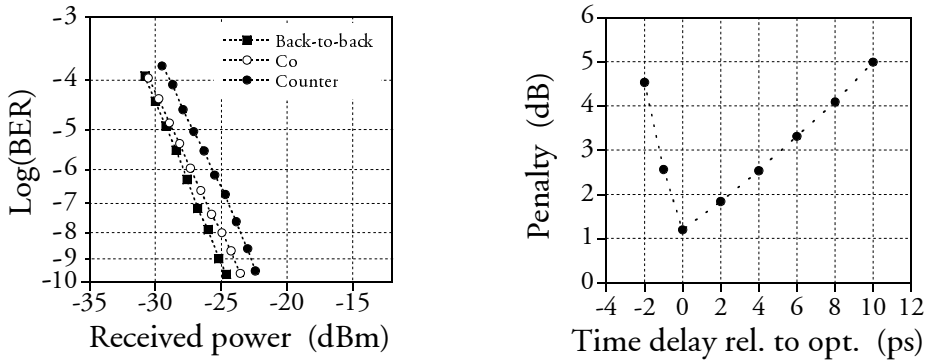

Fig. 4.18: (left) BER measurement of the back-to-back signal at 1550 nm and the converted signal for co- and counter propagation at 1545 nm. (right) Penalty vs. the time delay relative to optimum between the data and clock signal for co-directional propagation. The bit rate is 20 Gbit/s.

The right part of Fig. 4.18 shows the penalty as a function of the time delay relative to optimum between the data and clock signal, i.e., 0 ps corresponds to the optimum delay. This switching window is a measure of the jitter tolerance of the converter, i.e., the amount of jitter on the data signal that can be accepted for a given penalty. In this case the switching window is ~7 ps (@ 2 dB excess penalty), which has to be related to a time slot of 50 ps, i.e., corresponding to 14%. It should be emphasised, however, that the switching window could easily be increased if the pulse width of the clock signal was lower (in this case the pulse widths are equal). It can be noted that the tolerance is higher for an increasing delay than for a decreasing delay, which is due to the finite time response of the SOA as described in section 4.4.1.

4.5 Summary

The use of SOAs for XGM-based wavelength conversion has been described in this chapter and the main advantages and disadvantages of the scheme have been highlighted. Furthermore, guidelines for achieving high modulation bandwidths have been outlined by a theoretical large-signal investigation. It was found that long SOAs with high confinement factors using high bias currents together with high optical powers are beneficial to improve the performance. It has also been shown that an overshoot can appear in the modulation response of the converter, which can be utilised to further increase the modulation bandwidth, if the SOA is designed with care. Following this, a system experiment performed at 40 Gbit/s was described using two different SOAs, i.e., a 1200 μm and a 2200 μm long SOA with a confinement factor of 0.45 and 0.6, respectively. The eye diagrams of the converted signals were in both cases clear and open with the RZ signal format preserved indicating that a high modulation bandwidth was achieved, although with a noticeable degradation in extinction ratio.

Moreover, the differences between co- and counter-directional coupling of the data signal and CW light have been explained. The counter-directional scheme has some advantages since filter-less operation and conversion to the same wavelength is possible. There are, however, also some disadvantages due to a dynamic movement of the carrier distribution inside the SOA that does not occur for co-directional coupling. First of all, the noise figure is higher for the counter-directional case. Secondly, the dynamic movement of the carrier distribution results in jitter on the wavelength converted signal that accumulates as the converters are cascaded. Thirdly, transit time effects become a limiting factor for long SOAs operated at high bit rates and can decrease the modulation bandwidth compared to the co-directional case. Although, these detrimental effects can be minimised by proper design of the amplifier, the co-directional scheme does not impose any of these limitations. Therefore, if conversion to the same wavelength is unimportant and the added complexity of a filter is of no concern, the co-directional scheme should be applied.

An investigation of a scheme that can be used as part of all-optical re-timing has also been carried out. In this scheme, an optical clock signal is used instead of CW light, why proper synchronisation to the data signal has to be assured. Achieving this, however, results in good performance with a high suppression of original clock pulses in the converted zeros. Since the scheme offers all-optical re-timing, there is the benefit that the shape of the converted signal to some degree is determined by the shape of the clock signal. One of the benefits is that it is easier to obtain a high extinction ratio of the converted signal since the clock signal already has a finite extinction ratio. Another benefit is that the pulse width of the converted signal depends on the width of the clock signal so that short output pulses can be obtained even though the data input pulses are broad. Finally, a system experiment carried out at 20 Gbit/s for both co- and counter-directional coupling was demonstrated resulting in a penalty of 1.2 and 2.5 dB, respectively. Due to an inherently higher noise figure of the SOA for counter propagation, a higher penalty was experienced for that set-up. In addition to the low penalties, polarisation independent and loss-less operation with an output power of more than 6 dBm was achieved.

Chapter 5

High-speed cross-phase modulation in SOAs

In the previous chapter XGM converters were described. Although these types of converters are very simple and compact, two major drawbacks of the scheme are the wavelength dependency [15] and chirped output signals [112]. A technique that eliminates these disadvantages and shows very promising results over-all, is based on cross-phase modulation (XPM) in interferometers incorporating SOAs. These converters have been realised as TOADs [51] and UNIs [53], that are partly fiber-based, or as monolithically integrated Mach-Zehnder interferometers (MZI) [58] and Michelson interferometers (MI) [59].

This chapter will focus on the performance of the monolithically integrated converters, i.e., MZIs and MIs. To set the scene, a list of the most important advantages and disadvantages of interferometric wavelength converters (IWCs) is given below:

+ Potentially polarisation independent.
+ High-speed operation (40 Gbit/s shown in [p19,60-62]).
+ High optical bandwidth and extinction ratio at 40 Gbit/s [61,p19].
+ Conversion efficiency above 10 dB can be obtained.
+ OSNR above 40 dB in 0.1 nm can be obtained [p23].
+ Impressive cascadability performance [p34,35,36]
+ Low and controllable chirp [15].
+ Regenerative capabilities [p16,p23,35,36,82].
÷ Limited input power dynamic range (3-4 dB).
÷ Requires well-established fabrication techniques to realise an interferometer.
÷ Control of the interferometer needs special attention.

Although only 40 Gbit/s wavelength conversion has been demonstrated so far, the potential bandwidth should be much higher as indicated by theoretical studies carried out in [101] and the fact that 168 Gbit/s conversion has been achieved with the delayed-interference signal wavelength converter [65,66]. Due to this and the other attractive features listed above, IWCs are believed to be closest to commercial utilisation. There are, however, also some important challenges that need to be solved. First of all, fabrication of good devices is by no means straightforward and only a few manufacturers are able to accomplish this task satisfactory. Secondly, the devices are sensitive to changes in the operating conditions. Therefore, some kind of active control of the interferometer is essential before commercial deployment will

be realistic. Still, very promising results have been obtained with IWCs either for wavelength conversion or regeneration and many people are pursuing the task of solving the above-mentioned problems.

In section 5.1, the operating principle as well as two ways of realising IWCs will be described. Furthermore, the basic performance at 10 Gbit/s will be demonstrated experimentally. The high-speed capabilities will be the topic of section 5.2, where system experiments carried out at 20 and 40 Gbit/s will be shown together with a scheme for increasing the IPDR. Section 5.3 is concerned with the problem of converting to the same wavelength as the input signal. Two schemes for this will be presented, where the first is a dual-stage converter consisting of an XGM and XPM converter. The second scheme is based on a new type of IWC called a dual order mode (DOMO) Mach-Zehnder interferometer [125,126]. Finally, section 5.4 presents a new scheme for wavelength conversion in IWCs that results in high-speed operation, while maintaining good transmission properties.

5.1 Wavelength conversion by XPM in SOA-based IWCs

The objective of this section is to explain the operating principle of IWCs and discuss the two approaches used today to realise these types of converters, namely active/passive and all-active integration. The difference in the two approaches seen from a system perspective will be highlighted and, following this, the performance of all-active MZIs and MIs will be demonstrated experimentally at 10 Gbit/s.

5.1.1 Principle of operation and physical realisation of MZIs and MIs

In IWCs it is exploited that the refractive index, and therefore the phase shift of a signal traversing the SOA, depends on the optical input power. So, by placing the SOA in an interferometric configuration, the interference of CW light can be controlled by an amplitude modulated signal. A schematic of the MZI and MI is shown in the left part of Fig. 5.1 and in the following, the operating principle of the converters will be described.

In the MZI, the CW light is coupled into the interferometer, where it splits equally between the two interferometer arms and recombines again at the output either constructively or destructively depending on the phase difference between the two interferometer arms. By injecting a modulated signal into only one of the arms, this phase difference can be controlled and thereby the amplitude modulation on the data signal is transferred to the CW light. In the figure, co-directional coupling is illustrated, but counter-directional coupling is also possible in MZIs with the advantages and drawbacks described for XGM in chapter 4.

The operating principle of the MI is similar to the MZI except that the CW light traverses the interferometer arms twice due to the reflective facets and recombines

again at the input. Since the CW light enters and leaves at the same port, a circulator is needed to separate the signals. Furthermore, an optical filter is always needed to reject the original data signal.

There are two main differences between the MZI and MI. First of all, for the MI the data signal is injected directly into one of the interferometer arms, whereby losses from input sections and couplers are avoided, resulting in a higher power to the interferometer arm. Secondly, as mentioned above, the CW light traverses the interferometer arms twice, which resembles SOAs with a higher effective length. According to the guidelines described in chapter 4, this increases the modulation bandwidth, why it could be expected that MIs have a better performance than MZIs when the length of the interferometer arms are equal. However, since the operation in MIs is partly co- and counter-propagation, this will only be the case at moderate bit rates and with interferometer arms that are not too long due to the transit time effects outlined in chapter 4. Still, although MZIs have the highest potential bandwidth [101], the first successful 40 Gbit/s experiments on IWCs were in fact performed with MIs [60-62]. It should be emphasised, though, that the higher modulation bandwidth for MZIs has not been experimentally verified yet.

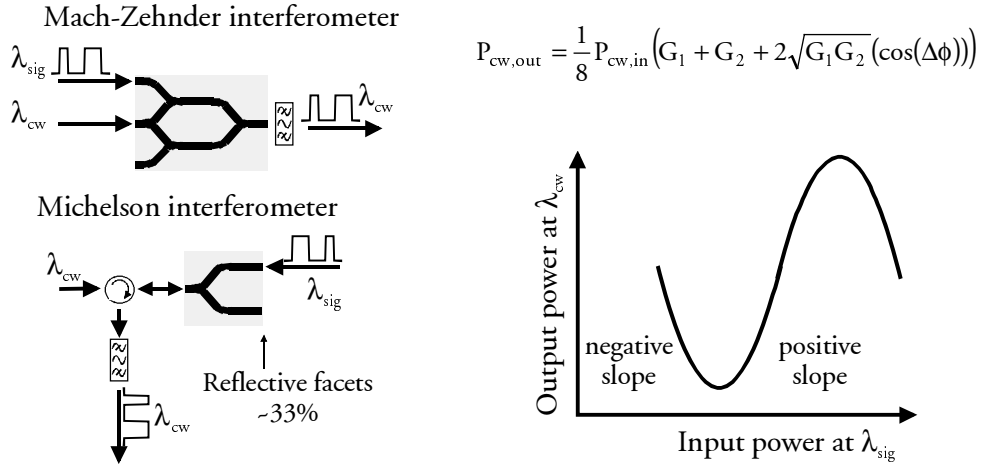

Fig. 5.1: (left) Illustration of a Mach-Zehnder and Michelson interferometer, where co-directional coupling is shown for the Mach-Zehnder interferometer. (right) Schematic of the transfer function for IWCs together with the mathematical expression, where G_1 and G_2 is the gain in the upper and lower interferometer arm, respectively. $\Delta\phi$ is the phase difference between the two interferometer arms.

The transfer function of IWCs is shown in right part of Fig. 5.1. Since conversion is based on interference, the resulting transfer function is sinusoidal as illustrated in the figure. Also shown in the figure is the mathematical expression for the output power at the converted wavelength. In the expression G_1 and G_2 are the gains in the upper and lower interferometer arm, while $\Delta\phi$ is the phase difference between the two interferometer arms. As seen, a phase shift of π will change the output power from minimum to maximum or vice versa, yielding the highest extinction ratio of the

converted signal. It can be noted that operation on a negative and a positive slope is possible, which means that conversion with inverting and non-inverting polarity is possible. Inverting operation results in the highest modulation bandwidth since XGM has a beneficial influence. However, the converted signal is also associated with a small positive chirp that limits transmission on non-dispersion shifted fiber [15]. Non-inverting operation, on the other hand, results in a small negative chirp [15] but a lower modulation bandwidth.

The converters can be realised either as an active/passive structure [127,128], where only the interferometer arms are active, or as an all-active structure [129], where the input/output sections and splitters also are active. The benefits of an active/passive device is that it is easier to control since only two electrodes are necessary, i.e., one for each interferometer arm. As a consequence of having only two electrodes, another benefit is that the electrical power consumption is lower compared to all-active devices. However, the all-active devices require fewer epitaxial and processing steps [129] and are therefore easier and potentially less expensive to fabricate. Furthermore, the absence of active/passive transitions avoids parasitic reflections that are especially critical for high bias currents [129]. Additional benefits of the all-active structures are that the input sections can be used as pre-amplifiers [130] allowing low input powers [131] and that they can be used for fast power equalisation of the input signal as described in chapter 3 or as shown experimentally in [132,p19]. Moreover, the output section can be used as a booster amplifier ensuring a high power of the converted signal. This also ensures that a conversion efficiency above 10 dB can be obtained, whereas this typically is below -10 dB for the active/passive structures.

The downside to the all-active integration is that the electrical power consumption is higher and that control of the interferometer is more complex. Furthermore, since modulation is only needed in the interferometer arms, the input/output SOAs add unnecessary noise and can result in extinction ratio degradation. Due to this, it is very important that these sections are as short as possible so that the noise figure is low and the saturation input power high (see chapter 3). Taking only the conversion performance into account, the active/passive structures are therefore probably better, although this has not been verified by experiments. Still, the all-active devices have some benefits, as mentioned above, that are important in a system perspective, e.g., high conversion efficiency and potentially lower cost, making them preferable by some manufacturers. It should be emphasised, however, that the all-active devices have shown a high extinction ratio and OSNR of the converted signal even at 40 Gbit/s [p23] as well as an impressive cascadability performance [p34,35,36].

The results presented in this chapter, and throughout the rest of this thesis, are based on IWCs fabricated by Alcatel Opto+ and except for two results presented in section 5.2.2, all devices are all-active structures.

5.1.2 Basic performance of MZIs and MIs at 10 Gbit/s

Since the phase shift in SOAs is governed by the differential refractive index[10], an important advantage of IWCs is that they are nearly wavelength independent[11] [58], a feature that is in strong contrast to the XGM-based converters. This wavelength independence will be illustrated experimentally here for an MZI and an MI both having 1200 μm long SOAs in the interferometer arms with a confinement factor of ~0.45.

Mach-Zehnder interferometer

Fig. 5.2 shows the measured eye diagram of a wavelength converted signal at 10 Gbit/s for conversion from 1555 to 1550 nm (left) and the resulting BER (right). Clearly, the 5 nm down-conversion is achieved with a very good performance, i.e., the eye diagram is open with an extinction ratio above 12 dB and with short rise and fall times indicating potential for an even higher bit rate. The BER measurements verify the excellent performance in that conversion is achieved without penalty.

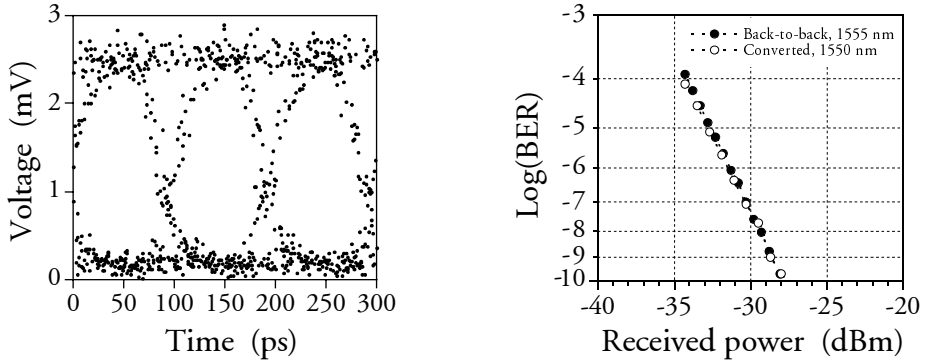

Fig. 5.2: Eye diagram of the wavelength converted signal at 10 Gbit/s in an MZI (left) and the resulting BER curves for the back-to-back signal and the converted signal (right). Co-directional coupling is used.

In Fig. 5.3 a similar result is illustrated but for a 5 nm up-conversion from 1555 to 1560 nm. Also in this case, conversion is achieved with an excellent performance as indicated by the clear and open eye diagram with an extinction ratio above 13 dB and the BER measurements showing negligible penalty.

[10] The differential refractive index is given by $\partial n/\partial N$, where n is the refractive index and N is the carrier density in the SOA.

[11] The wavelength independence is usually experienced in a range of $\pm 15 \rightarrow 20$ nm around the gain peak of the interferometer.

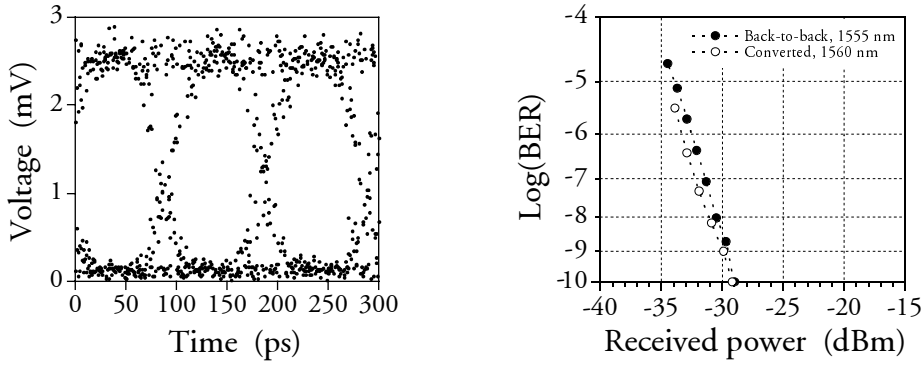

Fig. 5.3: Eye diagram of the wavelength converted signal at 10 Gbit/s in an MZI (left) and the resulting BER curves for the back-to-back signal and the converted signal (right). Co-directional coupling is used.

It should be emphasised that even though these results only show wavelength independence over 10 nm, similar results have been obtained for MZIs over the entire EDFA window [101,p30]. That this also is the case for MIs will be demonstrated in the following.

Michelson interferometer

The performance of an MI at 10 Gbit/s for up-conversion from 1545 to 1550 nm is shown in Fig. 5.4, giving the measured eye diagram of the converted signal (left) and the optical spectrum at the output of the converter (right). Comparing the eye diagram in Fig. 5.4 to those illustrated in Fig. 5.2 and 5.3, it is seen that an even higher modulation bandwidth is obtained with the MI, i.e., the rise and fall times are shorter. As discussed in section 5.1.1, the reason is that for moderate bit rates and not too long interferometer arms, MIs usually have a higher conversion speed than MZIs. From the optical spectrum it can be noted that the power of the converted signal is ~0 dBm and that the OSNR is ~40 dB in 0.1 nm, clearly indicating a very good performance.

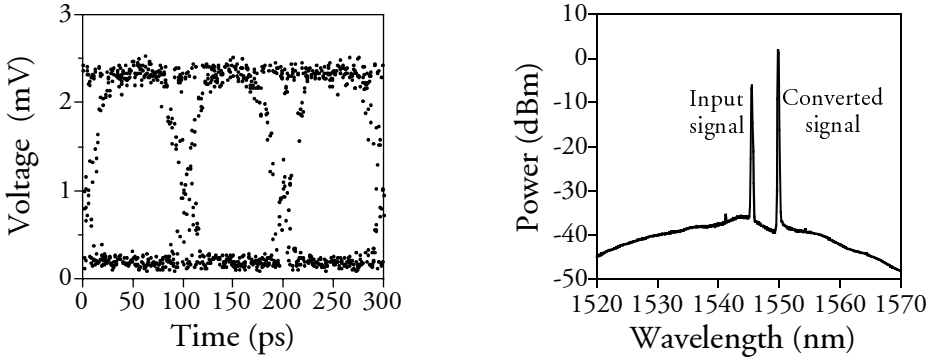

Fig. 5.4: Eye diagram of the wavelength converted signal at 10 Gbit/s in an MI (left) and the optical spectrum at the output of the converter in 0.1 nm (right). Conversion is from 1545 to 1550 nm.

In order to demonstrate the wavelength independence of the MI, Fig. 5.5 shows the measured penalty as a function of the signal wavelength (left) and CW wavelength (right). As seen, an excellent performance is achieved over the entire EDFA window with a pre-amplified penalty below 1 dB. The reason for a higher penalty at long wavelengths is that the gain peak of the MI is situated at ~1525 nm. The negative penalty at short wavelengths is caused by an increase in extinction ratio of the converted signal compared to the back-to-back signal. As mentioned in chapter 2, and in the beginning of this chapter, this regenerative capability is one of the features that characterise IWCs and is a consequence of the non-linear transfer function shown in Fig. 5.1. Chapter 6 deals with all-optical regeneration in IWCs in more detail.

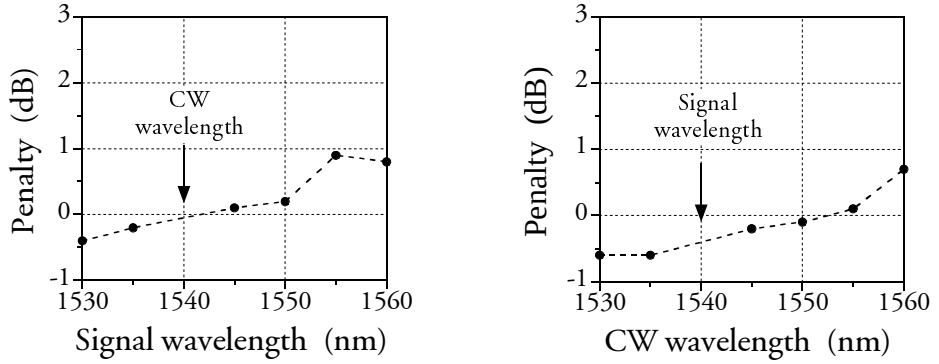

Fig. 5.5: Penalty at 10 Gbit/s in an MI vs. the signal wavelength with the CW wavelength at 1540 nm (left) and vs. the CW wavelength with the signal wavelength at 1540 nm (right).

5.2 High-speed performance of IWCs

By following the guidelines for high-speed XGM conversion described in chapter 4, high-speed operation of IWCs is also possible. This will be demonstrated in the present section, giving experimental results for conversion at 20 Gbit/s in both MZIs and MIs and at 40 Gbit/s in an MZI. Furthermore, a scheme for increasing the IPDR of MZIs will be illustrated at 40 Gbit/s.

5.2.1 20 Gbit/s wavelength conversion in IWCs

The possibility of operating MZIs and MIs at 20 Gbit/s will be demonstrated in the following starting with conversion in a single MZI and then moving on to a straight-line experiment with two MIs. The results are based on [p17] and [p4], respectively.

20 Gbit/s conversion in an all-active MZI

The set-up used for the experiment is depicted in Fig. 5.6. A gain-switched DFB laser at 1554 nm generates optical pulses at 10 GHz that are compressed to ~6 ps in a DCF, modulated at 10 Gbit/s and finally multiplexed to 20 Gbit/s. This signal is then launched into the MZI co-directionally with CW light at 1549 nm. After

conversion, the converted signal is filtered out and detected by the pre-amplified receiver, where an EA is used to demultiplex the signal to 10 Gbit/s before BER measurements. In order to allow for conversion at 20 Gbit/s, the MZI has been optimised according to the guidelines for high-speed operation, i.e., the interferometer arms are long (1200 μm), the input/output sections are relatively short (~200 μm) and the confinement factor is 0.45. Additional information about the MZI can be found in [129].

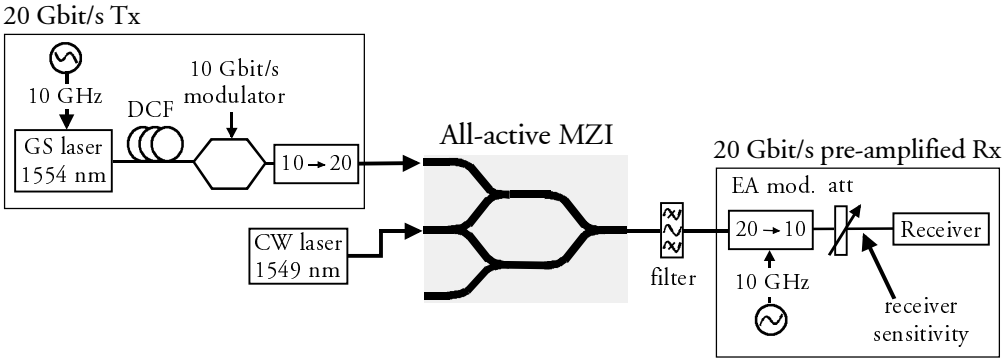

Fig. 5.6: Experimental set-up for 20 Gbit/s wavelength conversion in an all-active MZI converter.

Fig. 5.7 shows the back-to-back signal (left), the converted signal (middle) and the resulting BER measurements after demultiplexing to 10 Gbit/s (right). As seen, good performance has been achieved, however, pulse broadening and extinction ratio degradation can also be noted, which is the reason for the small pre-amplified penalty below 1 dB.

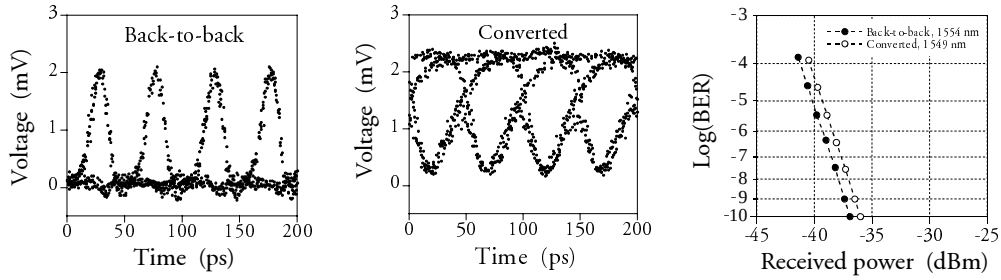

Fig. 5.7: Eye diagrams at 20 Gbit/s of the back-to-back signal at 1554 nm (left) and the converted signal at 1549 nm (middle). (right) The resulting BER curves after demultiplexing to 10 Gbit/s.

Straight-line experiment at 20 Gbit/s with 2 all-active MIs

As pointed out in section 5.1, the conversion speed of MIs is higher compared to MZIs at moderate bit rates. To evaluate this, the performance of a cascade of two all-active MIs will be illustrated here.

Fig. 5.8, showing the experimental set-up, illustrates that the back-to-back signal at 1563 nm is wavelength converted to 1559 nm after the first MI and to 1555 nm after the second MI.

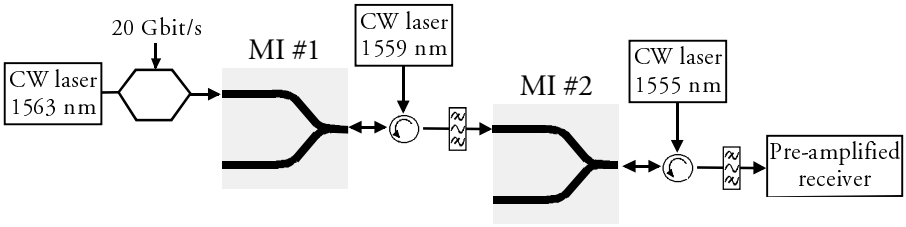

Fig. 5.8: Experimental set-up for 20 Gbit/s wavelength conversion in two all-active MIs in cascade. The pre-amplified receiver contains demultiplexing to 10 Gbit/s.

The measured eye diagrams are given in Fig. 5.9 for the back-to-back signal (left) and the converted signals after the first (middle) and second MI (right). As can be seen, the large conversion bandwidth of the MIs is confirmed in that both converted signals are clear and open with fast rise and fall times together with a high extinction ratio in both cases.

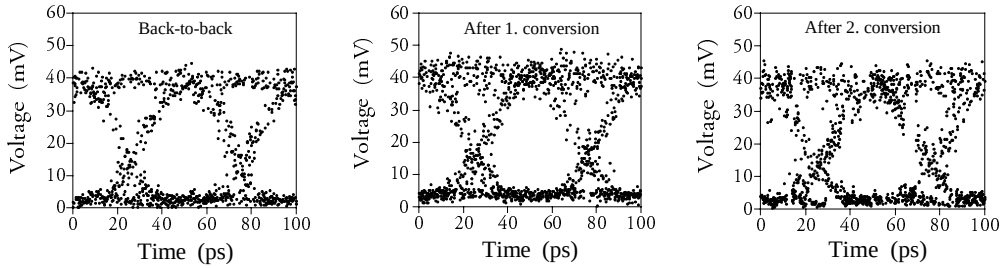

Fig. 5.9: Measured eye diagrams at 20 Gbit/s of the back-to-back signal at 1563 nm (left), after the first converter at 1559 nm (middle) and after both converters at 1555 nm (right).

The good performance is also verified by the BER measurements in Fig. 5.10, where a penalty of ~0.5 dB is achieved after the first converter and a negligible penalty after the second converter. The reason for the lower penalty after the second MI is due to an increased extinction ratio, which is caused by the fact that the second converter has longer interferometer arms (1150 μm compared to 800 μm for the first converter) resulting in a higher modulation bandwidth.

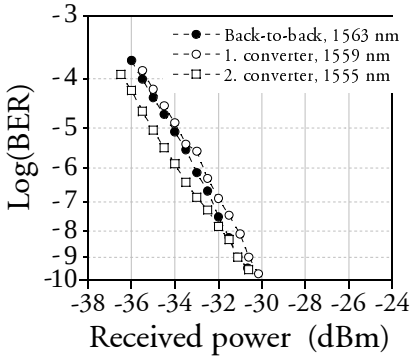

Fig. 5.10: BER curves after demultiplexing from 20 to 10 Gbit/s for the back-to-back signal and the converted signal after one and two MIs, respectively.

Besides the high modulation bandwidth obtained after two converters, another advantage of the all-optical IWCs is their flat phase response compared to electro-optical solutions. Therefore, the cascadability of these devices is superior as demonstrated theoretically in [101,133] and experimentally in [133].

5.2.2 40 Gbit/s wavelength conversion in an all-active MZI

The 20 Gbit/s wavelength conversion experiment described in section 5.2.1, using the all-active MZI, shows that the converted signal is substantially broader than the input signal. The broadening is caused by the limited carrier lifetime, making operation at 40 Gbit/s impossible with the specific device. Although the guidelines for high-speed operation discussed in chapter 4 can be followed to obtain a device with a higher modulation bandwidth, the carrier lifetime will always set an upper limit on how fast conversion can be achieved. In this section, a technique that minimises the influence of the carrier lifetime will be described [134] and following this, the feasibility of the technique will be demonstrated by a system experiment carried out at 40 Gbit/s. The results are based on [p19,p23].

The technique, which is called the differential control scheme [134], is illustrated in Fig. 5.11 for an MZI using co-directional propagation of the data signal and CW light. It is noted, however, that counter-directional propagation also can be applied and that also MIs can be used, although co-directional operation in an MZI results in the highest modulation bandwidth. Turning back to Fig. 5.11, the input signal is split in two and injected into both the upper and lower interferometer arm. As shown in the figure, the upper pulse is unaltered, whereas the lower pulse is attenuated and delayed by $\Delta\tau$ compared to the upper pulse. As in the case of standard conversion (see Fig. 5.1), the input pulses control the interference of the CW light at the output of the MZI.

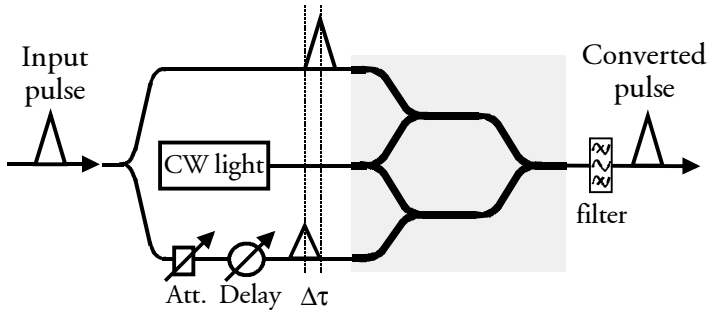

Fig. 5.11: Illustration of the differential control scheme for high-speed RZ wavelength conversion in an MZI. An input pulse is split in two, where the pulse in the lower part is attenuated and delayed with $\Delta\tau$ compared to the pulse in the upper part. Thereby, a short switching window is created for the CW light.

The purpose of injecting a pulse in both interferometer arms is illustrated in Fig. 5.12. The pulse that enters the MZI first, i.e., the pulse in the upper interferometer arm, causes a phase shift (Phase 1) as depicted in the top of the figure, where the tail is caused by the limited carrier lifetime. The pulse in the lower interferometer arm causes a similar phase shift (Phase 2), but since the power of the pulse is lower compared to the first pulse, the phase shift is smaller. Remembering that it is the phase difference between the interferometer arms that is important for the performance of the MZI, it can be seen that by having a correct time delay ($\Delta\tau$) between the pulses, the detrimental effect of the slow carrier recovery can be avoided. Note that since one of the phase shifts has to cancel the tail of the other phase shift, it is very important that they have different values. Since the effect of the slow carrier recovery is cancelled, the differential control scheme can result in very short switching windows allowing for higher conversion speeds than with the standard conversion technique. It should be mentioned, though, that the scheme is only applicable for RZ signals. Furthermore, due to the added complexity, the differential scheme is only attractive for high-speed conversion (>10 Gbit/s). It is emphasised, however, that at high bit rates, RZ signals are likely to be used due to superior transmission properties compared to NRZ [135].

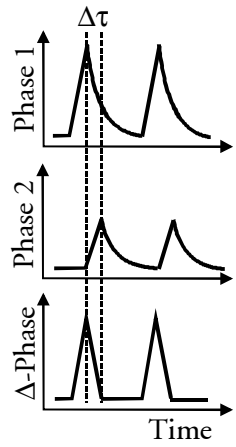

Fig. 5.12: Illustration of the effect of the differential scheme. The two pulses create a phase shift in the interferometer arms so that a short switching window is obtained.

The influence of the differential control scheme is demonstrated experimentally in Fig. 5.13, giving measured eye diagrams of converted signals using the MZI described in section 5.2.1. The figure shows eye diagrams using standard conversion (left), non-optimised differential control, i.e., non-optimised $\Delta\tau$ (middle) and fully optimised differential control (right). Clearly, the tail of the converted signal caused by the relatively slow recovery time is suppressed as $\Delta\tau$ is optimised.

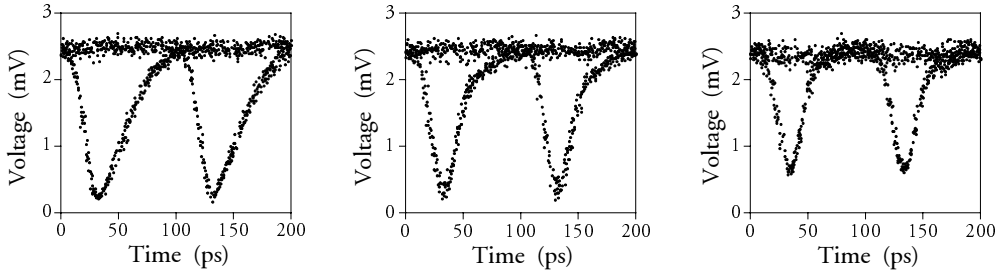

Fig. 5.13: Eye diagrams of a converted signal at 10 Gbit/s using an MZI without differential control (left), with partial differential control (middle) and with fully optimised differential control (right).

Fig. 5.13 clearly shows the strength of the differential control scheme for high-speed operation, and the scheme is therefore assessed at 40 Gbit/s with the experimental set-up depicted in Fig. 5.14. The set-up is in principle the same as for the 20 Gbit/s experiment (see Fig. 5.6) except that the differential control scheme is implemented and that the MUX and DMUX is a 10 to 40 Gbit/s and 40 to 10 Gbit/s, respectively. It is emphasised that the employed MZI is the one used for 20 Gbit/s standard conversion (see section 5.2.1) and that standard conversion at 40 Gbit/s is not possible with this specific device.

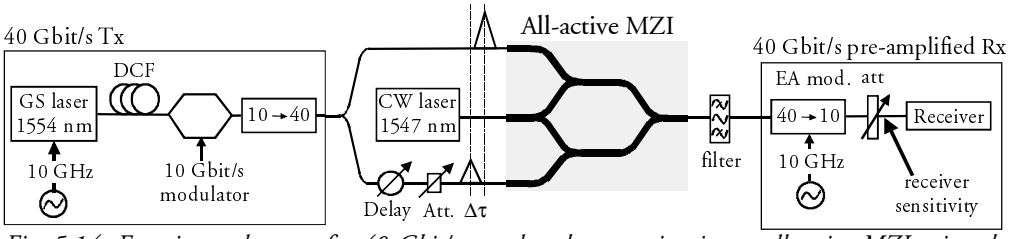

Fig. 5.14: Experimental set-up for 40 Gbit/s wavelength conversion in an all-active MZI using the differential control scheme.

The performance of the wavelength converter at 40 Gbit/s is illustrated in Fig. 5.15, showing eye diagrams of the input signal at 1554 nm (left), the converted signal at 1547 nm (middle) and the optical spectrum in 0.1 nm at the output of the MZI (right). As is evident, the eye diagram of the converted signal is both clear and open (extinction ratio in excess of 10 dB). Furthermore, the OSNR at the output is as high as ~40 dB, clearly a very attractive feature when considering cascadability of these devices. Another attractive feature is a high optical output power of ~0 dBm from the converter. The small peaks, which can be seen in the optical spectrum, are FWM products. These are of no importance, however, since the signal-to-FWM ratio is in excess of 35 dB before the optical filter.

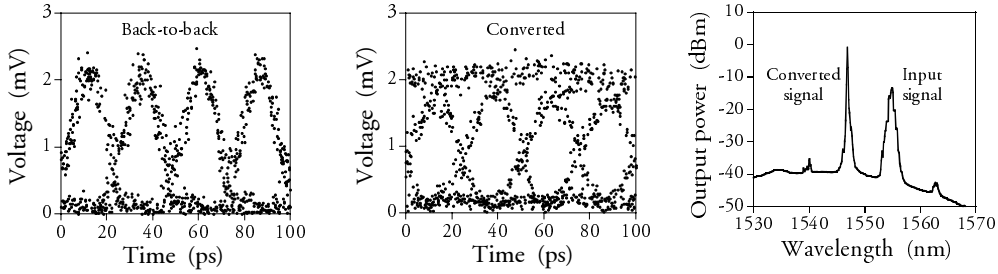

Fig. 5.15: Measured eye diagrams at 40 Gbit/s of the back-to-back signal at 1554 nm (left) and the converted signal at 1547 nm (middle). (right) Optical spectrum in 0.1 nm after the MZI.

It should be noted that the RZ signal format at the input is transformed to an NRZ format at the output of the converter due to the relatively wide switching window seen in Fig. 5.13. A higher modulation bandwidth could in fact be obtained by decreasing $\Delta\tau$ even more than was done in the experiment but at the expense of a

lower extinction ratio as also seen in Fig. 5.13. Despite the NRZ format, very good performance is obtained as is evident from the BER measurements in Fig. 5.16, showing that conversion at 40 Gbit/s is achieved with a pre-amplified penalty of only 0.6 dB. Comparing this result with the result given in section 5.2.1, it can be concluded that the use of the differential control scheme has resulted in an increase of the bit rate by a factor of two, while slightly reducing the penalty.

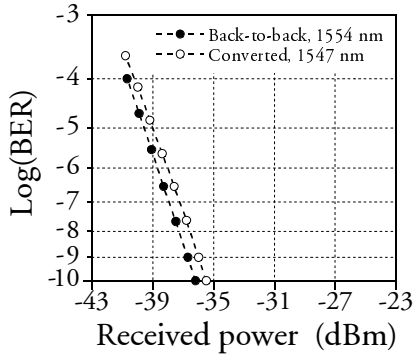

Fig. 5.16: BER curves after demultiplexing from 40 to 10 Gbit/s for the back-to-back signal and the converted signal.

As demonstrated in this section, the differential control scheme is a powerful tool to obtain high-speed operation. This is achieved at the expense of added complexity, however, since the length of the two paths to the interferometer arms has to be controlled very accurately. It is therefore still very attractive to realise IWCs that are capable of high-speed operation with the standard conversion technique since it is a less expensive solution.

Recently, a new generation MZIs incorporating 2000 μm long interferometer arms have been developed by Opto+ showing promising performance for 40 Gbit/s standard conversion. Furthermore, the output section of these new devices has been made passive in order to optimise the performance of the differential control scheme. As mentioned in the beginning of this chapter, an active output section has the advantage that a high output power is ensured. The drawback, however, is that the converted signal experiences XGM by the original data signal. In the case of the differential control scheme, two original data signals propagate through the output section making the performance even more sensitive to unwanted XGM. In addition, the XGM will also be influenced by interferometric cross talk since the two signals are at the same wavelength.

The results of an experiment at 40 Gbit/s with this new device can be seen in Fig. 5.17, giving eye diagrams of the converted signal using standard conversion (left) and the differential scheme (right). Although the eye diagram in the left part of Fig. 5.17 has a low extinction ratio and is quite noisy, it is emphasised that, to the author's knowledge, it is the first open eye diagram that is obtained at 40 Gbit/s

using the standard conversion technique in an MZI. The fast conversion speed is also indicated by the fact that the signal has not been fully transformed to an NRZ signal. In the right part of Fig. 5.17 it can be observed that the RZ format is preserved when the differential control scheme is used, which also indicates the high-speed potential. In addition, the extinction ratio of the converted signal using the differential scheme is above 9 dB.

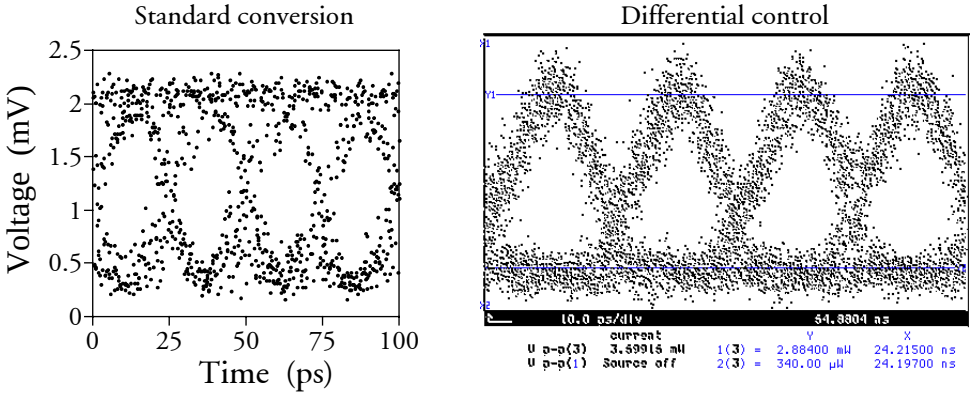

Fig. 5.17: Eye diagram of a converted signal at 40 Gbit/s using the standard conversion technique (left) and the differential control scheme (right). The all-active MZI used in these experiments incorporates 2000 µm long interferometer arms for high-speed operation. T. Fjelde, M. L. Nielsen and H. Wessing from Research Center COM have obtained the result in the right part of the figure.

Wavelength conversion at 40 Gbit/s using the differential scheme in an MZI has already resulted in RZ formats [61], however, with an active/passive device. This, together with the results demonstrated above, indicates that the highest speed potential is indeed obtained with devices incorporating passive output sections so that unwanted XGM is avoided, although it has not been finally verified yet.

5.2.3 Scheme for increased input power dynamic range of IWCs

As demonstrated so far, IWCs have several desirable features such as wavelength independence, high-speed capability and the ability to convert to signals with a high extinction ratio and OSNR. One of the concerns of IWCs, however, is that their IPDR is limited to 3-4 dB due to the sinusoidal transfer function. This will be a problem in an all-optical network because of signals entering optical nodes with different power levels, ageing of EDFAs, etc. Some kind of power equalisation is therefore required to ensure good performance. Concerning all-active IWCs, a straightforward solution is to control the bias current to the input sections according to the optical input power. This is possible since all sections in the all-active devices are individually biased. An advantage of this approach is that the SOAs used for power equalisation are already monolithically integrated into the structure yielding a compact solution. Furthermore, the scheme is inherently fast (~ns range) and therefore only limited by the choice of electronics.

Here, an experiment carried out at 40 Gbit/s, using the above-mentioned technique to increase the IPDR of an MZI, will be described. The results are obtained with the MZI described in section 5.2.1 and are based on [p19]. Fig. 5.18 shows the all-active MZI in a set-up exploiting the differential control scheme, why the bias currents for both the upper and lower input section have to be controlled. Except for this, the experimental set-up is similar to that shown in Fig. 5.14. As seen, the input power variation is defined at the point before the input pulse is split in two. So, depending on the input power to the converter, the bias currents are adjusted in both input sections so that optimum performance is maintained.

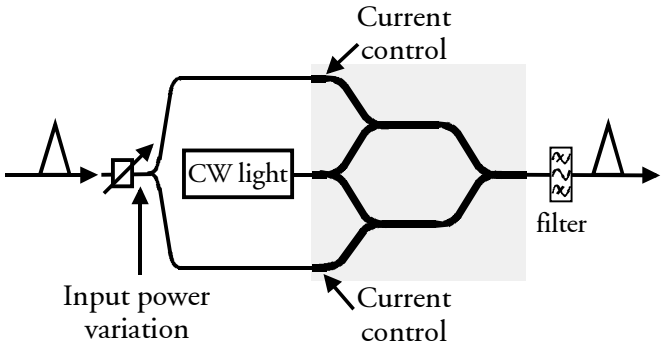

Fig. 5.18: Schematic of an MZI exploiting the differential control scheme. In order to increase the input power dynamic range, the bias current to the upper and lower input section is controlled in accordance with the input power variations. The attenuator and delay line necessary to achieve correct operation with the differential control scheme is not shown in the figure for simplicity.

In order to assess the feasibility of this scheme, Fig. 5.19 shows the measured penalty as a function of the input power variation to the two input sections with and without control of the bias currents.

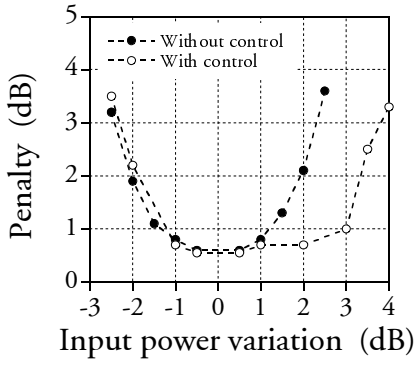

Fig. 5.19: Measured penalty at 40 Gbit/s as a function of the input power variation to the MZI with and without control of the bias currents to the two signal input sections.

As seen, an improvement is achieved at high input powers since the increase in input power is counteracted by a decrease in the bias currents from 105 to 85 mA. The resulting IPDR is ~6 dB at 40 Gbit/s (at an excess penalty of 2 dB). It can also be

observed that contrary to what is expected, there is no improvement at low input powers but this was not achieved in the specific experiment.

Whether an IPDR of ~6 dB is enough will depend on the application, where in the network the converter is placed, etc. Another solution to perform power equalisation is to place an amplifier in front of the IWCs, e.g., an SOA [131] as described in chapter 3 or an EDFA [131,132] and as shown experimentally at 10 Gbit/s in [132] this led to an IPDR of ~28 and ~40 dB, respectively. The drawback, however, is the added complexity due to an extra amplifier in front of the IWC and furthermore, the solution incorporating an EDFA only allows for power equalisation on a ms scale.

5.3 Conversion to the same wavelength

In optical networks deploying optical wavelength conversion, there will be a need to convert to the same wavelength as the input signal. Although this may sound strange at first, since it simply equals the situation where no conversion is performed, it is a natural requirement for full flexibility in the network. Given that a wavelength converter is deployed in specific nodes and depending on the wavelength usage throughout the network, it might be advantageous to keep the wavelength assignment on a specific channel, i.e., conversion to the same wavelength. Another application, where conversion to the same wavelength is a very attractive feature, is for internal use in an OXC. Here, the functionality can be used to design a more flexible architecture, a feature that has been exploited in the OPEN OXC [31].

It can be argued that conversion to the same wavelength can be accomplished simply by bypassing the converter. However, to decide whether the converter has to be bypassed or not requires an optical space switch before the converter. Furthermore, the quality of an optical signal is not necessarily the same after a space switch and a wavelength converter, which means that the performance is dependent on whether conversion to the same wavelength is performed or not. Therefore, conversion to the same wavelength will most likely be accomplished in the converter itself.

Both XGM in SOAs and XPM in MZIs can enable conversion to the same wavelength if counter-directional propagation is used. As pointed out in chapter 4, however, the main drawbacks of the counter-directional scheme are a lower speed potential than the co-directional scheme [56] and accumulation of jitter if many converters are cascaded [114]. Alternative solutions are therefore necessary and consequently, this section presents two different schemes based on SOAs, where conversion to the same wavelength is possible without having the disadvantages of the counter-directional scheme.

5.3.1 Dual-stage wavelength converter

The first solution for conversion to the same wavelength is based on a dual-stage converter employing XGM and XPM [136,p9]. The scheme is depicted in Fig. 5.20, which illustrates conversion of an incoming signal at λ_{in} to a fixed internal wavelength at $\lambda_{internal}$ by XGM in the first stage and then to the output wavelength by XPM in the second stage. Co-directional coupling is used in the first stage to ensure a high modulation bandwidth and jitter-free conversion. As a consequence of co-directional coupling, a fixed filter is needed at the output of the SOA to remove the original data signal before the second stage. The second stage is here depicted as an MI, but it could be an MZI as well. In the MI, the internal signal is converted to the output signal at the desired wavelength. By choosing the wavelength of the internal signal different than the input and output wavelengths, conversion to any network wavelength is possible, including conversion to the same wavelength.

There are many advantages related to the dual-stage converter since it exploits the advantages from both XGM and XPM. The XGM converter ensures polarisation independent operation and a high IPDR. The XPM converter, on the other hand, ensures wavelength independent operation, a small chirp associated with the converted signal and 2R regeneration.

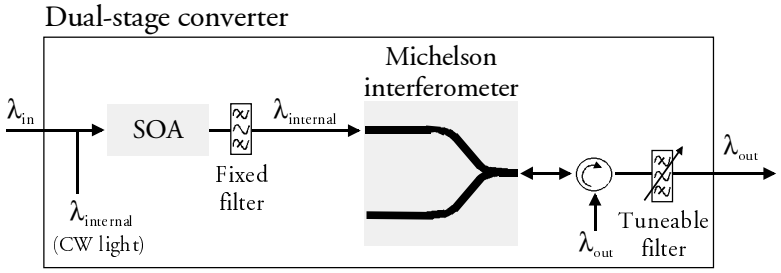

Fig. 5.20: Schematic of the dual-stage converter employing XGM in the first stage and XPM in the second stage. If the internal wavelength is chosen different than the input and the output wavelengths, then conversion to any network wavelength is possible, including conversion to the same wavelength. Here, an MI is shown, but the scheme is also applicable for an MZI.

In order to assess the performance of the dual-stage converter and to demonstrate the ability to convert to the same wavelength, an experiment at 20 Gbit/s has been carried out [p9]. The experimental set-up is similar to the one illustrated in Fig. 5.20 and conversion is performed from 1560 nm (input wavelength) to 1555 nm (internal wavelength) and back to 1560 nm (output wavelength). Fig. 5.21 shows the recorded eye diagrams at 20 Gbit/s of the back-to-back or input signal (left), the internal signal after the XGM converter (middle) and the output signal after the XPM converter (right). As seen, both the internal and output eye diagrams are clear and open indicating a good performance. Furthermore, the extinction ratio degradation that can be observed after the XGM converter is almost fully regenerated after second stage employing the XPM converter.

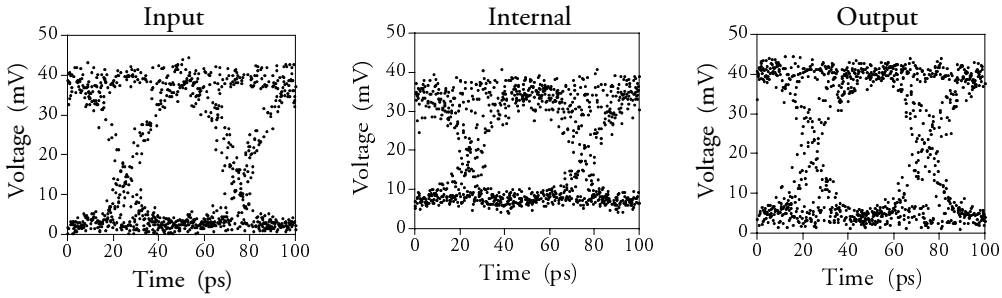

Fig. 5.21: Eye diagrams at 20 Gbit/s of the back-to-back signal at 1560 nm (left), the signal after XGM conversion at 1555 nm (middle) and the signal after XPM conversion at 1560 nm (right).

The resulting BER measurements are shown in Fig. 5.22, where it is demonstrated that insertion of the XGM converter results in a pre-amplified penalty of ~3.5 dB due to extinction ratio degradation. After the XPM converter, where the extinction ratio is partly recovered, the total penalty of the dual-stage converter is ~1.5 dB.

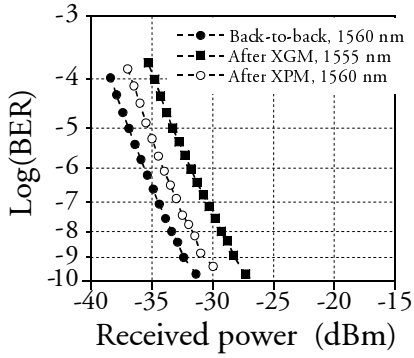

Fig. 5.22: BER curves after demultiplexing from 20 to 10 Gbit/s for the dual-stage converter.

The good performance of the dual-stage converter has also been demonstrated in a similar set-up [136], where a re-circulating loop experiment allowed for 10 round trips at 10 Gbit/s. The performance was primarily limited by jitter accumulation from the first stage caused by counter-propagation in the XGM converter.

5.3.2 Dual-order mode Mach-Zehnder wavelength converter

In a recently developed all-active dual-order mode (DOMO) MZI, conversion to the same wavelength is possible in the co-directional propagation scheme [126]. This has been made possible, as shown in Fig. 5.23, by exploiting mode separation between the input signal and CW light achieved by multi-mode interference (MMI) couplers [125] at the input and output of the interferometer arms. Thereby, the original input signal is suppressed in the device itself, which also has the advantage that filter-less operation is possible, clearly attractive if a tuneable output wavelength is required.

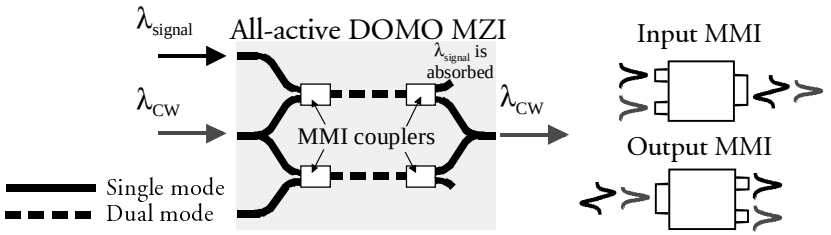

Fig. 5.23: Schematic of an all-active dual-order mode (DOMO) Mach-Zehnder converter incorporating MMI couplers at the input and output of the interferometer arms. Conversion to the same wavelength is achieved by mode separation of the signal and CW light in the MMIs. Consequently, the active waveguides in the interfero-meter arms are designed to sustain two lateral modes, whereas all other active waveguides are single-mode.

The operation of the device is as follows: The input signal and CW light are coupled into the first-order and fundamental mode by the input MMI. After traversing the SOA in the interferometer arm, which is designed to sustain two lateral modes, the signal and CW light are separated in the output MMI (identical to the input MMI). Consequently, the signal light is absorbed in an unpumped waveguide, whereas the converted signal is guided to the output of the converter.

Here, a DOMO MZI with 1800 μm long interferometer arms will be assessed at 10 Gbit/s using the set-up in Fig. 5.24 for conversion to the same wavelength as well as different combinations of the signal and CW wavelengths. It is emphasised that no filter was used at the output of the MZI in the experiments. A detailed description of the device and structure is given in [137] and the presented results are based on [p24] and [p30], respectively.

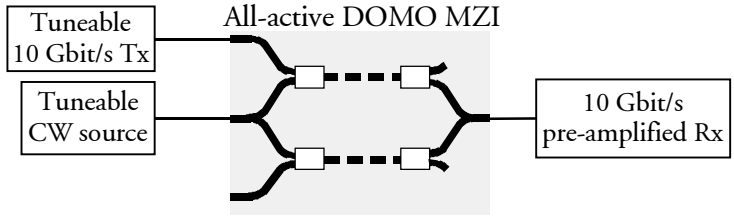

Fig. 5.24: Experimental set-up for assessment of the performance of the DOMO MZI at 10 Gbit/s.

The performance of the DOMO MZI is illustrated in Fig. 5.25, showing the eye diagram of the back-to-back signal at 1545 nm (left), the converted signal at 1550 nm (middle) and the corresponding spectrum at the output of the DOMO (right). As seen, a clear and open eye diagram of the converted signal is obtained. It can also be observed, however, that this specific DOMO causes extinction ratio degradation even though the converter obviously is not limited by speed.

Since no filter is supposed to be applied at the output of the DOMO, a high input signal suppression ratio (ISSR) is of course crucial for this type of device in order to avoid influence from cross talk. The output spectrum demonstrates in this case a high ISSR and OSNR of ~25 dB and ~38 dB, respectively.

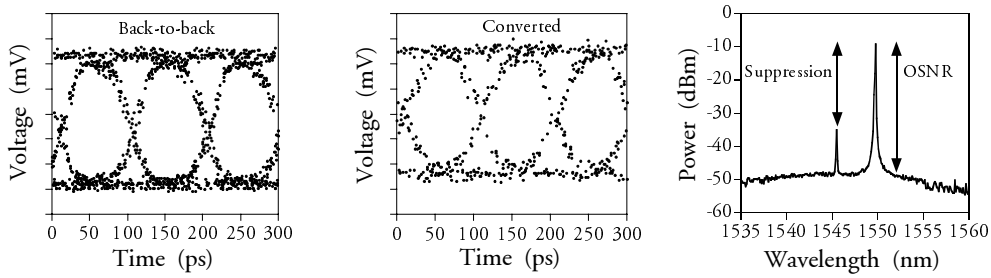

Fig. 5.25: Measured eye diagram of the back-to-back signal at 1545 nm (left), the converted signal at 1550 nm (middle) and the optical spectrum at the output of the converter in 0.1 nm (right).

The capability of the DOMO as a wavelength independent device is demonstrated in Fig. 5.26, showing the pre-amplified penalty and ISSR at 10 Gbit/s as a function of the signal wavelength (left) and CW wavelength (right). Not taking conversion from 1550 to 1530 nm into account, it can be seen that nearly wavelength-independent conversion is achieved with a resulting penalty between ~1.2 and ~2.4 dB. This penalty is mainly caused by the extinction ratio degradation observed in Fig. 5.25. The penalty of ~4.5 dB for conversion from 1550 to 1530 nm is caused by a low ISSR of ~7 dB resulting in a degradation due to cross-talk. The reason for this low ISSR is that the converted signal is far from the gain peak resulting in a low output power and therefore also a low ISSR.

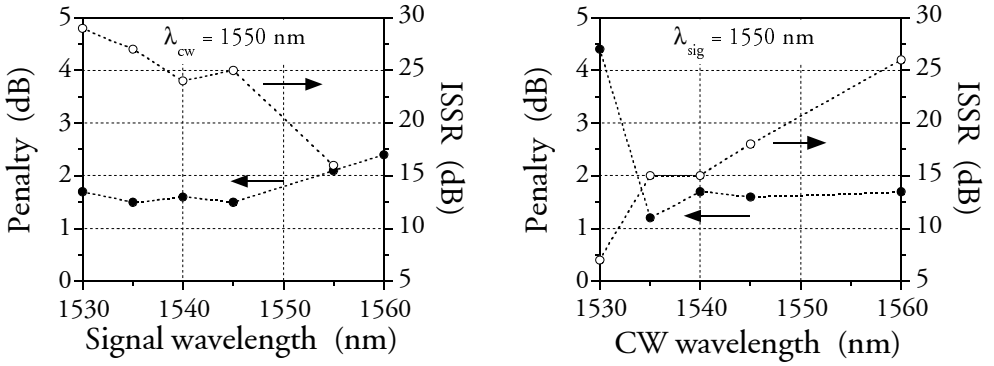

Fig. 5.26: Measured penalty and input signal suppression ratio (ISSR) at 10 Gbit/s as a function of the signal wavelength for a fixed CW wavelength of 1550 nm (left) and CW wavelength for a fixed signal wavelength of 1550 nm (right).

In the case of conversion to the same wavelength, a high ISSR is even more important due to the influence of interferometric cross-talk. This is illustrated in Fig. 5.27, showing eye diagrams of the converted signal in the following cases: (left) difference of 0.1 nm between the signal and CW wavelength, (middle) identical wavelengths and (right) identical wavelengths but with optimised power levels. With a wavelength difference of 0.1 nm (~12.5 GHz), the original data signal is outside the receiver bandwidth and is therefore power-addition cross-talk. An approximate ISSR of 20 dB (see Fig. 5.26) is therefore enough to make the influence negligible, which

is also verified by the eye diagram. On the other hand, when the wavelengths are identical (ensured by the use of a wavemeter), the cross-talk is within the electrical bandwidth and is therefore interferometric cross-talk. Keeping in mind that the operating conditions for the DOMO MZI does not change for a wavelength shift of 0.1 nm, the poor performance seen in Fig. 5.27 (middle) can only be caused by the influence of interferometric cross-talk. By changing the power levels, however, it is possible to increase the ISSR and obtain the eye diagram given in the right part of the figure. Comparing the result with the eye diagram in the left part of the figure, it can be observed, though, that the performance is still affected by cross-talk.

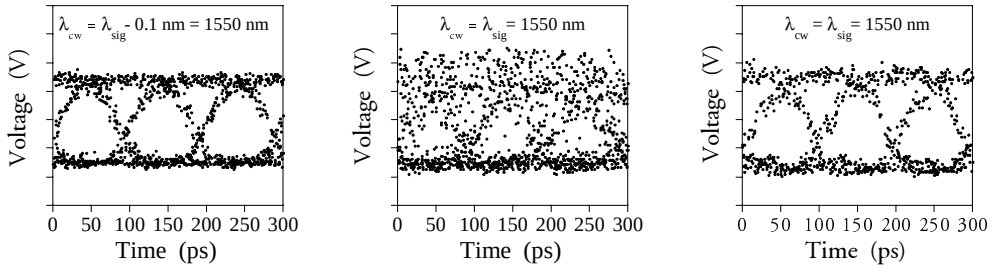

Fig. 5.27: Eye diagrams of the converted signal at 10 Gbit/s when signal and CW wavelength differ with 0.1 nm (left), exact same wavelength (middle) and exact same wavelength but after optimisation of the ISSR (right).

The poorer performance for conversion to the same wavelength can also be seen in Fig. 5.28, showing the penalty as a function of the signal and CW wavelength. A penalty between ~3 to ~4 dB is obtained, which corresponds to an excess penalty of ~2 dB compared to conversion to different wavelengths. Still, the penalty is also in this case almost independent of wavelength indicating that the operation of the MMIs also is nearly wavelength-independent within the examined range.

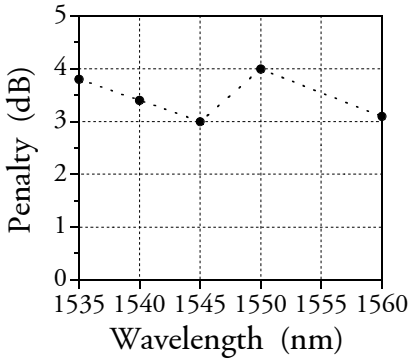

Fig. 5.28: Penalty at 10 Gbit/s as a function of the wavelength. Conversion is performed to the same wavelength as the input signal, i.e., equal signal and CW wavelength.

The high-speed potential of the DOMO MZI is illustrated in Fig. 5.29, showing the eye diagram of a converted signal (1555 to 1550 nm conversion) at 20 Gbit/s with an RZ input signal (left) and the corresponding spectrum at the output of the converter

(right). As seen, a noisy but nevertheless open eye diagram is obtained. Furthermore, the optical spectrum demonstrates that the conversion has been achieved with an OSNR of ~30 dB and an ISSR of ~27 dB. As mentioned, the DOMO MZI incorporates 1800 µm long interferometer arms, which, judging from the results on the standard converter in section 5.2, should result in a better performance than observed in Fig. 5.29. A probable reason for the lower conversion speed is that there is a smaller mode overlap between the signal and CW light in the DOMO compared to the standard converter. The smaller mode overlap in the DOMO results in a smaller effective confinement factor in the interferometer arms and therefore also a lower modulation bandwidth. In addition, a broad width of the waveguide has to be used to sustain two lateral modes. The broad width increases the optical area, which also decreases the modulation bandwidth (see comments in section 4.2.2).

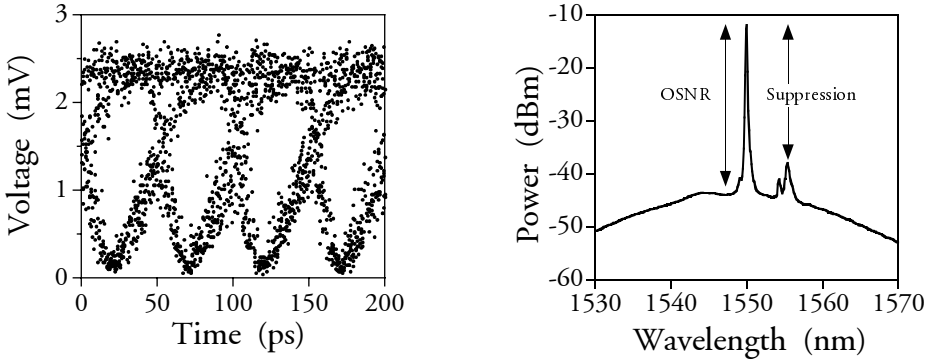

Fig. 5.29: Eye diagram at 20 Gbit/s of a converted signal from 1555 to 1550 nm (left) and the optical spectrum at the output of the DOMO MZI measured in 0.1 nm (right).

5.4 Novel scheme for wavelength conversion in IWCs

As mentioned in the beginning of this chapter, the chirp properties of IWCs are superior compared to, e.g., XGM-based converters. Still, as explained in section 5.1, the following trade-off between speed and transmission properties normally exists in IWCs: Inverting operation results in the highest modulation bandwidth but also in a small positive chirp that limits transmission on standard fiber. Non-inverting operation has a lower modulation speed but results in good transmission properties.

In this section, a novel conversion scheme, that shows good transmission properties and high-speed performance in IWCs simultaneously, will be demonstrated. The results are based on [p28,p38].

5.4.1 Principle of operation of the novel conversion scheme

For comparison, Fig. 5.30 shows an illustration of the conventional (left) and novel scheme (right) for wavelength conversion in IWCs (here shown for MZIs). In the conventional scheme, a data and CW signal is coupled into the interferometer as

shown, resulting in an inverted or non-inverted signal at λ_{CW} (non-inverted shown in the figure). In the novel scheme an additional clock signal (with a repetition rate corresponding to the bit rate) is injected into the lower interferometer arm and, as in the conventional scheme, the wavelength converted signal of interest is at λ_{CW}. Here, inverted and non-inverted operation is also possible, however with a different appearance of the converted signal. When a logical one is present in the data signal, i.e., the clock and data signals are identical, the CW light will experience equal phase conditions in the interferometer arms resulting in a constant output power. On the other hand, with a zero in the data signal, the interferometer will be unbalanced resulting in a pulse at the output. The right part of Fig. 5.30 shows an inverted signal. To assure good performance, the clock signal will have to be synchronised to the data signal, which means that clock recovery has to be applied.

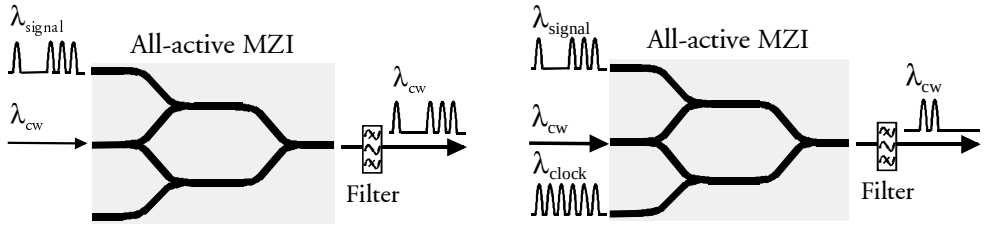

Fig. 5.30: Illustration of the conventional (left) and the novel scheme (right) for wavelength conversion in an SOA-based interferometric device. It is noted that the novel scheme is only compatible with RZ signals since a clock signal is used. The novel scheme is also applicable for MIs.

There are several advantages by applying the clock signal as will be shown in the following section. One is low chirp of the converted signal resulting in transmission properties, which are similar to those obtained for non-inverting operation of the conventional scheme. This can be understood by noting that the converted pulses are created by the clock signal, i.e., the data signal only serves to suppress pulses in the clock signal. If the converted pulses have the same polarity as the clock pulses (as is the case in the figure), this will therefore result in negative chirp on the converted signal, i.e., the same as for non-inverting operation with the conventional conversion scheme. Another advantage is that the modulation bandwidth is maintained or even improved compared to the conventional scheme since the clock signal allows for additional optimisation of the operating conditions of the IWC. It should be mentioned that the advantages are obtained at the expense of increased complexity.

5.4.2 Speed performance and transmission properties of the novel scheme

In order to make a fair assessment of the modulation bandwidth and transmission properties of the novel scheme, the results will be compared to what can be obtained using the conventional scheme using the same MZI for both conversion schemes. The experimental set-up illustrated in Fig. 5.31 is used for assessment of the novel scheme. The MZI used in the experiments is that used for 20 and 40 Gbit/s wavelength conversion described in section 5.2.1 and 5.2.2, respectively.

Two gain-switched lasers generate 10 GHz pulses at 1546 and 1553 nm with pulse widths of ~25 ps. Here, the same electrical clock generator drives the gain-switched lasers, i.e., clock recovery has not been performed. After modulation of the data signal at 10 Gbit/s, it is injected into the MZI together with the clock signal and CW light at 1556 nm. At the output of the MZI, a filter selects the converted signal before detection and BER measurements. Note that an optical delay line is used before the MZI to obtain optimum alignment of the data and clock signal. The ~25 km of standard fiber in the set-up is inserted for the transmission experiments.

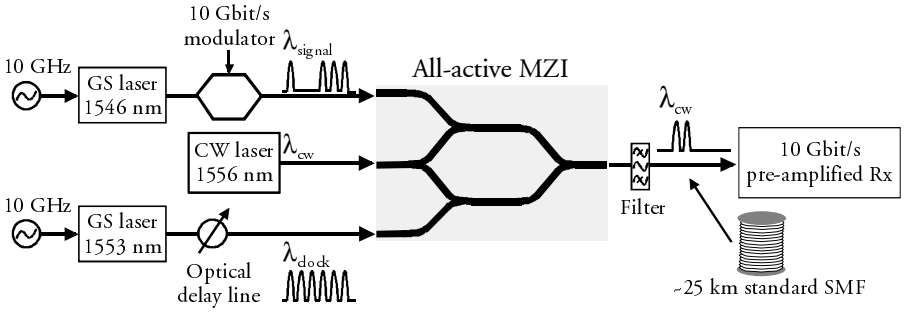

Fig. 5.31: Experimental set-up for assessment of the novel conversion scheme at 10 Gbit/s. The ~25 km of standard fiber is used for the transmission experiments.

The performance of the new scheme is illustrated in Fig. 5.32, giving pulse patterns of the back-to-back signal (left), the converted signal (middle) and the resulting BER measurements (right). As seen, conversion is achieved with a very good quality of the converted pulses with almost complete suppression of the original data pulses. This is even more evident from the right part of Fig. 5.33. The good performance is also illustrated by the BER curves in the right part of Fig. 5.32, showing that conversion has been obtained with negligible penalty. Note that even though the converted pulses have the shape of non-inverted RZ pulses, the polarity is indeed inverted compared to the input signal as explained above.

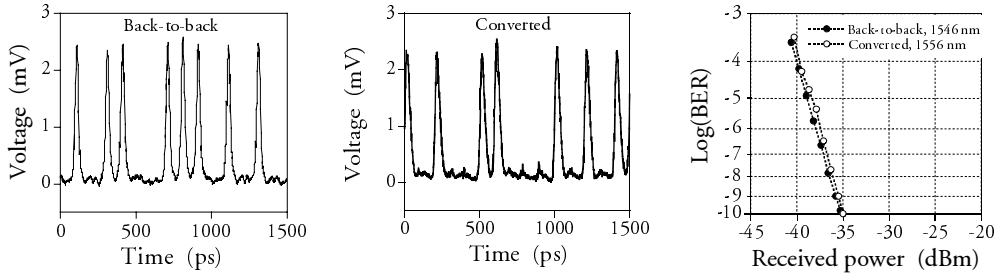

Fig. 5.32: Pulse patterns at 10 Gbit/s of the back-to-back signal at 1546 nm (left), the converted signal at 1556 nm (middle) and the corresponding BER measurements (right).

As mentioned, the novel scheme can result in a conversion speed that is comparable to or even better than what can be obtained with the conventional scheme. This is verified in Fig. 5.33, showing eye diagrams of the converted signal using the

conventional scheme (non-inverted and inverted in the left and middle part of the figure) and the converted signal using the novel scheme (right). It is emphasised that all results are obtained using the same MZI and that the device has been optimised for each specific experiment. As seen, superior speed performance is clearly achieved with the novel scheme, a clear separation between the eyes can be observed.

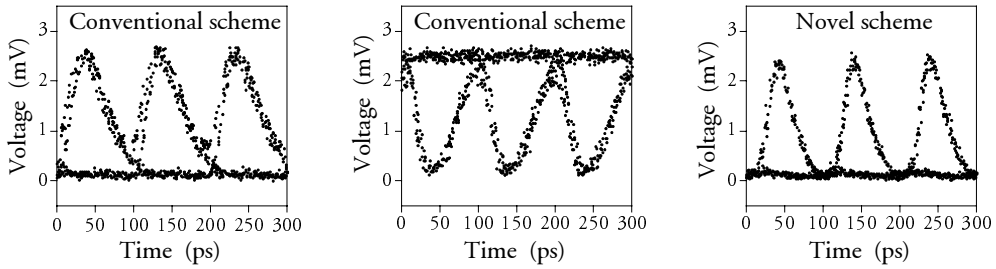

Fig. 5.33: Eye diagrams at 10 Gbit/s of the converted signal using the conventional scheme for non-inverting (left) and inverting operation (middle). (right) Eye diagram of the converted signal using the novel scheme for inverting operation.

To assess the transmission properties of the converted signals, a comparison of the two methods has been performed. The results can be seen in Fig. 5.34, giving the BER for the back-to-back signal and the converted signals using the conventional and novel scheme before (left) and after (right) transmission over ~25 km standard fiber. Note that operation of the MZI has been optimised for conversion and not transmission.

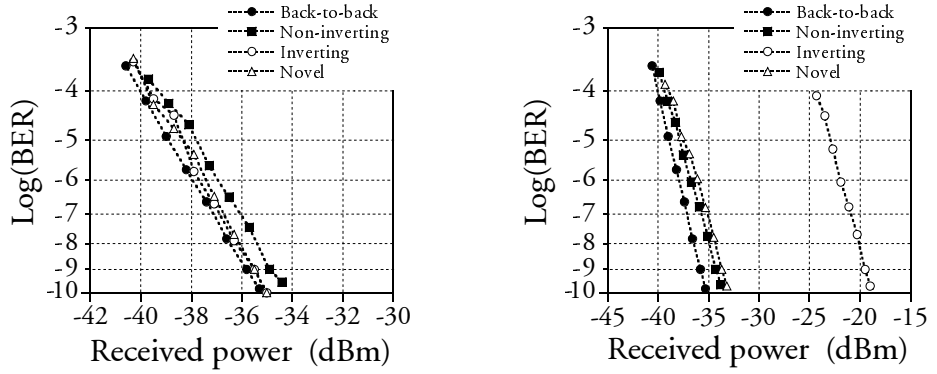

Fig. 5.34: BER measurements at 10 Gbit/s of the back-to-back signal and the converted signals using the conventional and novel scheme before (left) and after (right) transmission over 25 km standard fiber. Transmission is carried out after wavelength conversion.

As seen in the left part of the figure, nearly penalty-free conversion is achieved with the two schemes. The highest penalty is observed for conventional non-inverting operation, which primarily is due to the lower modulation bandwidth (see Fig. 5.33). As seen in the right part of Fig. 5.34, however, there is a difference after transmission. Inverting operation using the conventional scheme results in a pre-amplified penalty of ~17 dB due to the chirped output signal, whereas non-inverting

operation using the conventional scheme and conversion using the novel scheme results in an almost equal pre-amplified penalty of only ~2 dB.

The transmission characteristics are also evident from Fig. 5.35, showing the eye diagrams after transmission. Clearly, inverting operation with the conventional scheme (middle part of the figure) results in a very distorted eye diagram due to the small amount of positive chirp associated with the signal. On the other hand, the remaining eye diagrams are both clear and open after transmission, although the signal in the left part of Fig. 5.35 indicates a slightly better quality than the signal in the right part of the figure, which also explains the lower penalty. These results verify the important advantage of the novel conversion scheme, namely good transmission properties while at the same time exhibiting a high modulation bandwidth.

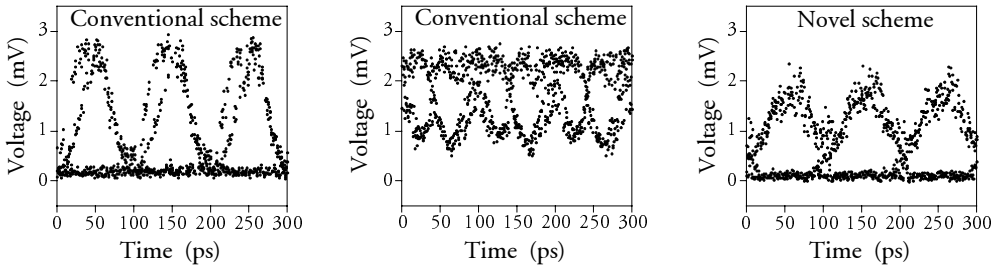

Fig. 5.35: Eye diagrams at 10 Gbit/s of the converted signals after ~25 km transmission over standard fiber using the conventional scheme for non-inverting (left) and inverting operation (middle). (right) For inverting operation using the novel scheme.

What could seem as a drawback of the novel scheme, is that the widths of the data and clock pulses have to be equal or comparable. Experimental work has shown, however, that the width of the clock pulses can be smaller than the width of the data signal by at least a factor of 4 (in the experimental results shown here, they are equal). This means that the novel conversion scheme also offers re-timing. This can also be obtained with the conventional scheme if a clock signal is used instead of the CW signal [81,p23]. In this case, however, the transmission properties of the converted signal will be strongly dependent on the spectral properties of the clock signal. This is not the case for the novel scheme since conversion is performed onto a CW signal, which in addition relaxes the requirements to the clock signal.

Finally, it should be mentioned that using the novel scheme with non-inverting operation results in just the opposite characteristics, i.e., a small positive chirp and lower conversion speed. This is illustrated in Fig. 5.36, giving the eye diagram after conversion (left) and after transmission over ~25 km standard fiber (right). By comparing the eye diagram in the left part of Fig. 5.36 to those shown in Fig. 5.33, it can be observed that the conversion speed is comparable to what is achieved with the conventional scheme for inverting operation but lower than for the novel scheme with inverting operation. In addition, the transmission properties are comparable to

those obtained with the conventional scheme for inverting operation (middle part of Fig. 5.35) verifying that inverting operation of the novel scheme by all means has the best performance.

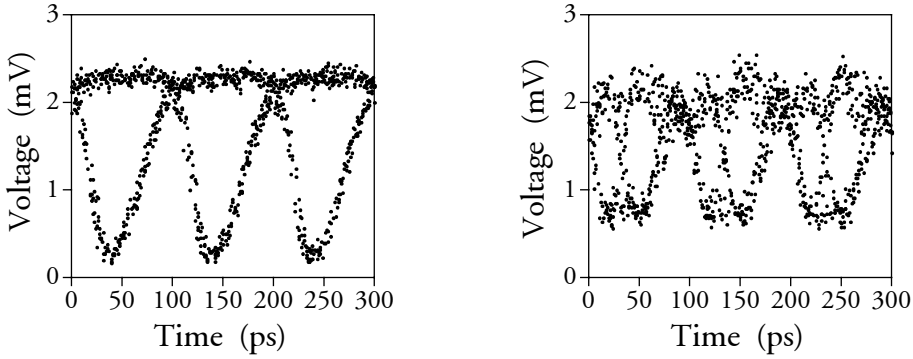

Fig. 5.36: Eye diagram at 10 Gbit/s of the converted signal using the novel conversion scheme for non-inverting operation before (left) and after (right) transmission over 25 km of standard fiber.

5.5 Summary

This chapter has focused on the description of monolithically integrated SOA-based IWCs, starting with an explanation of the operating principle of these devices. Furthermore, a discussion of the main differences between active/passive and all-active realisation of IWCs has been given with focus on the system aspects. Except for two results, only work using all-active IWCs have been presented in this chapter.

The wavelength-independent operation of IWCs has been verified at 10 Gbit/s and it was demonstrated that the converted signals typically exhibit a high OSNR and extinction ratio. The high-speed operation of IWCs has also been demonstrated by experiments carried out at 20 and 40 Gbit/s, respectively. Conversion at 20 Gbit/s was achieved in a single MZI and a cascade of two MIs with penalties of ~0.8 and ~0 dB, respectively. In order to perform successful conversion at 40 Gbit/s using the MZI, a differential control scheme was applied, whereby the influence from the limited carrier recovery time can be reduced. Using this technique, conversion at 40 Gbit/s resulted in a penalty of ~0.6 dB (extinction ratio and OSNR of ~10 and 40 dB, respectively). In addition, a recently developed MZI incorporating 2000 μm long interferometer arms and a passive output section showed very promising results for 40 Gbit/s conversion. A noisy but nevertheless open eye diagram was obtained at 40 Gbit/s using standard conversion. Differential control resulted in an RZ output signal with an extinction ratio in excess of 9 dB, clearly demonstrating the high modulation bandwidth. Finally, a scheme to increase the IPDR of IWCs was described and demonstrated at 40 Gbit/s showing an increase from ~4.5 to 6 dB.

The problem of conversion to the same wavelength has been discussed and two approaches have been described and demonstrated experimentally. The first solution

was based on a dual-stage converter employing XGM in the first stage and XPM in the second stage so that the benefits of the two conversion techniques were utilised. An assessment of the dual-stage converter at 20 Gbit/s showed good performance with a total insertion penalty of ~1.5 dB. The second approach was based on a DOMO MZI, where conversion to the same wavelength has been made possible for co-directional coupling. A device was investigated at 10 Gbit/s, showing almost wavelength-independent operation from 1530 to 1560 nm. Conversion to the same wavelength resulted in penalties ranging from ~3 to ~4 dB, while conversion for different signal and CW wavelengths resulted in penalties from ~1.2 to ~2.4 dB. For conversion to different wavelengths, the penalty was caused by extinction ratio degradation, whereas the excess penalty of ~2 dB for conversion to the same wavelength was caused by non-ideal suppression of the original data signal resulting in degradations due to interferometric cross talk. In addition, 20 Gbit/s conversion was achieved with a high suppression of the original data signal, showing that this is indeed possible even at bit rates beyond 10 Gbit/s.

Finally, a novel conversion scheme has been presented, where good transmission properties and high-speed performance is achieved simultaneously, something that is not easily obtained with the conventional conversion scheme. The feasibility of the scheme has been investigated by experiments carried out at 10 Gbit/s and in order to have a fair assessment, the results have been compared to what can be obtained using the conventional scheme. In these experiments, it was verified that the novel conversion scheme results in superior speed performance and transmission properties that are comparable to what could be obtained using the conventional scheme.

Chapter 6

All-optical regeneration in SOA-based IWCs

One of the main limitations in building large-scale transparent optical networks is the fact that the detrimental effects that the signals undergo during transmission are accumulated. So, even if transparent all-optical networking employing switching, dynamic wavelength allocation, etc., becomes a reality, there will still be a limitation on the size of the network before termination becomes necessary. The all-optical regenerator will therefore be as important for large-scale transparent networks as the EDFA was for the commercial success of WDM systems [21] and consequently, there are very intensive research activities in this area around the world.

As described in chapter 2, all-optical IWCs have regenerative capabilities that together with the other advantages (see chapter 5) make them very attractive candidates for realisation of an all-optical regenerator. The purpose of the present chapter is therefore to assess the regenerative capabilities of IWCs, especially at bit rates above 10 Gbit/s. Part of the work presented here is based on work performed in the European ACTS project REPEAT[12] for which the aim was to investigate and assess the feasibility of different solutions for electrical and all-optical regeneration. The part on all-optical regenerators was mainly focussed on soliton techniques and IWCs, of which some of the most important results are summarised in chapter 2.

In section 6.1, the basic concepts of signal regeneration will be explained with special focus on the definition of 1R, 2R and 3R regeneration. An investigation of the regenerative properties of IWCs at 40 Gbit/s will be given in section 6.2, where an assessment of the novel conversion scheme described in section 5.4 also will be presented. Finally, section 6.3 describes a pass-through scheme in IWCs [p13], where regeneration is achieved without the normally accompanying wavelength conversion.

6.1 Introduction to all-optical regeneration

As optical signals are transmitted over optical fibers, noise from optical amplifiers, fiber dispersion and non-linearities cause the signal quality to deteriorate. This limits the transmission distance and regeneration of the signals becomes necessary. Fig. 6.1 illustrates a deteriorated amplitude modulated signal that is regenerated in three steps, i.e., 1R, 2R and 3R regeneration. 1R regeneration is re-amplification, which is performed by amplifiers, e.g., EDFAs in optical systems and only serves to ensure that the power levels of the optical signals are above the system sensitivity. In a large-

[12] REPEAT: REgeneration of PulsE shape, Amplitude and Timing.

scale network, however, where the signals are amplified many times and transmitted over long distances, 2R or 3R regeneration becomes necessary. In addition to re-amplification, 2R regeneration serves to re-shape the signal, i.e., suppress the power fluctuations on the logical zeros and ones and restore the extinction ratio, whereas 3R regeneration also performs re-timing to avoid influence from jitter. With the emerging optical 3R regenerator, the analogue nature of optical signal processing will evolve to digital signal processing, making large-scale transparent optical networks possible [35,36].

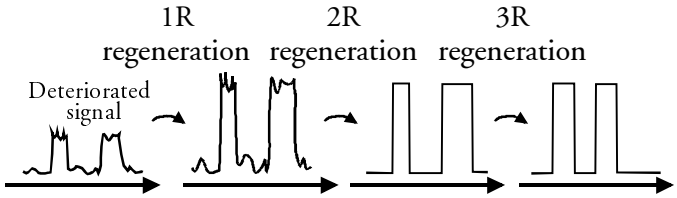

Fig. 6.1: Schematic of a deteriorated signal that experiences 1R (re-amplification), 2R (re-shaping) and 3R (re-timing) regeneration, respectively.

Due to the non-linear transfer function of all-optical IWCs, 2R regeneration of amplitude modulated signals is an inherent part of the device. Note that 2R in IWCs normally only refers to re-shaping and not re-amplification because net gain is not always ensured in IWCs. However, an amplifier after the IWC would solve this problem and consequently IWCs are referred to as 2R regenerators. Fig. 6.2 shows 2R regeneration of a noisy input signal, where the transfer function of an ideal decision gate and an IWC is given. Because of the flat parts of the transfer function of the decision gate, complete suppression of the amplitude fluctuations on the input signal is achieved as shown in the figure.

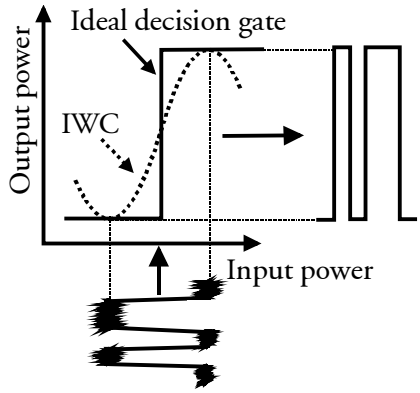

Fig. 6.2: Illustration of 2R regeneration of a noisy input signal. The figure shows the transfer function of an IWCs and an ideal decision gate. The ideal decision gate results in complete suppression of the amplitude fluctuations on the input signal, as shown in the figure. Due to the sinusoidal transfer function of IWCs, they are also capable of 2R regeneration (result not shown in the figure).

Since the decision gate causes complete suppression of amplitude noise, it is the ideal transfer function for 2R regeneration. As discussed in chapter 5 and illustrated in

Fig. 6.2, the transfer function of IWCs is sinusoidal and ideal 2R regeneration is therefore not possible with these devices. Still, if operated on the flat parts of the transfer function, good 2R regenerative properties can be obtained as will be demonstrated in this chapter. Furthermore, if IWCs are cascaded, the effective transfer function will approach that of an ideal decision gate and therefore improve the 2R regenerative capabilities [p3,35].

To demonstrate the re-shaping capabilities of IWCs, the left part of Fig. 6.3 shows a schematic of an experimental set-up used for assessment of an MI at 20 Gbit/s [p4]. For simulation of transmission through many EDFAs, a noise generator, consisting of an attenuator and an EDFA, is placed in front of the MI. Thus, by varying the input power to the EDFA, the OSNR into the MI is varied. Note that an optical bandpass filter is used after the EDFA, which is done in order to simulate a wavelength demultiplexer, as would be the case in a WDM system. The right part of Fig. 6.3 shows the eye diagrams and power density distribution at the input (top) and output (bottom) of the MI, respectively. Note that a low input power to the EDFA is used in this experiment to ensure a low OSNR at the input of the MI.

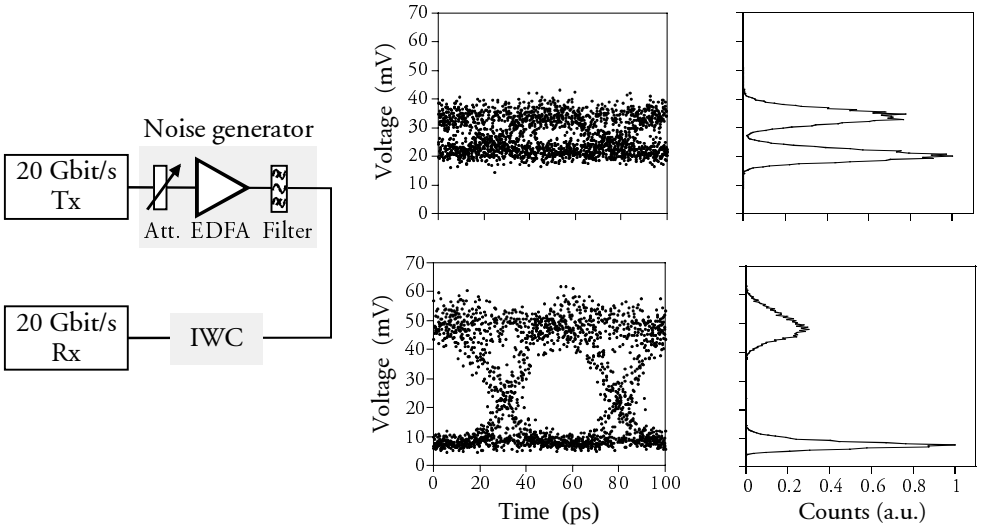

Fig. 6.3: Illustration of the 2R regenerative capabilities of IWCs at 20 Gbit/s. (left) Schematic of the experimental set-up for assessment of an IWC. By adjusting the input power to the EDFA in the noise generator, the OSNR of the optical signal to the IWC is varied. (right) Eye diagram and power density distribution at the input (top) and output (bottom) of the IWC, respectively.

Clearly, 2R regeneration is achieved in the MI. The input signal, which is very noisy and has a low extinction ratio due to the added ASE, is both clear and open at the output of the converter. The enhancement in extinction ratio is made possible by the steep slopes in the transfer function as shown in Fig. 6.2. A suppression of amplitude noise, obtained by the flat parts of the transfer function, can also be observed in Fig. 6.3. Since inverting operation of the MI is carried out, the power density

distribution of the logical ones at the input has to be compared to the distribution of the logical zeros at the output. As seen, there is a clear difference in the width of the two distributions, verifying the re-shaping capability of the MI.

It should be mentioned that the amount of re-shaping that is witnessed in Fig. 6.3 can seem miraculous since a nearly closed eye diagram is almost completely restored. The main reason for this is probably that, although the modulation bandwidth is high enough for 20 Gbit/s operation, the high-frequency amplitude fluctuations caused by ASE is removed by low-pass filtering in the IWC. It should be pointed out, though, that it is a fine balance since a too low modulation bandwidth obviously will result in poor performance. However, an investigation that explains the relationship between the modulation bandwidth and the regenerative properties in greater detail has, to the author's knowledge, not been reported so far.

As will be illustrated in section 6.2.2, it is straightforward to also achieve re-timing in IWCs, i.e., 3R regeneration. This requires a re-timed clock signal and an important part of the 3R regenerator is therefore also clock recovery, which can be electrical or all-optical. Regarding all-optical clock recovery, impressive results have been obtained with self-pulsating DFB lasers, where 40 GHz operation has been achieved [138,139]. The focus in the following, however, will not be on the clock recovery part but solely on the regenerative properties of IWCs.

6.2 High-speed all-optical regeneration in MZIs

This section presents an investigation of the regenerative capabilities of the MZI used for the 20 and 40 Gbit/s conversion experiments described in section 5.2. The results are based on [p20,p23,p28].

6.2.1 All-optical 2R regeneration at 40 Gbit/s in an all-active MZI

The set-up for 2R regeneration at 40 Gbit/s is illustrated in Fig. 6.4 and except for the noise generator, the set-up is identical to the one in Fig. 5.14. As a means to assess the regenerative properties of the MZI, the OSNR is measured with a spectrum analyser before the optical filters at the input and output of the converter.

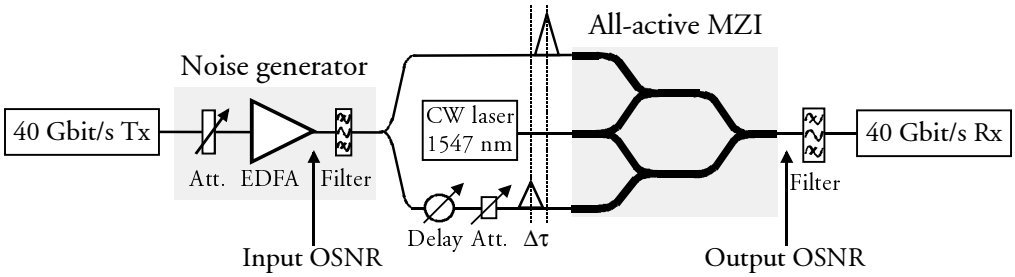

Fig. 6.4: Set-up for assessment of the 2R regenerative capabilities of an MZI. Except for the noise generator, the set-up is identical to the one in Fig. 5.14 used for 40 Gbit/s wavelength conversion.

The left part of Fig. 6.5 shows the OSNR at both the input and output of the converter as a function of the input power to the EDFA. As illustrated, the MZI is capable of preserving a very high OSNR regardless of the OSNR at the input. This is possible since the spectrum after the device is determined by the spectrum of the CW source and the low ASE level from the converter. For this experiment the OSNR is kept above 37 dB even for an OSNR at the input as low as ~13 dB thus resulting in an improvement of ~24 dB. Clearly, the ability to ensure a high OSNR of regenerated signals even at high bit rates is very important when considering cascadability of the all-optical 2R regenerator. It has to be emphasised, though, that an improvement in the OSNR is not a guarantee that regeneration has actually occurred. This is because the OSNR in itself does not give any information on whether the regenerated signal has a high extinction ratio, etc. Therefore, penalty measurements are the only way to ensure that regeneration has actually taken place. Such measurements are illustrated in the right part of Fig. 6.5, showing the excess penalty versus the input power to the EDFA with and without regeneration. The excess penalty is depicted in order to focus on the regenerative capabilities of the MZI alone (the insertion penalty at 40 Gbit/s is ~0.6 dB as shown in section 5.2.2). It can be seen that a noise suppression capability is obtained for input powers below -20 dBm. As an example, a ~2 dB lower input power to the EDFA is allowed at an excess penalty of 2 dB (compared at a penalty of 2 dB since a pre-amplified receiver is used). This noise suppression can be used to increase the repeater spacing, relax the power budget on a transmission link or to increase the total transmission distance.

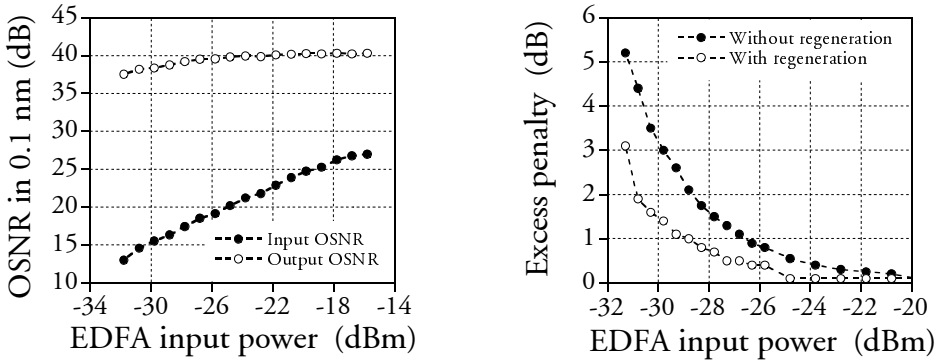

Fig. 6.5: OSNR at the input and output of the MZI (left) and excess penalty with and without regeneration (right) at 40 Gbit/s as a function of the input power to the EDFA.

6.2.2 All-optical 3R regeneration at 40 Gbit/s in an all-active MZI

For large-scale optical networks, 2R regeneration will not be sufficient to maintain good signal quality. The reason is that jitter accumulation will start to limit the performance and 3R regeneration is consequently necessary. This functionality is straightforward to obtain in IWCs as illustrated in Fig. 6.6, showing the difference in using the MZI for 2R and 3R regeneration, respectively.

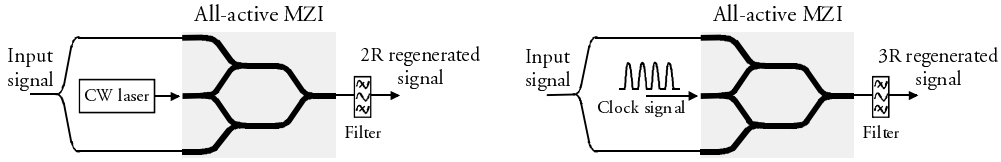

Fig. 6.6: Schematic of an MZI used for 2R (left) and 3R regeneration (right). The use of a clock signal instead of CW light ensures that re-timing is possible. The differential control scheme is illustrated without the use of an attenuator and optical delay line.

3R regeneration is accomplished simply by replacing the CW light with a clock signal. Hereby, jitter on the input data signal will result in amplitude variations on the clock signal but due to the non-linear transfer function of the MZI, these variations will be suppressed resulting in a 3R regenerated signal [81]. Obviously, the clock signal has to be extracted through clock recovery from the incoming data signal and synchronised to the data signal. As pointed out in section 4.4, the use of a clock signal instead of CW light has some additional benefits. First of all, it is easier to obtain a high extinction ratio of the converted signal due to the finite modulation of the clock signal. Secondly, short output pulses can be obtained since the width of the converted pulses is dependent on the width of the clock pulses.

These characteristics are clearly observed in Fig. 6.7, showing the eye diagram of a converted signal at 10 Gbit/s using the differential control scheme in the MZI together with CW light (left) and a 10 GHz clock signal instead (right), i.e., using the two set-ups shown in Fig. 6.6.

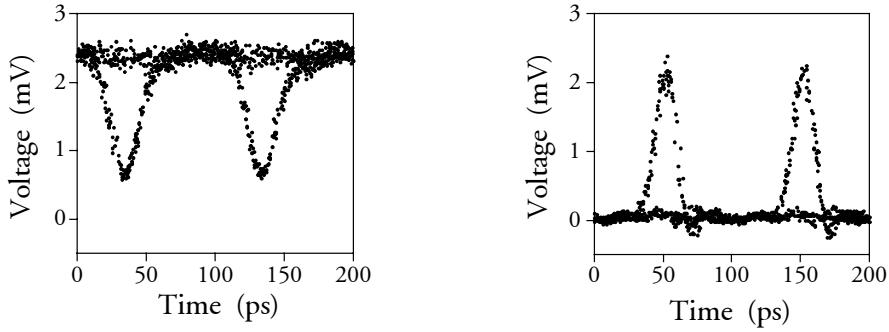

Fig. 6.7: Eye diagram at 10 Gbit/s of a wavelength converted signal using the differential control scheme in an MZI together with CW light (left) and a 10 GHz clock signal (right).

The system performance of the 3R regenerator is investigated at 40 Gbit/s in a set-up identical to the one illustrated in Fig. 5.14, where a clock signal is used instead of CW light. Note that clock recovery is not carried out in this experiment since no transmission is carried out. For simulation of the clock signal, pulses from a gain-switched laser multiplexed to 40 GHz are used (FWHM = 6 ps). The performance of the 3R regenerator is illustrated in Fig. 6.8, giving the back-to-back signal at 1554 nm (left), the converted and 3R regenerated signal at 1547 nm (middle) and the resulting BER measurements (right).

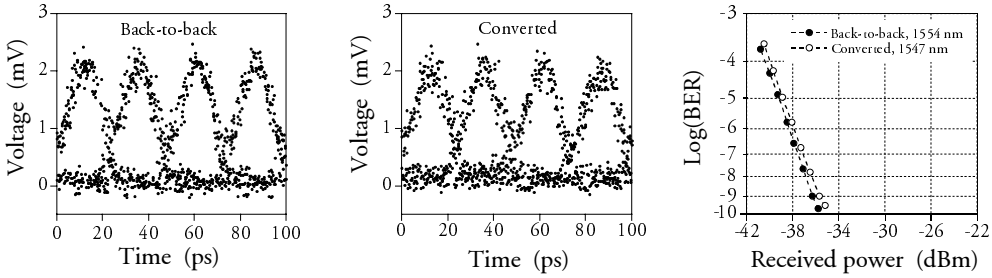

Fig. 6.8: Eye diagram at 40 Gbit/s of the back-to-back signal (left), the converted signal (middle) and the resulting BER curves after demultiplexing to 10 Gbit/s (right).

As seen, the converted eye diagram is both clear and open with little difference compared to the back-to-back signal. The resulting penalty is as low as ~0.5 dB and note that due to the use of a clock signal, the RZ signal format is preserved at the output of the 3R regenerator emphasising the feasibility of this scheme at high-bit rates. As a comparison, the 40 Gbit/s wavelength conversion experiment described in section 5.2.2, using CW light instead of a clock signal, resulted in a transformation from RZ to NRZ.

The scheme depicted in the right part of Fig. 6.6 has been used in an architecture for a 3R regenerator consisting of two stages, each employing an MZI [35,36]. In that architecture, 3R regeneration is accomplished in the first stage, where inverting operation is used since this improves the speed capability of the MZI, as discussed in chapter 5. The second stage performs additional 2R regeneration, thus improving the overall 2R regeneration capability [35,p3], and adaptation for transmission over standard fiber, i.e., non-inverting operation (see section 5.4). Thereby, it was possible to cascade 1000 3R regenerators at 10 Gbit/s using standard conversion in both MZIs [35] and 200 regenerators at 20 Gbit/s using the differential control scheme in the second stage [36]. Clearly, this demonstrates the impressive cascadability performance of IWCs at high bit rates. In connection with these experiments, transmission over 170.000 km at 10 Gbit/s and 20.000 km at 20 Gbit/s was achieved, showing that global distances indeed can be covered when all-optical regenerators are used.

6.2.3 Simultaneous demultiplexing, conversion and 3R regeneration

As the channel bit rate in optical networks increases to 40 Gbit/s or more, optical time division multiplexing (OTDM) techniques become increasingly attractive due to the finer granularity obtained thereby. A combination of both OTDM and WDM will therefore offer a flexible network, where switching and add/drop functionalities can be accomplished in both the wavelength and time domain. As wavelength conversion is attractive in WDM networks, all-optical demultiplexing is attractive in an OTDM network. Therefore, an important need will be for optical building blocks capable of demultiplexing in time. The ability of the IWCs to perform wavelength

conversion has been demonstrated in chapter 5 as well as in this section. In addition to this, IWCs are also capable of performing demultiplexing as shown experimentally in [140,141]. Here, a scheme that is capable of both wavelength conversion and demultiplexing simultaneously will be described [142,p23]. The fact that wavelength conversion and demultiplexing is achieved simultaneously is attractive in a combined OTDM/WDM network since a 10 Gbit/s channel can be dropped from a channel at 40 Gbit/s and converted to a new wavelength channel within a single component.

The scheme is illustrated schematically in Fig. 6.9, showing demultiplexing in an MZI using the traditional scheme [140,141] (left) and the new scheme (right). Both schemes result in 40 to 10 Gbit/s demultiplexing if a 10 GHz clock signal and a 40 Gbit/s data signal is used. In the traditional scheme, the clock signal is injected into the interferometer arms, while the data signal is injected into the middle arm. In the scheme depicted in the right part of the figure, the data and clock signals are injected the same way as for 3R regeneration (see the right part of Fig. 6.6).

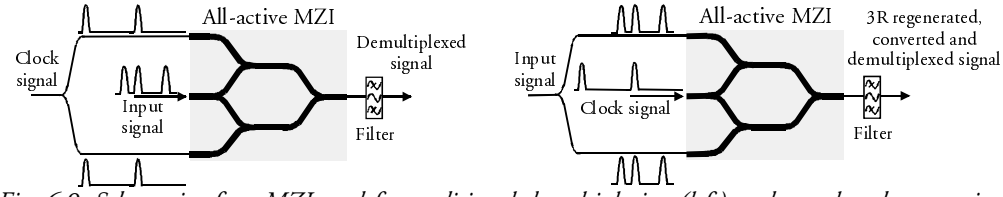

Fig. 6.9: Schematic of an MZI used for traditional demultiplexing (left) and wavelength conversion and demultiplexing simultaneously using the new scheme (right). The scheme in the right part also exhibits a 3R regenerative capability since conversion is performed with a re-timed clock signal. The differential control scheme is illustrated without the use of an attenuator and optical delay line.

The advantage of the new scheme is that in addition to demultiplexing, both wavelength conversion and 3R regeneration is obtained. The drawback, however, is that the MZI has to be able to operate at the speed of the data signal, whereas in the traditional scheme, it only has to be able to operate at the speed of the clock signal.

Still, good performance can be achieved if a high-speed MZI is used as will be shown in the following. An experimental set-up similar to that in Fig. 5.14 is used for the investigation, except that a 10 GHz clock signal is used instead of the CW light. In addition, an electrical time delay controls the time alignment of the clock signal compared to the data signal. So, by controlling the time delay of the 10 GHz clock signal, any of the four multiplexed 10 Gbit/s signals in the 40 Gbit/s signal can be demultiplexed. To verify this, Fig. 6.10 shows the pulse trace of a 40 Gbit/s signal at 1554 nm (top), and two different converted and demultiplexed pulse traces at 1547 nm (middle and bottom). It must be mentioned that the reason for the pulse overlap in the top of the figure is due to the limited bandwidth of the photo detector (~32 GHz). As seen, the wavelength converted and demultiplexed pulse traces (‘1110’ and ‘1011’, respectively) clearly demonstrate that demultiplexing is achieved with a strong suppression of the other three OTDM channels (extinction ratio >10 dB).

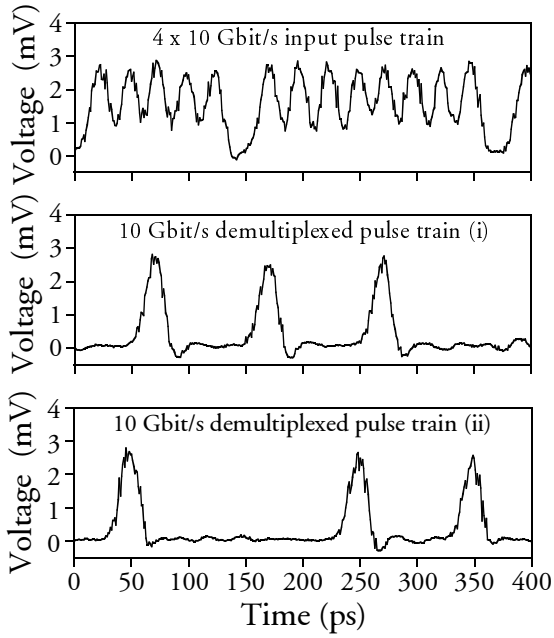

Fig. 6.10: 40 Gbit/s input signal to the MZI (top) and two different pulse traces of wavelength converted and demultiplexed pulse traces at 10 Gbit/s (middle and bottom).

In order to assess the performance of the technique, Fig. 6.11 shows the eye diagram of the demultiplexed signal (left) and the BER performance of the back-to-back signal at 10 Gbit/s and the demultiplexed signal. The eye diagram verifies that demultiplexing is performed with a high suppression of the other OTDM channels, while the BER curves shows that the scheme has introduced a pre-amplified penalty of ~3 dB for wavelength conversion and demultiplexing from 40 to 10 Gbit/s.

It is noted that simultaneous wavelength conversion and demultiplexing also can be performed with converters based on either cross-gain modulation [143] or four-wave mixing [144], however, neither of these schemes provides re-shaping.

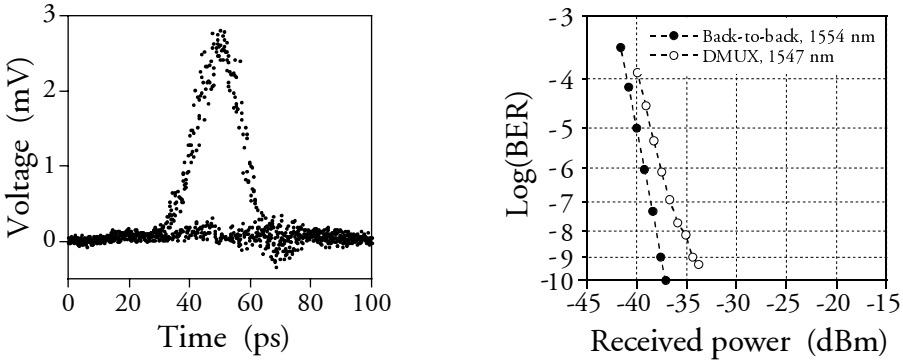

Fig. 6.11: Eye diagram of a wavelength converted and demultiplexed signal (left) and the BER performance of the back-to-back at 10 Gbit/s signal and the demultiplexed signal (right).

6.2.4 Regenerative capabilities of the novel conversion scheme

Here, the regenerative properties of the novel conversion scheme described in section 5.4 will be demonstrated at 10 Gbit/s. This is accomplished by placing a noise generator similar to the one illustrated in Fig. 6.3 in front of the converter. The left part of Fig. 6.12 gives the OSNR at the input and output of the converter, while the right part of the figure shows the penalty with and without regeneration, both as a function of the input power to the EDFA in the noise generator. As illustrated, the converter is capable of preserving a high OSNR regardless of the OSNR at the input. In addition, noise suppression is obtained for EDFA input powers below -25 dBm.

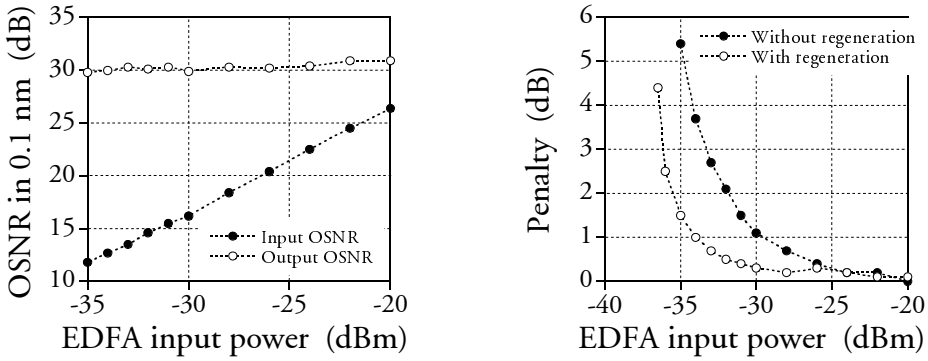

Fig. 6.12: OSNR in 0.1 nm at the input and output of the converter using the novel conversion scheme described in section 5.4 (left) and the penalty with and without regeneration (right) both as a function of the input power to the EDFA in the noise generator.

The novel conversion scheme has been exploited in an architecture for a 3R regenerator consisting of two stages, both employing an all-active MZI [p34]. In the first stage, 3R regeneration is performed using the scheme illustrated in section 6.2.2, while the second scheme employs the novel conversion scheme. The purpose of the second stage is therefore twofold; first of all, the overall re-shaping capabilities of the regenerator are improved due to the regenerative properties illustrated in Fig. 6.12. Secondly, the novel conversion scheme can result in very good transmission properties, while preserving high-speed operation as demonstrated in section 5.4. A re-circulating loop experiment, including 50 km standard fiber without dispersion compensation, confirmed the good regeneration and transmission properties of this approach. More than 300 loop rounds were achieved at 10 Gbit/s without noise and jitter accumulation [p34].

6.3 All-optical regeneration using a pass-through scheme in IWCs

So far, the schemes for all-optical regeneration in IWCs described in this chapter have included wavelength conversion, which means that additional components are needed, e.g., CW laser, optical filter, etc. In this section, a scheme to obtain 2R regeneration without wavelength conversion, a so-called pass-through scheme, will

be presented and demonstrated experimentally. Since regeneration is achieved without wavelength conversion, the need for additional components is avoided thus making the scheme simpler and potentially less expensive.

6.3.1 Operating principle of the pass-through scheme

The operating principle of the pass-through scheme is illustrated in Fig. 6.13. As shown, the lower and upper interferometer arm of an MI is biased at I_1 and I_2, resulting in a gain and phase shift of (G_1,ϕ_1) and (G_2,ϕ_2), respectively. An input signal is injected into the MI, where it splits equally between the interferometer arms. After traversing these interferometer arms, the signal is reflected at the end facets and propagates in the opposite direction. Finally, the signal recombines at the input, either constructively or destructively depending on the phase difference between the interferometer arms. This phase difference is achieved by asymmetric biasing ($I_1 \neq I_2$). In the following it is assumed that I_2 is larger than I_1, which means that G_2 is higher than G_1 and that the saturation input power is lower in the upper interferometer arm compared to the lower interferometer arm (see chapter 3). Consequently, ϕ_2 will start to increase at a lower input power than ϕ_1. For input powers below P_1 and above P_2 (see Fig. 6.13), the phase difference will therefore be constant, while it increases for input powers between P_1 and P_2. This results in a total phase difference close to that of a decision gate and therefore, the same will apply to the transfer function of the input power. As observed in the figure, it is important that the saturation input powers are different so that there can be a change in the phase shift from a low to a high level. It is emphasised that even though an MI is shown, the operating principle is the same for an MZI.

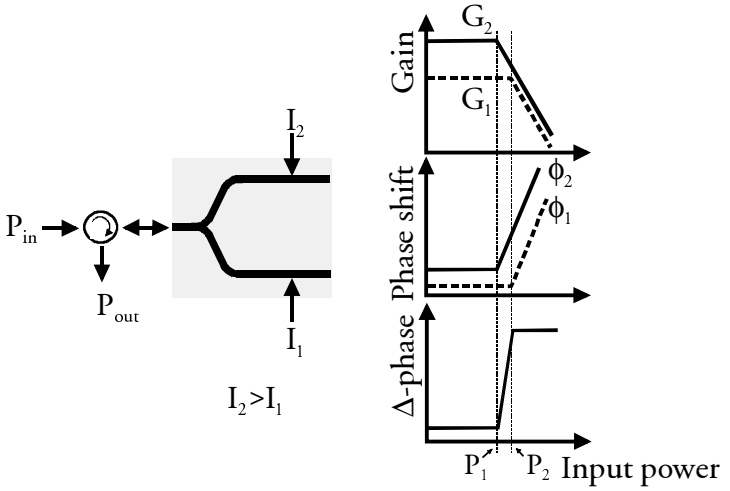

Fig. 6.13: Illustration of the pass-through scheme. (left) Schematic of an MI biased at I_1 and I_2 in the lower and upper interferometer arm, respectively. It is assumed that I_2 is larger than I_1. (right) Gain (G_1, G_2) (top) and phase shift (ϕ_1, ϕ_2) (middle) in the lower and upper interferometer arm, respectively. (bottom) The resulting phase difference that a signal experiences in the interferometer.

It should be mentioned that since there is a different gain in the interferometer arms, the destructive interference at low input powers is not perfect. The re-shaping capabilities are therefore better for a logical one than for a logical zero. The pass-through scheme was first proposed using GC-SOAs as the active elements in the interferometer arms [145,146], which therefore solves the problem of different gains. In GC-SOAs, asymmetric biasing results in different saturation input powers but equal gains as described in chapter 3. Seen from the static case, a solution with GC-SOAs is therefore preferable since perfect destructive interference can be obtained also at low input powers. However, as pointed out in chapter 3, GC-SOAs cause relaxation oscillations making regeneration difficult at high bit rates. The problem of different gains, when conventional SOAs are used in the interferometer arms, can be solved, though, by using SOAs with different lengths. In this way, asymmetric biasing can still result in equal gain but different saturation input powers as pointed out in chapter 3. It should be mentioned that a passive section would be necessary so that equal path length in the two interferometer arms is obtained. However, such a device has not been fabricated yet.

In the following section, the characteristics and regenerative capabilities of the pass-through scheme will be investigated experimentally at 2.5 and 10 Gbit/s in an MI.

6.3.2 2R regeneration at 2.5 and 10 Gbit/s in an all-active MI

The experimental set-up is shown in Fig. 6.14. The 1550 nm data signal, which is either at 2.5 or 10 Gbit/s, is first transmitted through a noise generator (described in connection with Fig. 6.3) and then coupled into the MI using the pass-through configuration. The optical circulator separates the output signal from the input signal before final detection. It is emphasised that no filter is applied at the output of the MI, i.e., no additional ASE filtering is performed compared to back-to-back. The presented results are based on [p13,p31].

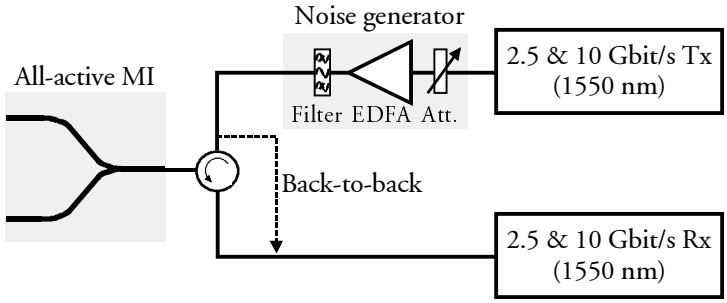

Fig. 6.14: Set-up for assessment of the regenerative capabilities of the pass-through scheme in an MI at 2.5 and 10 Gbit/s. The EDFA and attenuator in front of the MI is a noise generator.

2.5 Gbit/s operation

The performance of the MI at 2.5 Gbit/s is illustrated in Fig. 6.15, showing the eye diagram of the output signal (left) and the resulting BER measurements (right). Note that in this measurement, the input power to the EDFA in the noise generator is high so that the OSNR of the input signal to the MI also is high. As seen, a clear and open eye diagram is obtained at the output of the MI resulting in penalty-free operation.

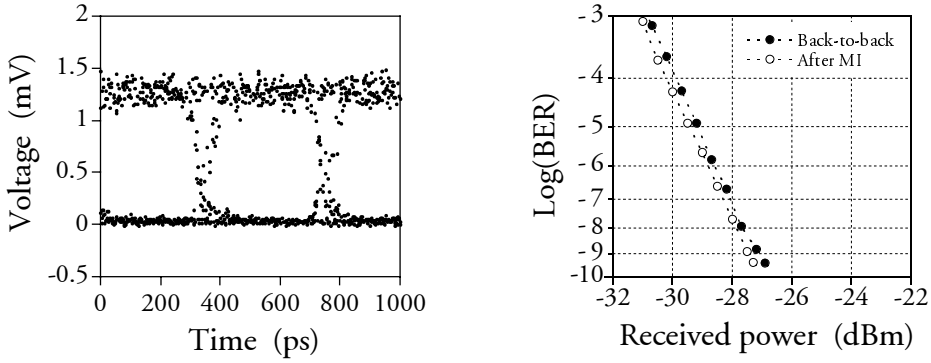

Fig. 6.15: Eye diagram at the output of the MI at 2.5 Gbit/s using the pass-through configuration (left) and the resulting BER curves of the input and output signal at 1550 nm.

The measured static transfer function of the MI is shown in the left part of Fig. 6.16. As observed, the transfer function is close to that of a decision gate as explained in section 6.3.1, clearly in contrast to what is obtained with IWCs performing wavelength conversion (see chapter 5). Note that a logarithmic scale is used on the x-axis in the figure. This has been done so that the properties of the transfer function can be seen at low input powers. An attractive feature resulting from the decision gate characteristic is a very large IPDR as demonstrated in the right part of Fig. 6.16. As seen, penalty-free operation is achieved over a range of ~7 dB, while the IPDR is ~8.5 dB (@ 1 dB penalty). In comparison, the IPDR of IWCs performing wavelength conversion is only~3-4 dB due to the sinusoidal transfer function.

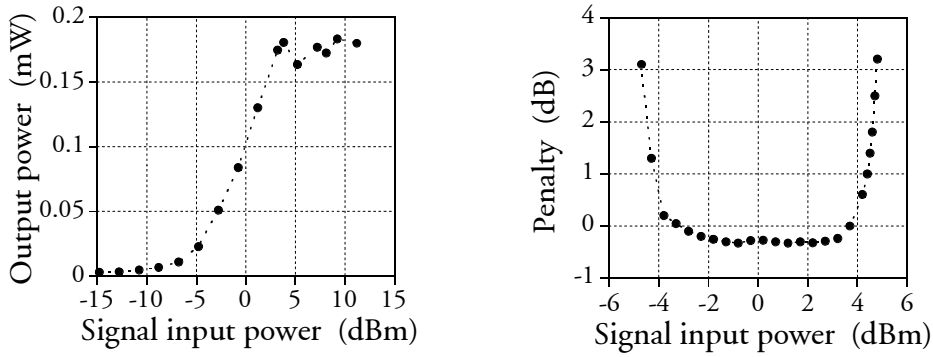

Fig. 6.16: Static transfer function of the MI in the pass-through configuration (left) and penalty at 2.5 Gbit/s vs. the input power to the MI (right). The signal wavelength is 1550 nm.

Due to the non-linear transfer function observed in the left part of Fig. 6.16, a regenerative capability can be obtained when using the pass-through scheme. This is demonstrated in Fig. 6.17, showing the output extinction ratio as a function of the input extinction ratio (left) as well as the penalty with and without regeneration as a function of the input power to the EDFA in the noise generator (right). Clearly, the input signal is regenerated. As seen, extinction ratio improvement is measured for input extinction ratios ranging from 3 to 13.5 dB. Also, very good noise suppression performance is achieved. As shown in the right part of Fig. 6.17, at a penalty of 1 dB, it is possible to use a ~4.5 dB lower input power to the EDFA when applying the MI.

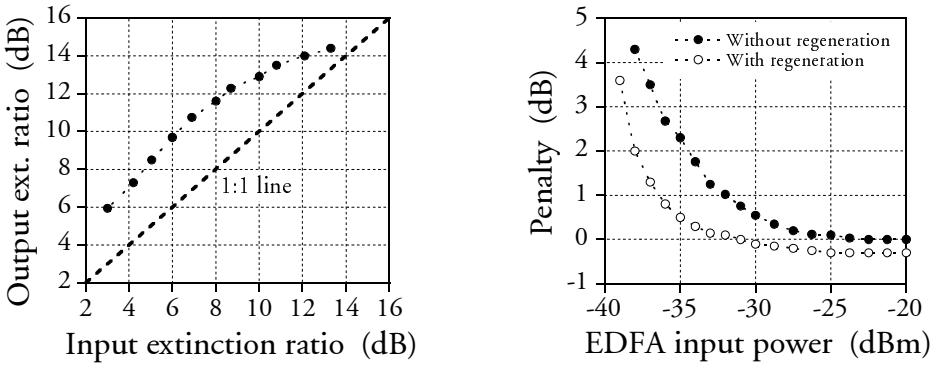

Fig. 6.17: Output extinction ratio vs. input extinction ratio (left) and penalty vs. the input power to the EDFA in the noise generator with and without regeneration (right). The signal wavelength is 1550 nm and the bit rate is 2.5 Gbit/s.

10 Gbit/s operation

The MI is also investigated at 10 Gbit/s and the results can be seen in Fig. 6.18. The figure shows the penalty as a function of the input power to the MI (left), the output versus input extinction ratio (middle) and the penalty with and without regeneration (right). The results illustrate the good performance of the pass-through scheme, i.e., an IPDR of ~8 dB (@ 2 dB penalty), extinction ratio improvement as well as excellent noise suppression properties.

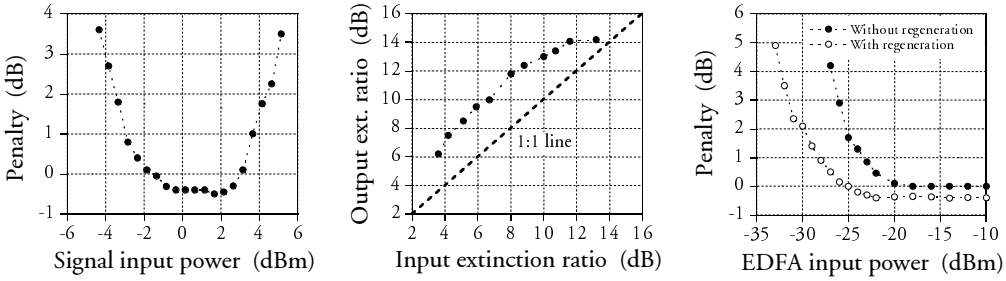

Fig. 6.18: Penalty vs. input power to the MI (left), output extinction ratio vs. input extinction ratio to the MI (middle) and penalty vs. the input power to the EDFA in the noise generator with and without regeneration in the MI (right). The signal wavelength is 1550 nm and the bit rate is 10 Gbit/s.

6.3.3 2R regeneration at 40 Gbit/s in an all-active MZI

In order to assess the properties of the pass-through scheme at 40 Gbit/s, the all-active MZI described in section 5.2.1 is used, i.e., the MZI used for 40 Gbit/s wavelength conversion. The results presented here are based on [p16]. Fig. 6.19 shows the eye diagram of the back-to-back signal (left), the output signal from the MZI (middle) and the resulting BER measurements. Clearly, the eye diagram at the output of the MZI is both clear and open (extinction ratio of ~13 dB), with little difference compared to the back-to-back signal. The excellent performance is also verified by the BER measurements, showing a negligible penalty of ~0.3 dB. In addition, it is noted that the MZI is inserted without loss, i.e., -5 dBm is measured in the fiber both at the input and output of the MZI.

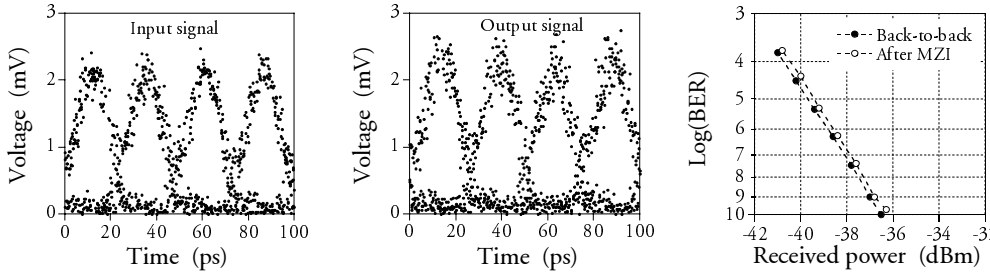

Fig. 6.19: Eye diagram at 40 Gbit/s of the back-to-back signal (left), the output signal from the MZI (middle) and the resulting BER curves after demultiplexing to 10 Gbit/s. The wavelength is 1554 nm.

The regenerative properties can be seen in Fig. 6.20, showing the excess penalty with and without regeneration as a function of the input power to the EDFA in the noise generator. As seen, noise suppression is achieved for input powers below -20 dBm. As an example, a ~2.5 dB lower input power to the EDFA is allowed at a pre-amplified penalty of 2 dB, clearly demonstrating the high-speed capability. Therefore, taking the simplicity of the regeneration scheme as well as the good performance into account, this approach is a feasible and competitive technique for all-optical 2R regeneration, where wavelength conversion is not needed.

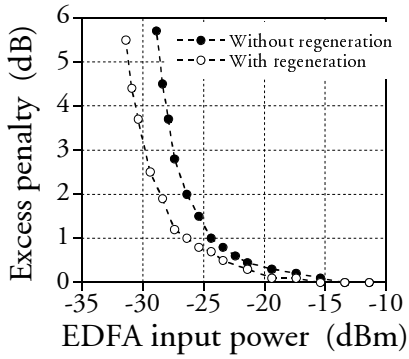

Fig. 6.20: Excess penalty at 40 Gbit/s with and without regeneration vs. the input power to the EDFA in the noise generator. The signal wavelength is 1554 nm.

6.3.4 Transmission performance of the pass-through scheme at 10 Gbit/s

Here, the transmission properties of the pass-through scheme will be investigated at 10 Gbit/s using the set-up in Fig. 6.21 [p31]. The signal from the transmitter is injected into the MZI and then transmitted over ~31 km of standard fiber before detection. In order to assess the transmission properties of the output signal from the MZI, the performance is compared to the transmitted signal directly from the transmitter. Consequently, the numbers 1 → 4 in the figure correspond to positions where measurements are performed.

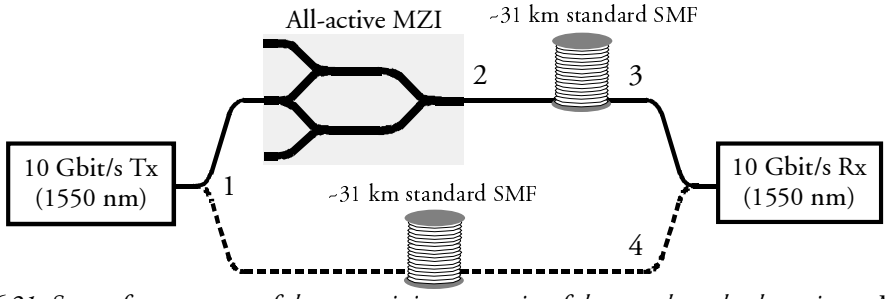

Fig. 6.21: Set-up for assessment of the transmission properties of the pass-through scheme in an MZI at 10 Gbit/s. The numbers 1 → 4 correspond to positions where measurements are performed.

It can be expected that the transmission properties of the pass-through scheme are good due to the non-inverting operation (see left part of Fig. 6.16). In order to verify this, the left part of Fig. 6.22 shows BER curves measured at 1 → 4.

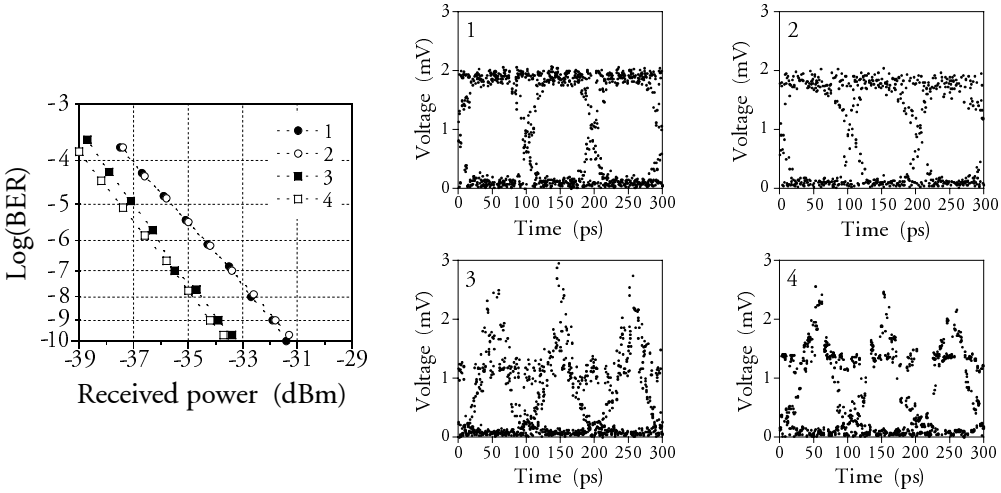

Fig. 6.22: BER curves (left) and eye diagrams (right) at 10 Gbit/s for the back-to-back signal and the signal after the MZI, before and after transmission over ~31 km of standard fiber. The numbers 1→4 refer to the places indicated in Fig. 6.21. The signal wavelength is 1550 nm.

First of all, it can be observed that there is no difference between the BER performance of the back-to-back signal and the signal after the MZI, i.e., 1 and 2 in Fig. 6.21. After transmission, i.e., 3 and 4, it can be seen that both sensitivities have

improved by ~2 dB. The reason for this is the chirp added by the electro-optical $LiNbO_2$ modulator used in the transmitter. This is also evident from the eye diagrams in the right part of Fig. 6.22, where it can be noticed that both signals have been compressed after transmission. By comparing the BER curves after transmission, it can be observed that traversing the MZI results in a penalty of only 0.3 dB, verifying that the pass-through scheme only has negligible influence on the transmission properties of the regenerated signal.

6.4 Summary

The focus in this chapter has been on the regenerative capabilities of all-optical SOA-based IWCs. After a short discussion on the definition of 1R, 2R and 3R regeneration, it was argued that the ideal decision gate imposes the best transfer function for all-optical re-shaping (2R). Due to the sinusoidal transfer function of IWCs, perfect re-shaping cannot be obtained in these devices but if operated at the flat parts of the transfer function, good re-shaping properties can nevertheless be achieved. This was verified by an experiment carried out at 20 Gbit/s, resulting in clear extinction ratio improvement as well as noise redistribution.

By using a noise generator, the regenerative capabilities of an MZI were investigated at 40 Gbit/s, resulting in very good 2R regenerative properties. It was demonstrated that the MZI is capable of preserving an OSNR of the converted signal above 37 dB (measured in 0.1 nm) even for an input OSNR as low as ~13 dB. The regenerative properties were also verified by the fact that a ~2 dB lower input power to an EDFA in a noise generator was allowed. Furthermore, a scheme to obtain 3R regeneration in IWCs has been discussed and shown feasible at 40 Gbit/s in an MZI. The good performance of the scheme was illustrated by the fact that the output signal had a high extinction ratio and operation of the MZI resulted in a pre-amplified penalty of only ~0.5 dB. In addition, a scheme for simultaneous wavelength conversion, demultiplexing and 3R regeneration has been presented and shown feasible in an experiment demonstrating conversion and demultiplexing from 40 to 10 Gbit/s.

Finally, a novel scheme for all-optical 2R regeneration in IWCs has been presented. The scheme, which is called the pass-through scheme, does not include wavelength conversion and is therefore simpler than the other techniques described in this chapter. After an explanation of the operating principle of the regeneration scheme, the performance was illustrated at 2.5 and 10 Gbit/s in an MI. The experiments verified the excellent performance of the pass-though scheme, i.e., a high IPDR, extinction ratio improvement and 2R regenerative capabilities were demonstrated. The high-speed capabilities of the pass-through scheme were demonstrated in an experiment carried out at 40 Gbit/s, where clear noise suppression also was achieved. Furthermore, an investigation of the transmission properties of the scheme revealed that the chirp added by an MZI had negligible influence after transmission over

~31 km of standard fiber. Therefore, taking the simplicity of the regeneration scheme as well as the good performance into account, this approach is a feasible and competitive technique for all-optical 2R regeneration, where wavelength conversion is not needed.

Chapter 7

Conclusion

In the light of the growing demand for transmission bandwidth, the current trend in optical networking is that more and more functionalities, which today are carried out electrically, are moving into the optical domain. This progress has already started with the emergence of commercial optical add-drop multiplexers and optical space switches. As it has been argued, however, the progress will most likely continue so that even more complex operations will be implemented in the optical domain with the use of optical cross-connects. Consequently, this thesis has been devoted to the design and evaluation of key components that will be important enablers for future all-optical networks, namely optical gates, wavelength converters and regenerators. Although different techniques have been discussed, the focus throughout this thesis has been on semiconductor optical amplifier (SOA)-based devices.

The use of SOA-based devices for all-optical space switching has been investigated and the performance has been analysed mainly with the use of a detailed large-signal model. It was found that a high bias current together with a high confinement factor and a long device results in a large gain, whereas a high optical bandwidth and low noise figure requires a low confinement factor and a short SOA. The main drawback of SOA-based gates is that the input power dynamic range (IPDR) is limited by gain saturation at high input powers and amplified spontaneous emission (ASE) at low input powers. The limited IPDR also results in a limited cascadability, why guidelines on how to optimise the IPDR have been established. It has been demonstrated that the largest IPDR is obtained using short SOAs with low confinement factors and a low applied bias current. In this context, the cascadability of SOAs for single channel operation has been investigated for two different cases: The SOA used as a loss compensator, i.e., biased to give a certain unsaturated gain, and as a power equaliser. In both cases the analysis clearly confirmed the above-mentioned guidelines to obtain a large IPDR. When biased to give a gain of 5 and 20 dB (loss compensator), the maximum number of 200 μm long SOAs that could be cascaded at a penalty of 1 dB was 19 and 5, respectively. Biased to give an output power of -10 and 0 dBm (power equaliser), the maximum number of 100 μm long SOAs that could be cascaded was 27 and 8, respectively.

The problem of gain saturation is partly overcome in gain-clamped SOAs (GC-SOAs) that have a much higher saturation input power. This is especially attractive for multi-channel operation, since cross-gain modulation between different channels thereby is minimised. It has been shown that the cascadability of GC-SOAs is superior at 2.5 Gbit/s compared to conventional SOAs for up to at least 16 channels.

At a channel bit rate of 10 Gbit/s the performance of GC-SOAs is still better but the advantage has been reduced substantially due to the influence from relaxation oscillations, a phenomena that does not exist in the conventional SOA. It has been demonstrated, however, that using RZ signal formats instead of NRZ improves the cascadability due to less influence from the relaxation oscillations.

The use of SOAs for XGM-based wavelength conversion has been described and guidelines on how to achieve high modulation bandwidths have been outlined by a theoretical large-signal investigation. It was found that using long SOAs with high confinement factors and high bias currents together with high optical powers is beneficial for improving the performance. Following this, an experiment performed at 40 Gbit/s was demonstrated. The eye diagrams of the converted signals, that were clear and open, indicated a high modulation bandwidth since the RZ signal format was preserved. Moreover, issues concerning counter-directional coupling in XGM-based converters have been discussed. Counter-directional coupling has the advantages that filter-less operation and conversion to the same wavelength is possible. There are, however, also some significant disadvantages caused by a dynamic movement of the carrier distribution in the SOA. The noise figure is inherently higher than for co-directional coupling and jitter, that accumulates as the converters are cascaded, is associated with the converted signal. In addition, transit time effects become a limiting factor for long SOAs operated at high bit rates, which can decrease the modulation bandwidth compared to the co-directional case. Therefore, if conversion to the same wavelength is unimportant and the added complexity of a filter is of no concern, the co-directional scheme should be applied.

Furthermore, a scheme that can be used as a part of all-optical re-timing has been investigated both theoretically and experimentally. In this scheme an optical clock signal is used instead of CW light, which has the benefit that a high extinction ratio of the converted signal is easy to obtain since the clock has a finite extinction ratio. Furthermore, using short clock pulses results in short converted pulses even though the data input pulses are broad. In a system experiment carried out at 20 Gbit/s for both co- and counter-directional coupling, a penalty of 1.2 and 2.5 dB was achieved, illustrating the good performance of the scheme.

Following the XGM-based converters, a description of SOA-based interferometric wavelength converters (IWCs) was given. It is noted that the guidelines obtained for XGM-based converters also apply for IWCs. Characteristics such as wavelength independent operation, high optical signal-to-noise ratio (OSNR) and extinction ratio of the converted signals were verified experimentally at 10 Gbit/s. Furthermore, conversion at 20 Gbit/s was achieved in a single Mach-Zehnder interferometer (MZI) and a cascade of two Michelson interferometers (MIs) with penalties of ~0.8 and ~0 dB, respectively. A differential control scheme was applied to perform conversion at 40 Gbit/s and resulted in a penalty of ~0.6 dB, clearly illustrating the

high-speed capabilities of IWCs. In addition, a recently developed MZI with 2000 μm long interferometer arms showed very promising results for 40 Gbit/s standard conversion.

The challenge of conversion to the same wavelength has been discussed and two approaches have been described and demonstrated experimentally. The first solution was based on a dual-stage converter employing an XGM-converter in the first stage and an IWC in the second stage. An assessment at 20 Gbit/s showed good performance with an insertion penalty of ~1.5 dB. The second approach was based on a dual-order mode (DOMO) MZI, where conversion to the same wavelength has been made possible for co-directional coupling. A device was investigated at 10 Gbit/s, showing almost wavelength-independent operation from 1530 to 1560 nm. Conversion for different signal and CW wavelengths resulted in penalties from ~1.2 to ~2.4 dB due to extinction ratio degradation, while conversion to the same wavelength resulted in excess penalties of ~2 dB due to influence from interferometric cross-talk. Promising results at 20 Gbit/s wavelength conversion were also obtained with the specific device.

A novel conversion scheme in IWCs, where a clock signal is used in addition to the data signal and CW light, has been presented. Using this scheme, good transmission properties and high-speed performance are achieved simultaneously, something that is not easily obtained with the conventional conversion scheme. The feasibility of the scheme has been investigated at 10 Gbit/s. By comparing the results with what can be obtained with the conventional scheme, it was shown that the novel scheme results in superior speed performance and transmission properties that are comparable to what could be obtained using the conventional scheme.

The focus has also been on the regenerative capabilities of IWCs, which are inherent due to the non-linear transfer function. Experiments carried out at 40 Gbit/s demonstrated the excellent 2R regenerative capabilities of an MZI. An OSNR of the converted signal above 37 dB was achieved (measured in 0.1 nm) even for an input OSNR as low as ~13 dB. The regenerative properties were also confirmed by the fact that a ~2 dB lower input power to an EDFA, used in a noise generator, was allowed. Furthermore, a scheme to obtain 3R regeneration in IWCs has been discussed and shown feasible in an MZI. The good performance was illustrated at 40 Gbit/s, which resulted in an insertion penalty of only ~0.5 dB. In addition, a scheme for simultaneous wavelength conversion, demultiplexing and 3R regeneration has been demonstrated experimentally. Good performance was achieved for conversion and demultiplexing from 40 to 10 Gbit/s.

Finally, a novel scheme for all-optical 2R regeneration in IWCs, without the normally accompanying wavelength conversion, has been presented. The performance was illustrated at 2.5 and 10 Gbit/s in an MI and the experiments

verified the excellent performance, i.e., a high IPDR, substantial extinction ratio improvement and 2R regenerative capabilities were demonstrated. The high-speed capabilities of the novel regeneration scheme were illustrated in an experiment carried out at 40 Gbit/s using an MZI, where clear noise suppression was achieved. Furthermore, an investigation of the transmission properties of the scheme revealed that the chirp added by the MZI had negligible influence on the transmission properties of the regenerated signal after ~31 km of standard fiber.

The question that remains unanswered is whether optical space switching, wavelength conversion and regeneration will be implemented in optical networks. That question, however, is really not that difficult to answer. Already vendors have started to offer optical cross-connect products employing space switches, which enables the implementation of optical meshed networks. This has been kick-started by the tremendous increase in demand for transmission bandwidth and the fact that optical techniques offer cost-effective solutions compared to their electrical counterparts. Since most surveys state that the demand will continue to increase at a rapid pace, there will be a need for even more complex optical functionalities. With respect to this, both wavelength conversion and regeneration are important in order to realise flexible large-scale networks. It has been demonstrated in this thesis, and in the literature, that IWCs offer very attractive features for both applications. In fact, if the overall performance of these devices is compared to other solutions for wavelength conversion and regeneration, they appear to be one of the most promising candidates at the moment. Therefore, when IWCs reach the maturity needed in commercial systems and cost-effective products with these devices are realised, they will be implemented.

Ph.D. publications

P1 B. Mikkelsen, S. L. Danielsen, D. Wolfson, H. N. Poulsen, R. J. S. Pedersen, K. S. Jepsen, A. Kloch, P. B. Hansen, A. T. Clausen and K. E. Stubkjaer, "*Wavelength converters and their use in optical networks*", In Proceedings of APCC'97, Sydney, Australia, 1997.

P2 S. L. Danielsen, P. B. Hansen, D. Wolfson, K. E. Stubkjaer, J. Y. Emery, F. Pommereau and M. Renaud, "*Detailed experimental and theoretical investigation and comparison of semiconductor optical amplifier gates and gain-clamped semiconductor optical amplifier gates*", In Technical Digest of OFC'98, paper TuH2, San Jose, USA, 1998.

P3 D. Wolfson, B. Mikkelsen, S. L. Danielsen, H. N. Poulsen, P. B. Hansen and K. E. Stubkjaer, "*Experimental and theoretical investigation of electro-optic and all-optical implementations of wavelength converting 2R-regenerators*", In Technical Digest of OFC'98, paper WB3, San Jose, USA, 1998.

P4 P. B. Hansen, A. Kloch, D. Wolfson, S. L. Danielsen, "*20 Gbit/s straight line cascade of two interferometric wavelength converters*", In Technical Digest of OECC'98, pp. 18-19, Chiba, Japan, 1998.

P5 D. Wolfson, S. L. Danielsen, H. N. Poulsen, P. B. Hansen and K. E. Stubkjaer, "*Experimental and theoretical investigation of the all-optical noise reduction capabilities of interferometric wavelength converters*", In Technical Digest of OECC'98, pp. 20-21, Chiba, Japan, 1998.

P6 K. E. Stubkjaer, S. L. Danielsen, A. Kloch, P. B. Hansen, K. S. Jepsen, H. N. Poulsen, D. Wolfson, A. T. Clausen, E. Limal and A. Buxens, "*All-optical wavelength converters*", In Technical Digest of OECC'98 (Invited paper), pp. 464-465, Chiba, Japan, 1998.

P7 A. Kloch, P. B. Hansen, D. Wolfson, S. L. Danielsen and K. E. Stubkjaer, "*Penalty free operation of two interferometric wavelength converters in cascade at 20 Gbit/s*", In Proceedings of The Rank Prize Funds, Mini Symposium on Ultra Fast Photonic Processing and Networks, Grasmere, Cumbria, 1998.

P8 K. E. Stubkjaer, K. S. Jepsen, A. T. Clausen, H. N. Poulsen, A. Buxens, S. L. Danielsen, P. B. Hansen, A. Kloch and D. Wolfson, "*High-speed photonic processing*", In Proceedings of The Rank Prize Funds, Mini Symposium on Ultra Fast Photonic Processing and Networks (Invited paper), Grasmere, Cumbria, 1998.

P9 A. Kloch, P. B. Hansen, D. Wolfson, S. L. Danielsen, K. E. Stubkjaer, J. Y. Emery, F. Pommereau, M. Renaud and M. Schilling, "*Assessment of dual-stage wavelength converter in OXC at 20 Gbit/s*", In Proceedings of ECOC'98, pp. 659-660, Madrid, Spain, 1998.

P10 D. Wolfson, S. L. Danielsen, C. Joergensen, B. Mikkelsen and K. E Stubkjaer, "*Detailed theoretical investigation of the input power dynamic range for gain-clamped semiconductor optical amplifier gates at 10 Gbit/s*", IEEE Photonics Technology Letters, Vol. 10, No. 9, pp. 1241-1243, 1998.

P11 D. Wolfson, S. L. Danielsen, H. N. Poulsen, P. B. Hansen and K. E. Stubkjaer, "*Experimental and theoretical investigation of the regenerative capabilities of electro-optic and all-optical interferometric wavelength converters*", IEEE Photonics Technology Letters, Vol. 10, No. 10, pp. 1413-1415, 1998.

P12 D. Wolfson and K. E Stubkjaer, "*Bit error rate assessment of 20 Gbit/s all-optical wavelength conversion for co- and counter-directional coupling scheme*", Electronics Letters, Vol. 34, No. 23, pp. 2259-2260, 1998.

P13 D. Wolfson, P. B. Hansen, A. Kloch and K. E. Stubkjaer, "*All-optical 2R regeneration based on interferometric structure incorporating semiconductor optical amplifiers*", Electronics Letters, Vol. 35, No. 1, pp. 59-60, 1999.

P14 K. E. Stubkjaer, A. Kloch, P. B. Hansen, H. N. Poulsen, D. Wolfson, K. S. Jepsen, A. T. Clausen, E. Limal and A. Buxens, "*Wavelength converter technology*", IEICE Transactions on Communications (Invited paper), Vol. E82-B, No. 2, pp. 390-400, 1999.

P15 D. Wolfson and K. E. Stubkjaer, "*Comparison of the cascadability of conventional and gain-clamped semiconductor optical amplifier gates in multi wavelength optical networks*", In Technical Digest of OFC'99, paper FB8, San Diego, USA, 1999.

P16 D. Wolfson, P. Hansen, A. Kloch, T. Fjelde, C. Janz, A. Coquelin, I. Guillemot, F. Gaborit, F. Poingt and M. Renaud, "*All-optical 2R regeneration at 40 Gbit/s in an SOA-based Mach-Zehnder interferometer*", In Technical Digest of OFC'99 (Post deadline paper), paper PD36, San Diego, USA, 1999.

P17 T. Fjelde, D. Wolfson P.B. Hansen, A. Kloch, C. Janz, A. Coquelin, I. Guillemot, F. Gaborit, F. Poingt, B. Dagens and M. Renaud, "*20 Gbit/s optical wavelength conversion in all-active Mach-Zehnder interferometer*", Electronics Letters, Vol. 35, No. 11, pp. 913-914, 1999.

P18 A. Kloch, P. B. Hansen, D. Wolfson, T. Fjelde and K. E. Stubkjaer, "*Wavelength converters*", IEICE Transactions on Communications (Invited paper), Vol. E82-B, No. 8, pp. 1209-1220, 1999.

P19 D. Wolfson, P. B. Hansen, T. Fjelde, A. Kloch, C. Janz, A. Coquelin, I. Guillemot, F. Gaborit, F. Poingt and M. Renaud, "*40 Gbit/s all-optical wavelength conversion in an SOA-based all-active Mach-Zehnder interferometer*", In Proceedings of ECOC'99, Vol. 2, pp. 170-171, Nice, France, 1999.

P20 D. Wolfson, P. B. Hansen, T. Fjelde, A. Kloch, C. Janz, A. Coquelin, I. Guillemot, F. Gaborit, F. Poingt and M. Renaud, "*40 Gbit/s all-optical 2R regeneration in an SOA-based all-active Mach-Zehnder interferometer*", In Proceedings of OECC'99, pp. 456-457, Beijing, China, 1999.

P21 T. Fjelde, P. B. Hansen, A. Kloch, D. Wolfson and K. E. Stubkjaer, "*Feasibility of optical packet switched WDM networks without packet synchronisation under bursty traffic conditions*", In Proceedings of OECC'99, pp. 462-464, Beijing, China, 1999.

P22 D. Wolfson, "*Detailed theoretical investigation and comparison of the cascadability of conventional and gain-clamped SOA gates in multi wavelength optical networks*", IEEE Photonics Technology Letters, Vol. 11, No. 11, pp. 1494-1496, 1999.

P23 D. Wolfson, A. Kloch, T. Fjelde, C. Janz, B. Dagens and M. Renaud, "*40 Gbit/s all-optical wavelength conversion, regeneration and demultiplexing in an SOA-based all-active Mach-Zehnder interferometer*", IEEE Photonics Technology Letters, Vol. 12, No. 3, pp. 332-334, 2000.

P24 D. Wolfson, T. Fjelde, A. Kloch, C. Janz, F. Poingt, I. Guillemot, F. Gaborit and M. Renaud, "*Detailed experimental investigation of an all-active Dual-Order Mode Mach-Zehnder wavelength converter*", In Technical Digest of OFC2000, paper TuF3, Baltimore, USA, 2000.

P25 T. Fjelde, D. Wolfson and A. Kloch, "*Influence of RZ and NRZ signal format on the high-speed performance of gain-clamped semiconductor optical amplifiers*", In Technical Digest of OFC2000, paper ThF5, Baltimore, USA, 2000.

P26 T. Fjelde, D. Wolfson, A. Kloch, C. Janz, A. Coquelin, I. Guillemot, F. Gaborit, F. Poingt, B. Dagens and M. Renaud, "*10 Gbit/s all-optical logic OR in monolithically integrated interferometric wavelength converter*", Electronics Letters, Vol. 36, No. 9, pp. 813-815, 2000.

P27 T. Fjelde, D. Wolfson, A. Kloch, C. Janz, A. Coquelin, I. Guillemot, F. Gaborit, F. Poingt, B. Dagens and M. Renaud, "*20 Gbit/s all-optical logic XOR using integrated interferometric wavelength converter*", In Technical Digest of OAA2000, paper OWB4, Quebec, Canada, 2000.

P28 D. Wolfson, T. Fjelde, A. Kloch, C. Janz, F. Poingt, I. Guillemot, F. Gaborit, A. Coquelin, B. Dagens and M. Renaud, "*Novel scheme for all-optical wavelength conversion in SOA-based interferometric devices*", In Technical Digest of OAA2000, paper OWB5, Quebec, Canada, 2000.

P29 D. Wolfson, A. Kloch, T. Fjelde, C. Janz, F. Poingt, I. Guillemot, F. Gaborit, A. Coquelin, B. Dagens and M. Renaud, "*High-speed all-optical wavelength conversion using SOAs*", In Technical Digest of IPR2000 (Invited paper), paper IFE1, Quebec, Canada, 2000.

P30 D. Wolfson, T. Fjelde, A. Kloch, C. Janz, F. Poingt, F. Pommereau, I. Guillemot, F. Gaborit and M. Renaud, "*Detailed experimental investigation of all-active Dual-Order Mode Mach-Zehnder wavelength converter*", Electronics Letters, Vol. 36, No. 15, pp. 1296-1297, 2000.

P31 D. Wolfson, T. Fjelde, A. Kloch, C. Janz, A. Coquelin, I. Guillemot, F. Gaborit, F. Poingt and M. Renaud, "*Experimental investigation at 10 Gbit/s of the noise suppression capabilities in a pass-through configuration in SOA-based interferometric structures*", IEEE Photonics Technology Letters, Vol. 12, No. 7, pp. 837-839, 2000.

P32 X. Zheng, F. Liu, D. Wolfson and A. Kloch, "*Suppression of crosstalk and ASE noise using a polarisation multiplexing technique and an SOA*", IEEE Photonics Technology Letters, Vol. 12, No. 8, pp. 1091-1093, 2000.

P33 H. N. Poulsen, A. T. Clausen, A. Buxens, L. Oxenloewe, C. Peucheret, C. Rasmussen, F. Liu, J. Yu, A. Kloch, T. Fjelde, D. Wolfson and P. Jeppesen, "*Ultra fast all-optical signal processing in semiconductor and fiber based devices*" In Proceedings of ECOC2000 (Invited paper), Vol. 3, pp. 59-62, Munich, Germany, 2000.

P34 P. Guerber, B. Lavigne, C. Janz, A. Jourdan, D. Wolfson, T. Fjelde and A. Kloch, "*Chirp optimised operation of an optical 3R regenerator*", In Proceedings of ECOC2000, Vol. 3, pp. 121-122, Munich, Germany, 2000.

P35 X. Zheng, F. Liu, J. Yu, D. Wolfson, A. Kloch and T. Fjelde, "*Simultaneous interferometric crosstalk suppression in WDM channels using polarisation multiplexing technique and SOA*", In Proceedings of ECOC2000, Vol. 3, pp. 169-170, Munich, Germany, 2000.

P36 D. Wolfson, A. Kloch and T. Fjelde, "*Detailed investigation of the cascadability of SOA-based gates for all-optical switching*", In Proceedings of ECOC2000, Vol. 3, pp. 163-169, Munich, Germany, 2000.

P37 T. Fjelde, A. Kloch, D. Wolfson, C. Janz, A. Coquelin, I. Guillemot, F. Gaborit, F. Poingt, B. Dagens and M. Renaud, "*Novel scheme for efficient label-swapping using simple XOR gate*", In Proceedings of ECOC2000, Vol. 4, pp. 63-64, Munich, Germany, 2000.

P38 D. Wolfson, T. Fjelde, A. Kloch, C. Janz, F. Poingt, I. Guillemot, F. Gaborit and M. Renaud, "*Novel scheme for all-optical wavelength conversion in SOA-based interferometric devices*", Electronics Letters, Vol. 36, No. 21, pp. 1794-1795, 2000.

P39 A. Kloch, D. Wolfson, T. Fjelde and K. E. Stubkjaer, "*New technologies for ultra high speed switching*", In Conference Program of OSA Annual meeting 2000 (Invited paper), paper Th1, Providence, USA, 2000.

P40 T. Fjelde, D. Wolfson, A. Kloch, B. Dagens, A. Coquelin, I. Guillemot, F. Gaborit, F. Poingt, and M. Renaud, "*Demonstration of 20 Gbit/s all-optical logic XOR in integrated SOA-based interferometric wavelength converter*", Electronics Letters, Vol. 36, No. 22, pp. 1863-1864, 2000.

P41 F. Liu, X. Zheng, H. N. Poulsen, D. Wolfson and P Jeppesen, "*Reduction of interferometric crosstalk induced penalty using a saturated semiconductor optical amplifier*", In Proceedings of LEOS2000, Vol. 1, pp. 273-274, Rio Grande, Puerto Rico, 2000.

P42 K. E. Stubkjaer, T. Fjelde, D. Wolfson, A. Kloch, H. N. Poulsen and A. T. Clausen, "*Functional elements for high-speed optical processing*", In Technical Digest of CPT2001 (Invited paper), pp. 55-58, Tokyo, Japan, 2001.

P43 T. Fjelde, A. Kloch and D. Wolfson, B. Dagens, A. Coquelin, I. Guillemot, F. Gaborit, F. Poingt and M. Renaud, "*Novel scheme for simple label-swapping employing logic XOR in an integrated interferometric wavelength converter",* Submitted to IEEE Photonics Technology Letters.

P44 D. Wolfson, T. Fjelde and A. Kloch, "*SOA-based devices for all-optical wavelength conversion and regeneration*", Submitted to OECC/IOOC2001 (Invited paper), Sydney, Australia, 2001.

P45 T. Fjelde, A. Kloch, D. Wolfson, B. Dagens, R. Brenot, A. Labrousse, E. Roux, F. Gaborit, F. Poingt and M. Renaud, "*Simultaneous 2x10 to 20 Gbit/s time-division multiplexing and wavelength conversion using an integrated SOA-based Mach-Zehnder interferometer"*, Submitted to OECC/IOOC2001, Sydney, Australia, 2001.

P46 D. Wolfson, T. Fjelde and A. Kloch, "*Technologies for all-optical wavelength conversion in DWDM networks*", Submitted to CLEO Pacific Rim 2001 (Invited paper), Chiba, Japan, 2001.

P47 T. Fjelde, D. Wolfson, A. Kloch, "*Semiconductor All-Optical Functional Devices*", Submitted to ITCom2001 (Invited paper), Denver, USA, 2001.

References

[1] T. Freeman, "*Bandwidth boom*", In Fibre Systems Europe, Vol. 5, No. 1, pp.18, 2001.

[2] T. W. Chung, J. Coulter, J. Fitchett, S. Mokbel and B. S. Arnaud, "*Architectural and engineering issues for building an optical Internet*", CANARIE Inc, see http://www.canet2.net

[3] SN 10000 Intelligent Optical Transport System from Sycamore.

[4] R. C. Alferness, H. Kogelnik and T. H. Wood, "*The evolution of optical systems: Optics everywhere*", Bell Labs Technical Journal, Vol. 5, No. 1, January-March, pp. 188-202, 2000.

[5] E. Desurvire, J. R. Simpson and P. C. Becker, "*High-gain erbium-doped travelling-wave fiber amplifier*", Optical Letters, Vol. 12, Issue 11, pp. 888-890, 1987.

[6] D. Sadot and E. Boimovich, "*Tunable optical filters for dense WDM networks*", IEEE Communications Magazine, December, 1998.

[7] Ericsson Optical Networking (ERION™). A DWDM ring structure.

[8] L. Y. Lin, E. L. Goldstein and R. W. Tkach, "*Free-space micromachined optical switches with submillisecond switching time for large-scale optical crossconnects*", IEEE Photonics Technology Letters, Vol. 10, No. 4, pp. 525-527, 1998.

[9] Ericsson Optical Networking (ERION™).

[10] M. Renaud, M. Bachmann and M. Erman, "*Semiconductor optical space switches*", IEEE Journal of Selected Topics in Quantum Electronics, Vol. 2, No. 2, pp. 277-288, 1996.

[11] R. E. Wagner, R. C. Alferness, A. A. M. Saleh and M. S. Goodman, "*MONET: Multiwavelength Optical Networking*", IEEE Journal of Lightwave Technology, Vol. 14, No. 6, pp. 1349-1355, 1996.

[12] L. Berthelon, S. Bjørnstad, P. Bonno, P. Bousselet, M. Chbat, C. Coeurjolly, P. J. Gødsvang, R. Grønvold, P. M. Kjeldsen, A. Kleivstul, A. Jourdan, J. S. Mapsen, A. Noury, T. Olsen and G. Soulage, "*A cross-boarder WDM networking field trial with all-optical wavelength-translating crossconnects*", In Technical Digest of OFC'98 (Post-deadline paper), paper PD26, San Jose, USA, 1998.

[13] WaveStar™ LambdaRouter from Lucent Technologies.

[14] S. J. B. Yoo, "*Wavelength conversion technologies for WDM network applications*", IEEE Journal of Lightwave Technology, Vol. 14, No. 6, pp.955-966, 1996.

[15] T. Durhuus, B. Mikkelsen, C. Joergensen, S. L. Danielsen and K. E Stubkjaer, "*All-optical wavelength conversion by semiconductor optical amplifiers*", IEEE Journal of Lightwave Technology, Vol. 14, No. 6, pp. 942-954, 1996.

[16] B. Ramamurthy and B. Mukherjee, "*Wavelength conversion in WDM networking*", IEEE Journal on Selected Areas in Communications, Vol. 16, No. 7, pp. 1061-1073, 1998.

[17] K.-I. Sato "*Advances in transport network technologies*", Artech House Inc. 1996, Norwood.

[18] O. Gerstel, R. Ramaswami and G. Sasaki, "*Benefits of limited wavelength conversion in WDM ring networks*", In Technical Digest of OFC'97, paper WD1, Dallas, USA, 1997.

[19] N. Wauters, W. Van Parys, B. Van Caenegem and P. Demeester, "*Reduction of wavelength blocking through partitioning with wavelength converters*", In Technical Digest of OFC'97, paper WD4, Dallas, USA, 1997.

[20] K.-C. Lee and V. O. K. Li, "*A wavelength-convertible optical network*", IEEE Journal of Lightwave Technology, Vol. 11, No. 5/6, pp. 962-970, 1993.

[21] A. Jourdan, F. Bakhti, L. Berthelon, F. Bruyere, M. Chbat, D. Chiaroni, C. Drion, G. J. Eilenberger, M. Garnot, F. Masetti, P. A. Perrier and M. Renaud, "*Key building blocks for high-capacity WDM photonic transport networks*" IEEE Journal on Selected Areas in Communications, Vol. 16, No. 7, pp. 1286-1297, 1998.

[22] J. C. Simon, L. Billès, A. Dupas and L. Bramerie, "*All optical regeneration techniques*", In Proceedings of ECOC'99, Vol. 2, pp. 256-259, 1999.

[23] H. Takara, T. Ohara, K. Mori, K. Sato, E. Yamada, T. Morioka and K-I. Sato, "*Over 1000 channel optical frequency chain generation from a supercontiniuum source with 12.5 GHz channel spacing for DWDM and frequency standards*", In Proceedings of ECOC2000 (Post-deadline paper), paper 3.1, Munich, Germany, 2000.

[24] M. Nakazawa, T. Yamamoto and K. R. Tamura, "*1.28 Tbit/s – 70 km OTDM transmission using third- and fourth-order simultaneous dispersion compensation with phase modulator*", In Proceedings of ECOC2000 (Post-deadline paper), paper 2.6, Munich, Germany, 2000.

[25] P. Lagasse, P. Demeester, A. Ackaert, W. Van Parys, B. Van Caenegem, M. O'Mahony, A. Tzanakaki, K. Stubkjaer and J. Benoit, "*Roadmap towards the optical communication age*", A European view by the Horizon project and the ACTS photonic domain, November 1999 draft edition.

[26] T. Ito, K. Fukuchi, K. Sekiya, D. Ogasahara, R. Ohhira and T. Ono, "*6.4 Tbit/s (160x40 Gbit/s) WDM transmission experiment with 0.8 bit/s/Hz spectral efficiency*", In Proceedings of ECOC2000 (Post-deadline paper), paper 1.1, Munich, Germany, 2000.

[27] N. DeVito, "*How will the optical layer change today's networks?*", Lightwave Magazine, Vol. 16, Nov. 1999.

[28] A. McGuire and P. Bonenfant, "*Standards: The blueprints for optical networking*", IEEE Communications magazine, February, 1998.

[29] P. Bonenfant, "*Optical networking standards*", In Tutorial Sessions of OFC200, paper TuI, Baltimore, USA, 2000.

[30] Alcatel 1901 ICM, 10 Gbit/s all-optical interferometric wavelength converter.

[31] M. W. Chbat, E. Grard, L. Berthelon, A. Jourdan, P. A. Perrier, A. Leclert, B. Landousies, A. Ramdane, N. Parnis, E. V. Jones, E. Limal, H. N. Poulsen, R. J. S. Pedersen, N. Flaaronning, D. Vercauteren, M. Puelo, E. Ciaramella, G. Marone, R. Hess, H. Melchior, W. Van Parys, P. Demeester, P. J. Godsvang, T. Olsen and D. R. Hjelme, "*Towards wide-scale all-optical transparent networking: The ACTS Optical Pan-European Network (OPEN) project*", IEEE Journal on Selected Areas in Communications, Vol. 16, No. 7, pp. 1226-1244, 1998.

[32] See http://www.intec.rug.ac.be/research/projects/horizon/eeoc98pres/open.pdf

[33] P. Gambini, M. Renaud, C. Guillemot, F. Callegati, I. Andonovic, B. Bostica, D. Chiaroni, G. Corazza, S. L. Danielsen, P. Gravey, P. B. Hansen, M. Henry, C. Janz, A. Kloch, R. Krahenbuhl, C. Raffaelli, M. Schilling, A. Talneau and L. Zucchelli, "*Transparent optical packet switching: network architecture and demonstrations in the KEOPS project*", IEEE Journal on Selected Areas in Communications, Vol. 16, No. 7, pp. 1245-1259, 1998.

[34] C. Guillemot, M. Renaud, P. Gambini, C. Janz, I. Andonovic, R. Bauknecht, B. Bostica, M. Burizo, F. Callegati, M. Casoni, D. Chiaroni, F. Clerot, S. L. Danielsen, F. Dorgeuille, A. Dupas, A. Franzen, P. B. Hansen, D. K. Hunter, A. Kloch, R. Krahenbuhl, B. Lavigne, A. le Corre, C. Raffaelli, M. Schilling, J. C. Simon and L. Zucchelli, "*Transparent optical packet switching: The European ACTS KEOPS Project Approach*", IEEE Journal of Lightwave Technology, Vol. 16, No. 12, pp. 2117-2134, 1998.

[35] B. Lavigne, D. Chiaroni, P. Guerber, L. Hamon and A. Jourdan, "*Improvement of regeneration capabilities in semiconductor optical amplifier-based 3R regenerator*", In Technical Digest of OFC'99, paper TuJ3, San Diego, USA, 1999.

[36] B. Lavigne, P. Guerber, C. Janz, A. Jourdan and M. Renaud, "*Full validation of an optical 3R regenerator at 20 Gbit/s*", In Technical Digest of OFC2000, paper ThF7, Baltimore, USA, 2000.

[37] T. Otani, T. Miyazaki and S. Yamamoto, "*40 Gbit/s signal transmission using optical 3R regenerator based on electroabsorption modulators*", In Technical Digest of OFC2000, paper ThP3, Baltimore, USA, 2000.

[38] P. Brindel, O. Leclerc, D. Rouvillain, B. Dany, E. Desurvire and P. Nouchi, "*Experimental demonstration of new regeneration scheme for 40 Gbit/s dispersion-managed long-haul transmissions*", Electronics Letters, Vol. 36, No. 1, pp. 61-62, 2000.

[39] K. Inoue, T. Hasegawa and H. Toba, "*Influence of stimulated brillouin scattering and optimum length in fiber four-wave mixing wavelength conversion*", IEEE Photonics Technology Letters, Vol. 7, No. 3, pp. 327-329, 1995.

[40] M. F. C. Stephens, D. Nesset, R. V. Penty, I. H. White and M. J. Fice, "*Wavelength conversion at 40 Gbit/s via four wave mixing in semiconductor optical amplifier with integrated pump laser*", Electronics Letters, Vol. 35, No. 5, pp. 420-421, 1999.

[41] A. Mecozzi, S. Scotti, A. D'Ottavi, E. Iannone and P. Spano, "*Four-wave mixing in travelling-wave semiconductor amplifiers*", IEEE Journal of Quantum Electronics, Vol. 31, No. 4, pp. 689-699, 1995.

[42] A. E. Kelly, A. D. Ellis, D. Nesset, R. Kashyap and D. G. Moodie, "*100 Gbit/s wavelength conversion using FWM in an MQW semiconductor optical amplifier*", Electronics Letters, Vol. 34, No. 20, pp. 1955-1956, 1998.

[43] S. Watanabe, S. Takeda and T. Chikama, "*Interband wavelength conversion of 320 Gb/s (32x10 Gb/s) WDM signal using polarisation insensitive fiber four-wave mixer*", In Proceedings of ECOC'98 (Post-deadline paper), Vol. 3, pp. 85-87, Madrid, Spain, 1998.

[44] A. D'Ottavi, P. Spano, G. Hunziker, R. Paiella, R. Dall'Ara, G. Guekos and K. J. Vahala, "*Wavelength conversion at 10 Gbit/s by four-wave mixing over a 30-nm interval*", IEEE Photonics Technology Letters, Vol. 10, No. 7, pp. 952-954, 1998.

[45] T. J. Morgan, J. P. R. Lacey and R. S. Tucker, "*Widely tunable four-wave mixing in semiconductor optical amplifiers with constant conversion efficiency*", IEEE Photonics Technology Letters, Vol. 10, No. 10, pp. 1401-1403, 1998.

[46] T. J. Morgan, R. S. Tucker and J. P. R. Lacey, "*All-optical wavelength translation over 80 nm at 2.5 Gbit/s using four-wave mixing in a semiconductor optical amplifier*", IEEE Photonics Technology Letters, Vol. 11, No. 8, pp. 982-984, 1999.

[47] S. Watanabe, H. Kuwatsuka, S. Takeda and H. Ishikawa, "*Polarisation-insensitive wavelength conversion and phase conjugation using bi-directional forward four-wave mixing in a lasing DFB-LD*", Electronics Letters, Vol. 33, No. 4, pp. 316-317, 1997.

[48] R. B. Lee, D. F. Geraghty, M. Verdiell, M. Ziari, A. Mathur and K. J. Vahala, "*Cascaded wavelength conversion by four-wave mixing in a strained semiconductor optical amplifier at 10 Gb/s*", IEEE Photonics Technology Letters, Vol. 9, No. 6, pp. 752-754, 1997.

[49] D. F. Geraghty, R. B. Lee, K. J. Vahala, M. Verdiell, M. Ziari and A. Mathur, "*Wavelength conversion up to 18 nm at 10 Gbit/s by four-wave mixing in a semiconductor optical amplifier*", IEEE Photonics Technology Letters, Vol. 9, No. 4, pp. 452-454, 1997.

[50] L. Oxenloewe, A. T. Clausen and H. N. Poulsen, "*Wavelength conversion in an electroabsorption modulator*", In Proceedings of ECOC2000, Vol. 3, pp. 303-304, Munich, Germany, 2000.

[51] J. P. Sokoloff, P. R. Prucnal and M. Kane, "*A terahertz optical asymmetric demultiplexer (TOAD)*", IEEE Photonics Technology Letters, Vol. 5, No. 7, pp. 787-790, 1993.

[52] N. J. Doran and D. Wood, "*Nonlinear-optical loop mirror*", Optical Letters, Vol. 13, Issue 1, pp. 56-58, 1988.

[53] N. S. Patel, K. A. Rauschenbach and K. L. Hall, "*40-Gb/s demultiplexing using an ultrafast nonlinear interferometer (UNI)*", IEEE Photonics Technology Letters, Vol. 8, No. 12, pp. 1695-1697, 1996.

[54] B-E. Olsson, P. Öhlén, L. Rau and D. J. Blumenthal, "*A simple and robust 40-Gb/s wavelength converter using fiber cross-phase modulation and optical filtering*", IEEE Photonics Technology Letters, Vol. 12, No. 7, pp. 846-848, 2000.

[55] A. E. Kelly, I. D. Phillips, R. J. Manning, A. D. Ellis, D. Nesset, D. G. Moodie and R. Kashyap, "*80 Gbit/s all-optical regenerative wavelength conversion using semiconductor optical amplifier based interferometer*", Electronics Letters, Vol. 35, No. 17, pp. 1477-1478, 1999.

[56] C. Joergensen, S. L. Danielsen, K. E. Stubkjaer, M. Schilling, K. Daub, P. Doussiere, F. Pommerau, P. B. Hansen, H. N. Poulsen, A. Kloch, M. Vaa, B. Mikkelsen, E. Lach, G. Laube, W. Idler and K. Wünstel, "*All-optical wavelength conversion at bit rates above 10 Gb/s using semiconductor optical amplifiers*", IEEE Journal of Selected Topics in Quantum Electronics, Vol. 3, No. 5, pp. 1168-1180, 1997.

[57] A. D. Ellis, A. E. Kelly, D. Nesset, D. Pitcher, D. G. Moodie and R. Kashyap, "*Error free 100 Gbit/s wavelength conversion using grating assisted cross-gain modulation in 2mm long semiconductor amplifier*", Electronics Letters, Vol. 34, No. 20, pp. 1958-1959, 1998.

[58] T. Durhuus, C. Joergensen, B. Mikkelsen, R. J. S. Pedersen and K. E. Stubkjaer, "*All optical wavelength conversion by SOAs in a Mach-Zehnder configuration*", IEEE Photonics Technology Letters, Vol. 6, No. 1, pp. 53-55, 1994.

[59] B. Mikkelsen, T. Durhuus, C. Joergensen, R. J. S. Pedersen, C. Braagaard and K. E. Stubkjaer, "*Polarisation insensitive wavelength conversion of 10 Gbit/s signals with SOAs in a Michelson interferometer*", Electronics Letters, Vol. 30, No. 3, pp. 260-261, 1994.

[60] B. Mikkelsen, M. Vaa, H. N. Poulsen, S. L. Danielsen, C. Joergensen, A. Kloch, P. B. Hansen, K. E. Stubkjaer, K. Wünstel, K. Daub, E. Lach, G. Laube, W. Idler, M. Schilling and S. Bouchoule, "*40 Gbit/s all-optical wavelength converter and RZ-to-NRZ format adapter realised by monolithic integrated active Michelson interferometer*", Electronics Letters, Vol. 33, No. 2, pp. 133-134, 1997.

[61] B. Mikkelsen, K. S. Jepsen, M. Vaa, H. N. Poulsen, K. E. Stubkjaer, R. Hess, M. Duelk, W. Vogt, E. Gamper, E. Gini, P. A. Besse, H. Melchior, S. Bouchoule and F. Devaux, "*All-optical wavelength converter scheme for high speed RZ signal formats*", Electronics Letters, Vol. 33, No. 25, pp. 2137-2139, 1997.

[62] C. Joergensen, S. L. Danielsen, P. B. Hansen, K. E. Stubkjaer, M. Schilling, K. Daub, E. Lach, G. Laube, W. Idler and K. Wünstel, "*All-optical 40 Gbit/s compact integrated interferometric wavelength converter*", In Technical Digest of OFC'97, paper TuO1, Dallas, USA, 1997.

[63] Y. Ueno, S. Nakamura, K. Tajima and S. Kitamura, "*3.8-THz wavelength conversion of picosecond pulses using a semiconductor delayed-interference signal-wavelength converter (DISC)*", IEEE Photonics Technology Letters, Vol. 10, No. 3, pp. 346-348, 1998.

[64] Y. Ueno, S. Nakamura, K. Tajima and S. Kitamura, "*New wavelength converter for picosecond RZ pulses*", In Proceedings of ECOC'98, Vol. 1, pp. 657-658, 1998.

[65] S. Nakamura, Y. Ueno and K. Tajima, "*Error-free all-optical data pulse regeneration at 84 Gbps and wavelength conversion at 168 Gbps with symmetric Mach-Zehnder all-optical switches*", In Technical Digest of OAA200 (Post-deadline paper), PDP4, Quebec, Canada, 2000.

[66] Y. Ueno, S. Nakamura, H. Hatakeyama, T. Tamanuki, T. Sasaki and K. Tajima, "*168-Gb/s OTDM wavelength conversion using an SMZ-type all-optical converter*", In Proceedings of ECOC2000, Vol. 1, pp. 13-14, Munich, Germany, 2000.

[67] J. Leuthold, C. H. Joyner, B. Mikkelsen, G. Raybon, J. L. Pleumeekers, B. I. Miller, K. Dreyer and C. A. Burrus, "100 Gbit/s all-optical wavelength conversion with an integrated SOA delayed-interference configuration" In Technical Digest of OAA200, paper OWB3, Quebec, Canada, 2000.

[68] P. Öhlen and E. Berglind, "*Noise accumulation and BER estimates in concatenated nonlinear optoelectronic repeaters*", IEEE Photonics Technology Letters, Vol. 9, No. 7, pp. 1011-1013, 1997.

[69] P. S. Cho, D. Mahgerefteh and J. Goldhar, "*All-optical 2R regeneration and wavelength conversion at 20 Gb/s using an electroabsorption modulator*", IEEE Photonics Technology Letters, Vol. 11, No. 12, pp. 1662-1664, 1999.

[70] P. S. Cho, P. Sinha, D. Mahgerefteh and G. M. Carter, "*All-optical regeneration at the receiver of 10-Gb/s RZ data transmitted over 30000 km using an electroabsorption modulator*", IEEE Photonics Technology Letters, Vol. 12, No. 2, pp. 205-207, 2000.

[71] T. Miyazaki, N. Edagawa, M. Suzuki and S. Yamamoto, "*Novel optical-regenerator using electroabsorption modulators*", In Technical Digest of OFC'99, paper WM53, San Diego, USA, 1999.

[72] T. Otani, T. Miyazaki and S. Yamamoto, "*Optical 3R regenerator using wavelength converters based on electroabsorption modulator for all-optical network applications*", IEEE Photonics Technology Letters, Vol. 12, No. 4, pp. 431-433, 2000.

[73] M. Nakazawa, K. Suzuki and H. Kubota, "*10 Gbit/s soliton data transmission over one million kilometres*", Electronics Letters, Vol. 27, No. 14, pp. 1270-1272, 1991.

[74] M. Nakazawa, K. Suzuki, H. Kubota, A. Sahara and E. Yamada, "*160 Gbit/s WDM (20Gbit/s x 8 channels) soliton transmission over 10000 km using in-line synchronous modulation and optical filtering*", Electronics Letters, Vol. 34, No. 1, pp. 103-104, 1998.

[75] K. Suzuki, H. Kubota, A. Sahara and M. Nakazawa, "*40 Gbit/s single channel optical soliton transmission over 70000 km using in-line synchronous modulation and optical filtering*", Electronics Letters, Vol. 34, No. 1, pp. 98-100, 1998.

[76] M. Nakazawa, K. Suzuki and H. Kubota, "*Single-channel 80 Gbit/s soliton transmission over 10000 km using in-line synchronous modulation*", Electronics Letters, Vol. 35, No. 2, pp. 162-164, 1999.

[77] P. Brindel, B. Dany, O. Leclerc and E. Desurvire, "*'Black box' optical regenerator for RZ transmission systems*", Electronics Letters, Vol. 35, No. 6, pp. 480-481, 1999.

[78] O. Leclerc, B. Dany, D. Rouvillian, P. Brindel, E. Desurvire, C. Duchet, A. Shen, F. Devaux, A. Coquelin, M. Goix, S. Bouchoule, L. Fleury and P. Nouchi, "*Simultaneously regenerated 4x40 Gbit/s dense WDM transmission over 10.000 km using single 40 GHz InP Mach-Zehnder modulator*", Electronics Letters, Vol. 36, No. 18, pp. 1574-1575, 2000.

[79] B. Mikkelsen, S. L. Danielsen, C. Joergensen, R. J. S. Pedersen, H. N. Poulsen and K. E. Stubkjaer, "*All-optical noise reduction capability of interferometric wavelength converters*", Electronics Letters, Vol. 32, No. 6, pp. 566-567, 1996.

[80] A. Dupas, L. Billès, J. C. Simon, B. Landousies, M. Henry, I. Valiente, F. Ratovelomanana, A. Enard and N. Vodjdani, "*2R all-optical regenerator assessment at 2.5 Gbit/s over 3600 km using only standard fibre*", Electronics Letters, Vol. 34, No. 35, pp. 2424-2425, 1998.

[81] K. S. Jepsen, A. Buxens, A. T. Clausen, H. N. Poulsen, B. Mikkelsen and K. E. Stubkjaer, "*20 Gbit/s optical 3R regeneration using polarisation-independent monolithically integrated Michelson interferometer*", Electronics Letters, Vol. 34, No. 5, pp. 472-474, 1998.

[82] S. Fischer, M. Dülk, E. Gamper, W. Vogt, E. Gini, H. Melchior, W. Hunziker, D. Nesset and A. D. Ellis, "*Optical 3R regenerator for 40 Gbit/s networks*", Electronics Letters, Vol. 35, No. 23, pp. 2047-2049, 1999.

[83] N. A. Jackman, S. H. Patel, B. P. Mikkelsen and S. K. Korotky, "*Optical cross connects for optical networking*", Bell Labs Technical Journal, Vol. 4, No. 1, January-March, pp. 262-281, 1999.

[84] T. Ido, M. Koizumi, S. Tanaka, M. Suzuki and H. Inoue, "*Polarisation and wavelength insensitive MQW electroabsorption optical gates for WDM switching systems*", IEEE Photonics Technology Letters, Vol. 8, No. 6, pp. 788-790, 1996.

[85] R. Weinmann, D. Baums, U. Cebulla, H. Haisch, D. Kaiser, E. Kühn, E. Lach, K. Satzke, J. Weber, P. Wiedemann and E. Zielinski, "*Polarisation-independent and ultra-high bandwidth electroabsorption modulator in multiquantum-well deep-ridge waveguide technology*", IEEE Photonics Technology Letters, Vol. 8, No. 7, pp. 891-893, 1996.

[86] T. Ido, H. Sano, M. Suzuki, S. Tanaka and H. Inoue, "*High-speed MQW electroabsorption optical modulators integrated with low-loss waveguides*", IEEE Photonics Technology Letters, Vol. 7, No. 2, pp. 170-172, 1995.

[87] E. Lach, G. Laube, M. Schilling, A. Ambrosy, J. Hehmann and L. Dembeck, "*InP-based space switch module for 1.55 μm with wide wavelength span, low noise and 10 Gbit/s transparency*", In Proceedings of ECOC'95, Vol. 1, pp. 111-114, Brussels, Belgium, 1995.

[88] D. H. P. Maat, Y. C. Zhu, F. H. Groen, H. Van Brug, H. J. Frankena and X. J. M. Leijtens, "*Polarisation-independent dilated InP-based space switch with low crosstalk*", IEEE Photonics Technology Letters, Vol. 12, No. 3, pp. 284-286, 2000.

[89] H. Nishinoto, M. Iwasaki, S. Suzuki and M. Kondo, "*Polarisation independent $LiNbO_3$ matrix switch*", IEEE Photonics Technology Letters, Vol. 2, No. 9, pp. 634-636, 1990.

[90] D. Chiaroni, D. De Bouard, P. Doussière, C. Chauzat and M. Sotom, "*High performance semiconductor optical amplifier gate for fast WDM packet switching*", In Proceedings of ECOC'95, Vol. 1, pp. 115-118, 1995.

[91] T. Durhuus, "*Semiconductor optical amplifiers: amplification and signal processing*", Ph.D. thesis LD114, Technical University of Denmark, Department of Electromagnetic Systems, 1995.

[92] C. Joergensen, "*Optical amplifiers and processing in high-capacity photonic networks*", Ph.D. thesis LD124, Technical University of Denmark, Department of Electromagnetic Systems, 1997.

[93] J. Y. Emery, T. Doucellier, M. Bachmann, P. Doussière, F. Pommereau, R. Ngo, F. Gaborit, L. Goldstein, G. Laube and J. Barrau, "*High performance 1.55 μm polarisation-insensitive semiconductor optical amplifier based on low-tensile-strained bulk GaInAsP*", Electronics Letters, Vol. 33, No. 12, pp. 1083-1084, 1997.

[94] G. Soulage, P. Doussière, A. Jourdan and M. Sotom, "*Clamped gain travelling wave semiconductor optical amplifier as a large dynamic range optical gate*", In Proceedings of ECOC'94, Vol. 1, pp. 451-454, Florence, Italy, 1994.

[95] L. Lablonde, I. Valiente, E. Delevaque, S. Boj and J. C. Simon, "*Experimental and theoretical investigation of a gain clamped semiconductor optical amplifier*", In Proceedings of ECOC'94, Vol. 2, pp. 715-718, Florence, Italy, 1994.

[96] P. Doussière, P. Garabedian, C. Graver, D. Bonnevie, T. Fillion, E. Derouin, M. Mannot, J. G. Provost, D. Leclerc and M. Klenk, "*1.55 μm polarisation independent semiconductor optical amplifier with 25 dB fiber to fiber gain*", IEEE Photonics Technology Letters, Vol. 6, No. 2, pp. 170-172, 1994.

[97] G. P. Agrawal and N. K. Dutta, "*Long-wavelength semiconductor lasers*", Van Nostarnd Reinhold Company Inc. 1986, New York.

[98] T. Durhuus, B. Mikkelsen and K. E. Stubkjaer, "*Detailed dynamic model for semiconductor optical amplifiers and their crosstalk and intermodulation distortion*", IEEE Journal of Lightwave Technology, Vol. 10, No. 8, pp. 1056-1065, 1992.

[99] B. Mikkelsen, "*Optical amplifiers and their applications*", Ph.D. thesis LD112, Technical University of Denmark, Department of Electromagnetic Systems, 1994.

[100] B. R. Bennet, "*Carrier induced change in the refractive index of InP, GaAs and InPGaAsP*", IEEE Journal on Quantum Electronics, Vol. 26, No. 1, pp. 113-122, 1990.

[101] S. L. Danielsen, "*Traffic analysis and signal processing in high-capacity optical networks*", Ph.D. thesis LD133, Technical University of Denmark, Department of Electromagnetic Systems, 1997.

[102] P. B. Hansen, "*Optical packet switched networks*", Ph.D. thesis LD1, Technical University of Denmark, Research Center COM, 1999.

[103] J. L. Pleumeekers et al., "*Relaxation oscillations in the gain recovery of gain-clamped semiconductor optical amplifier: simulation and experiments*", In Technical Digest of OAA'97, paper WB5, pp. 224-227, Victoria, Canada, 1997.

[104] G. Soulage, A. Jourdan, P. Doussière, M. Bachman, J. Y. Emery, J. Da Loura and M. Sotom, "*4x4 space-switch based on clamped-gain semiconductor optical amplifiers in a 16x10 Gbit/s WDM experiment*", In Proceedings of ECOC'96, Vol. 4, pp. 145-148, Oslo, Norway, 1996.

[105] F. Dorgeuille, L. Noirie, J-P. Faure, A. Ambrosy, S. Rabaron, F. Boubal, M. Schilling and C. Artigue, "*1.28 Tbit/s throughput 8x8 optical switch based on arrays of gain-clamped semiconductor optical amplifier gates*", In Technical Digest of OFC2000 (Post-deadline paper), PD18, Baltimore, USA, 2000.

[106] Y. Arakawa and A. Yariv, "*Quantum well laser - gain, spectra, dynamics*", IEEE Journal of Quantum Electronics, Vol. 22, No. 9, pp. 1887-1899, 1986.

[107] S. L. Danielsen, B. Mikkelsen, C. Joergensen, T. Durhuus and K. E. Stubkjaer, "*WDM packet switch architectures and analysis of the influence of tuneable wavelength converters on the performance*", IEEE Journal of Lightwave Technology, Vol. 15, No. 2, pp. 219-227, 1997.

[108] S. L. Danielsen, P. B. Hansen and K. E. Stubkjaer, "*Wavelength conversion in optical packet switching*", IEEE Journal of Lightwave Technology, Vol. 16, No. 12, pp. 2095-2108, 1998.

[109] K. Sato, S. Okamoto and H. Hadama, "*Network performance and integrity enhancement with optical path layer technologies*", Journal on Selected Areas of Communications, Vol. 12, No. 1, pp. 159-169, 1994.

[110] B. Glance, J. M. Wiesenfeld, U. Koren, A. H. Gnauck, H. M. Presby and A. Jourdan, "*High performance optical wavelength shifter*", Electronics Letters, Vol. 28, No. 18, pp. 1714-1715, 1992.

[111] A. Tzanakaki, K. M. Guild, D. Simeonidu. M. J. O'Mahony, "*Penalty-free concatenation of 25 optical cross-connects performing reconfigurable wavelength routing*", In Proceedings of ECOC'99, Vol. 1, pp. 254-255, Nice, France, 1999.

[112] J. S. Perino, J. M. Wiesenfeld and B. Glance, "*Fibre transmission of 10 Gbit/s signals following wavelength conversion using a travelling-wave semiconductor optical amplifier*", Electronics Letters, Vol. 30, No. 3, pp. 256-258, 1994.

[113] A. Kloch, "*Circuit switched optical networks*", Ph.D. thesis LD8, Technical University of Denmark, Research Center COM, 1999.

[114] A. Kloch and K. E. Stubkjaer, "*Accumulation of jitter in cascaded wavelength converters based on semiconductor optical amplifiers*", In Technical Digest of OFC'99, paper FB4, San Diego, USA, 1999.

[115] N. Storkfelt, B. Mikkelsen, D. S. Olesen, M. Yamaguchi and K. E. Stubkjaer, "*Measurement of carrier lifetime and linewidth enhancement factor for 1.5 μm ridge-waveguide laser amplifier*", IEEE Photonics Technology Letters, Vol. 3, No. 7, pp. 632-634, 1991.

[116] F. Girardin, G. Guekos and A. Houbavis, "*Gain recovery of bulk semiconductor optical amplifers*", IEEE Photonics Technology Letters, Vol. 10, No. 6, pp. 784-786, 1998.

[117] D. D. Marcenac, A. E. Kelly, D. Nesset and D. A. O. Davies, "*Bandwidth enhancement via cross-gain modulation by semiconductor optical amplifier cascade*", Electronics Letters, Vol. 31, No. 17, pp. 1442-1443, 1995.

[118] C. Joergensen, S. L. Danielsen, M. Vaa, B. Mikkelsen, K. E. Stubkjaer, P. Doussiere, F. Pommerau, L. Goldstein and M. Goix, "*40 Gbit/s all-optical wavelength conversion by semiconductor optical amplifiers*", Electronics Letters, Vol. 32, No. 4, pp. 367-368, 1996.

[119] S. L. Danielsen, C. Joergensen, M. Vaa, B. Mikkelsen, K. E. Stubkjaer, P. Doussiere, F. Pommerau, L. Goldstein, R. Ngo and M. Goix, "*Bit error rate assessment of 40 Gbit/s all-optical polarisation independent wavelength converter*", Electronics Letters, Vol. 32, No. 18, pp. 1688-1689, 1996.

[120] J. Mørk, A. Mecozzi and G. Eisenstein, "*The modulation respeonse of a semiconductor optical laser*", IEEE Journal of Selected Topics in Quantum Electronics, Vol. 5, No. 3, pp. 851-860, 1999.

[121] T. Ducellier and D. Carpenter, "*Integrated GAG-SOA (Gain Attenuation Gain SOA) for ultra-high speed wavelength conversion*", COST 240 Workshop on SOA-based components for optical networks, pp. 11.1-11.3, Prague, Czech Republic, 1997.

[122] B. Mikkelsen, M. Vaa, H. N. Poulsen, S. L. Danielsen, C. Joergensen, A. Kloch, P. B. Hansen, K. E. Stubkjaer, K. Wünstel, K. Daub, E. Lach, G. Laube, W. Idler, M. Schilling and S. Bouchoule, "*40 Gbit/s all-optical wavelength converter and RZ-to-NRZ format adapter realised by monolithic integrated active Michelson interferometer*", Electronics Letters, Vol. 33, No. 2, pp. 133-134, 1997.

[123] A. E. Kelly, D. D. Marcenac and D. Nesset, "*40 Gbit/s wavelength conversion over 24.6 nm using FWM in a semiconductor optical amplifier with an optimised MQW active region*", Electronics Letters, Vol. 33, No. 25, pp. 2123-2124, 1997.

[124] D. Chiaroni, B. Lavigne, A. Jourdan, L. Hamon, C. Janz and M. Renaud, "*New 10 Gbit/s 3R NRZ optical regenerative interface based on semiconductor optical amplifiers for all-optical networks*", In Proceedings of ECOC'97 (Post-deadline paper), pp. 41-44, Edinburgh, U.K., 1997.

[125] J. Leuthold, J. Eckner, E. Gamper. P. A. Besse and H. Melchior, "*Multimode interference couplers for the conversion and combining of zero- and first-order modes*", IEEE Journal of Lightwave Technology, Vol. 16, No. 7, pp. 1228-1239, 1998.

[126] C. Janz, F. Poingt, F. Pommereau, F. Gaborit, D. Ottenwälder, I. Guillemot, B. Dagens and M Renaud, "*All-active dual-order mode Mach-Zehnder wavelength converter for co-propagative operation*", Electronics Letters, Vol. 34, No. 19, pp. 1848-1849, 1998.

[127] F. Ratovelomanana, N. Vodjdani, A. Enard, G. Glastre, D. Rondi, R. Blondeau, C. Joergensen, T. Durhuus, B. Mikkelsen, K. E. Stubkjaer, A. Jourdan and G. Soulage, "*An all-optical wavelength-converter with semiconductor optical amplifiers monolithically integrated in an asymmetric passive Mach-Zehnder interferometer*", IEEE Photonics Technology Letters, Vol. 7, No. 10, pp. 992-994, 1995.

[128] F. Ratovelomanana, N. Vodjdani, A. Enard, G. Glastre, D. Rondi, R. Blondeau, A. Jourdan, "*Monolithic integration of a Michelson all-optical wavelength converter*", In Technical Digest of OFC'96, paper WG3, San Diego, USA, 1996.

[129] B. Dagens, C. Janz, D. Leclerc, V. Verdrager, F. Poingt, I. Guillemot, F. Gaborit and D. Ottenwälder, "*Design optimisation of all-active Mach-Zehnder wavelength converters*", IEEE Photonics Technology Letters, Vol. 11, No. 4, pp. 424-426, 1999.

[130] L. H. Spiekman, J. M. Wiesenfeld, U. Koren, B. I. Miller and M. D. Chien, "*All-optical Mach-Zehnder wavelength converter with monolithically integrated preamplifiers*", IEEE Photonics Technology Letters, Vol. 10, No. 8, pp. 1115-1117, 1998.

[131] C. Janz, B. Dagens, A. Bisson, F. Poingt, F. Pommereau, F. Gaborit, I. Guillemot and M. Renaud, "*Integrated all-active Mach-Zehnder wavelength converter with -10dBm signal sensitivity and 15 dB dynamic range*", Electronics Letters, Vol. 35, No. 7, 1999.

[132] S. L. Danielsen, P. B. Hansen, K. E. Stubkjaer, W. Idler, P. Doussière and F. Pommerau, "*All optical wavelength conversion schemes for increased input power dynamic range*", IEEE Photonics Technology Letters, Vol. 10, No. 1, pp. 60-62, 1998.

[133] B. Mikkelsen, G. Raybon, T. N. Nielsen, U. Koren, B. I. Miller and K. Dreyer, "*Opto-electronic and all-optical wavelength translators and their cascadability*", In Technical Digest of OFC'99, paper FJ1, San Diego, USA, 1999.

[134] S. Nakamura, K. Tajima and Y. Sugimoto, "*Experimental investigation on high-speed switching characteristics of a novel symmetric Mach-Zehnder all-optical switch*", Applied Physics Letters, Vol. 65, No. 3, pp. 283-285, 1994.

[135] D. Breuer, K. Ennser and K. Petermann, "*Comparison of NRZ- and RZ-modulation format for 40 Gbit/s TDM standard-fibre systems*", In Proceedings of ECOC'96, Vol. 2, pp. 199-202, Oslo, Norway, 1996.

[136] B. Mikkelsen, R. S. J. Pedersen, B. F. Joergensen, M. Nissov, K. E. Stubkjaer, K. Wünstel, K. Daub, E. Lach, G. Laube, W. Idler, M. Schilling, P. Doussiere and F. Pommereau, "*Demonstration of a robust WDM cross-connect cascade based on all-optical wavelength converters for routing and wavelength slot interchange*", In Proceedings of ECOC'97, Vol. 2, pp. 245-248, Edinburgh, U.K, 1997.

[137] C. Janz, F. Poingt, F. Pommereau, W. Grieshaber, F. Gaborit, D. Leclerc, I. Guillemot and M. Renaud, "*New all-active dual-order mode (DOMO) Mach-Zehnder wavelength converter for 10 Gbit/s operation*", In Proceedings of ECOC'99, Vol. 2, pp. 172-173, Nice, France, 1999.

[138] C. Bornholdt, B. Sartorius and M. Möhrle, "*All-optical clock recovery at 40 Gbit/s*", In Proceedings of ECOC'99 (Post-deadline paper), paper PD3-5, Nice, France, 1999.

[139] B. Sartorius, C. Bornholdt, S. Bauer, M. Möhrle, P. Brindel and O. Leclerc, "*System application of 40 GHz all-optical clock in a 40 Gbit/s optical 3R regenerator*", In Technical Digest of OFC2000 (Post-deadline paper), paper PD11, Baltimore, USA, 2000.

[140] M. Vaa, K. S. Jepsen, B. Mikkelsen, K. E. Stubkjaer, R. Hess, W. Vogt, E. Gamper, E. Gini, H. Melchior, P. A. Besse and M. Duelk, "*Bit error rate assessment of 80 Gb/s all-optical demultiplexing by a monolithically integrated Mach-Zehnder interferometer with semiconductor optical amplifiers*", In Proceedings of ECOC'97, Vol. 3, pp. 31-33, Edinburgh, U.K, 1997.

[141] S. Diez, C. Schubert, R. Ludwig, H.-J. Ehrke, U. Fieste, C. Schmidt and H. G. Weber, "*160 Gbit/s all-optical demultiplexer using a hybrid gain-transparent SOA Mach-Zehnder-interferometer*", In Technical Digest of OAA2000, paper OWB6, Quebec, Canada, 2000.

[142] M. Duelk, St. Fischer, E. Gamper, W. Vogt, E. Gini, H. Melchior, W. Hunziker, M. Puleo and R. Girardi, "*Full 40 Gbit/s OTDM to WDM conversion: Simultaneous four channel 40:10 Gbit/s all-optical demultiplexing and wavelength conversion to individual wavelengths*", In Technical Digest of OFC'99 (Post-deadline paper), paper PD17, San Diego, USA, 1999.

[143] C. Joergensen, S. L. Danielsen, B. Mikkelsen, M. Vaa, K. E. Stubkjaer, P. Doussiere, F. Pommerau, L. Goldstein, R. Ngo and M. Goix, "*All-optical 40 Gbit/s OTDM to 2*20 Gbit/s signal-format translation*" Electronics Letters, Vol. 32, No. 15, pp. 1384-1386, 1996.

[144] R. Calvani, F. Cisternino, R. Girardi, E. Riccardi, "*Polarisation-independent all-optical demultiplexing using four wave mixing in dispersion shifted fibre*" Electronics Letters, Vol. 35, No. 1, pp. 72-73, 1996.

[145] G. Morthier, J. Sun, T. Gyselings and R. Baets, "*A novel optical decision circuit based on a Mach-Zehnder interferometer and gain-clamped semiconductor optical amplifiers*", In Technical Digest of OFC'98, paper WM19, San Jose, USA, 1998.

[146] G. Morthier, J. Sun, T. Gyselings and R. Baets, "*A novel decision circuit based on a Mach-Zehnder or Michelson interferometer and gain-clamped semiconductor optical amplifiers*", IEEE Photonics Technology Letters, Vol. 10, No. 8, pp. 1162-1164, 1998.